博士論文

ESTIMATION OF METHANE EMISSION FROM NATURAL WETLANDS IN THE NORTHERN PERMAFROST REGION BY REMOTE SENSING AND BIO-GEOPHYSICAL MODELING

(リモートセンシングと生物・地球物理学的モデルを用いた永久凍土地帯からのメタン発生量の推定)

苏德苏日古格

SUDESURIGUGE

37-117312

A thesis submitted in partial fulfillment
of the requirements for the degree of

Doctor of Engineering

Department of Civil Engineering
Graduate School of Engineering
The University of Tokyo
Tokyo, Japan

September, 2014

ESTIMATION OF METHANE EMISSION FROM NATURAL WETLANDS IN THE NORTHERN PERMAFROST REGION BY REMOTE SENSING AND BIO-GEOPHYSICAL MODELING

(リモートセンシングと生物・地球物理学的モデルを用いた永久凍土地帯からのメタン発生量の推定)

Examination Committee

Associate Professor	Wataru Takeuchi
Professor	Ryosuke Shibasaki
Professor	Sachiko Hayashida
Associate Professor	Ryoichi Imasu
Associate Professor	Kazuo Oki

苏德苏日古格

Ph.D thesis submitted to

Department of Civil Engineering, The University of Tokyo

ESTIMATION OF METHANE EMISSION FROM NATURAL WETLANDS IN THE NORTHERN PERMAFROST REGION BY REMOTE SENSING AND BIO-GEOPHYSICAL MODELING

Abstract

Wetland is one of the main sources of atmospheric methane. The increasing emission of atmospheric methane has brought great influence to global climate change and it is necessary to estimate wetland methane emission accurately. The methane has 20 times stronger greenhouse effect compared with the same amount of carbon dioxide. From the fifth report of the IPCC, by the end of the 21st century, global warming will cause that most of the active layer depth will increase by 30% to 40% of the northern hemisphere and the changes in climate will be expected to produce changes in the energy balance at the ground active layer. The increased active layer depth will provide greater anaerobic environment and increase methane emissions. Methane emission from anaerobic soil is released to the atmosphere by three ways including diffusion, ebullition and plant-mediated transport. These biochemical processes are greatly effected by the water condition in soil. The methane emission depends on the water table depth and therefore the land surface water coverage was considered in this study. The study site covers the whole Siberian (41°N~83°N, 27°E~180°E) permafrost area. The north coast of study area belongs to arctic climate, and the southernmost part has cold winters and fairly warm summer for at least 4 months. Methane estimation methods are evaluated as the two kinds of values, emission and concentration. In this study, bio-geophysical models were derived based on in-situ measurements integrated with vegetation index and temperature data which were obtained from satellite measurements to cover huge areas.

Firstly, the wetland selected from ENVISAT MERIS global land-cover data. The MERIS global land cover data has 300m spatial resolution with in 22 land cover classes. As a source of methane emission, 5 of them used to represent wetland in this study.

Secondly, the land surface dynamics were investigated by AMSR-E data. Land surface water coverage (LSWC) and snow coverage were computed by normalized polarization index. LSWC and snow coverage in wetland area were mapped over wetland land cover map from 2003 to 2010 in daily basis. The result indicated that LSWC gradually increased 3.31% of area in 2010 through 8 years from 2003; snow coverage shrunk about 2.11% of area at the same time. The results implied that summer season (LSWC onset time) started earlier and the continuing period was longer in 2010 than that in 2003.

Thirdly, bio-geophysical models are derived from the in-situ measurement published by Wille's. The models are defined as the function of land surface temperature (LST) and normalized difference vegetation index (NDVI) by MODIS from 2001 to 2012. The models are composed of three types including CH4_lst, CH4_ndvi and CH4_Ndl. They are applied to the wetland map derived from MERIS global land-cover data. Through applied models on different land cover types, we found that shurbland and grassland area are identified as the biggest source of methane in permafrost area. Moreover, through applied models on all land cover, the results showed positive methane growth rate, 0.24% (CH4_lst), 4.74% (CH4_ndvi) and 0.36% (CH4_Ndl) in 2012 respectively compare with those of 2003. This result indicated that the methane emissions would increase according as increase of melting permafrost due to climate warming.

Fourthly, the column averaged methane concentration data of SCanning Imaging

Absorption spectroMeter for Atmospheric CHartography (SCIAMACHY) were used to provide the seasonal variation of methane concentration from 2003 to 2010. From 2003 to 2010, around 13% of methane concentration growth rate over 8 years was observed by SCIAMACHY compared with the emission estimation mentioned above. The Pearson's correlations were carried out between SCIAMACHY concentration data and modeled methane emissions. The results showed that the models well represents seasonal dynamics of methane emissions over the years, however, some methane concentration anomalies were found in April and September. The Probable reasons for those anomalies were considered as sensor's degradation since 2005 and errors originated from lower tropopause height. The temperature anomaly were found in September when ground surface freeze quickly and pushed out amount of methane from the soil and in April when accumulated methane under the ground in previous year will released to the atmosphere along with ground melting.

Finally, the emission estimated derived from our models were compared with several inventory data and satellite observations including World Data Center of Greenhouse Gas (WDCGG), Emission Database for Global Atmospheric Research (EDGAR) and Greenhouse Gases Observing Satellite (GOSAT). WDCGG consist of measurement data and associated metadata of methane and the other related trace gas from various platforms. EDGAR is global anthropogenic emissions of greenhouse gases and air pollutants by country basis. GOSAT measures column averaged concentration of greenhouse gas since 2009. Its restriction is limited global coverage due to sampling pattern. In this study, one station (69.2N 35.1E) from WDCGG was used to do comparison analysis with methane estimation results and SCIAMACHY. Methane concentration of the satation indicated increasing tendency from 1999 to 2012, in which was consistant with the estimation results of this study. SCIAMACHY

concentration at that point also indicated increasing tendency but showed much bigger fluctuation than in WDCGG.

Uncertainties and limitations still remain in estimation models, satellite data and in-situ measurements. They are dependent on climate parameters such as soil moisture, wind speed, atmospheric pressure, topography, atmospheric circulation and tropopause height. That's why the satellite data appear abnormal values sometimes. In order to let emission and concentration value comparable, the atmospheric transport model should be considered. It is important that doing more investigations and exploring the fusion of scientific techniques is necessary to remedy those limitations.

Acknowledgement

My study at the University of Tokyo will soon come to an end and I wish to express my sincere appreciation to all those who have offered me invaluable help during three years of my PhD study in Japan.

My deepest gratitude goes first and foremost to Associate Professor Wataru Takeuchi, my supervisor, for his constant and patience guidance and encouragement. He has walked me through all the stages of my PhD study in Japan. Without his consistent and illuminating instruction, I could not have reached this present form. He is not only a very young and cool supervisor, but also a handsome and warm-hearted senior. Takeuchi sensei always introduces Japanese culture and encourages me to enjoy Japanese life. Under his guidance, I was fortunate to attend many international remote sensing conferences. Not only met many good professors who have a really wide range of knowledge about remote sensing, but also improved myself.

Second, I would like to express my heartfelt gratitude to Professor Sachiko Hayashida (Nara Women's University), who supports my research and thesis writing very patient and careful. I am also greatly indebted to the PhD thesis committee members: Professor Ryoichi Imasu, Professor Kazuo Oki and Professor Ryosuke Shibasaki, for their valuable comments, criticisms and suggestions for my research.

I would like to thank all friends and partners in Wataru Takeuchi laboratory. The precious and brilliant memories will stay in my heart for lifetime. Thanks due to my tutor Mr. Tatsuya Ishikawa, for helping me a lot in administrative aspects during my first step of life in Japan. Special thanks to Ms. Haemi Park and Mr. Hiromi Jonai, who helped my research could pass over the difficulties about coding and processing.

I am also grateful to Ms. Yoko Yoshimura, the secretary of Wataru Takeuchi laboratory, for her friendly support in handling many aspects during the course of my study. Thanks to other lab members: Ms. Minaco Adachi, Mr. Soni Darmawan, Ms. Li Xi, Mr. Naoki Katayama and Mr. Sho Tsunoda. I also express my sincere gratitude to all members not list above. I wish all the wishes for the bright life for them. All the people in Wataru Takeuchi laboratory contributed to an extremely nice laboratory atmosphere, which make me comfortable and enjoyable during three years' study.

I sincerely acknowledge the Ministry of Education, culture, Sports, Science & Technology (MEXT) scholarship for providing the financial assistance for my three year's study in Japan.

Last my thanks would go to my beloved family: my husband Hinggan and my parents, for their loving considerations and great confidence during my whole course of study. Special thanks to my brother Sodbilig, who helped me deal with C programing problems. I sincerely gratitude to my senior: Mr. Li Yuanheng and Mr. Guo Libiao who gave me their help and time for helping me work out my problems during the difficult course of the research.

September 2014

The University of Tokyo

Table of contents

List of Table

List of Figure

Chapter 1

INTRODUCTION

1.1. Background

Sea ice loss in arctic region is correlated with warming of northern hemisphere, which caused by global warming. Warming of northern hemisphere lead to thaw and melt of permafrost, which is one of the most vulnerable carbon pools of the Earth system [1][2] and release huge amount of greenhouse gases into the atmosphere [3]. Atmospheric CH_4 is the second most important anthropogenic greenhouse gas after CO_2 because of its influence on the Earth's radiation budget by infrared absorption and photochemical reactions in the atmosphere [5]. CH_4 sources can be divided into anthropogenic and natural. The anthropogenic sources include rice agriculture, livestock, landfills and waste treatment, some biomass burning, and fossil fuel combustion. Natural CH_4 is emitted from sources such as wetlands, oceans, forests, fire, termites and geological sources [6]. Methane has more than 20 times stronger greenhouse effect compare with the same amount of carbon dioxide. Therefore, increasing of methane in the atmosphere will increase greenhouse effect. Climatic warming, deeper permafrost thawing and subsequent vegetation changes have been associated with increases in landscape scale methane emissions in the range of 22–66% over the period 1970–2000 [8]. Changes in climate may be expected to produce changes in the energy balance at the ground and will provide more anaerobic environment to produce more methane emissions.

The response of trace gas emission to climate change, Anisimov [7] reported

increase of methane emissions due to soil warming is likely to be the short-term response to climate change, and in the longer-term warmer climate, more protracted growing periods and northward movement of productive vegetation may increase photosynthetic carbon uptake.

Water table position, soil moisture and temperature, type of substrate and vegetation as well as availability of organic carbon area the factors that influence the methane dynamics of permafrost wetland [9].

1.1.1 What is permafrost?

In Collins English Dictionary, geography definition of permafrost (permanently frozen ground) is ground that is permanently frozen, often to great depths, the surface sometimes thawing in the summer. In geology, permafrost is perennially frozen ground (soil or rock and included ice and organic material) that remains at or below 0°C for at least two consecutive years [10]. Most permafrost is located in high latitudes area include continuous and discontinuous permafrost. The distribution of discontinuous permafrost exists a surface table, which freezes and thaws annually and is called active layer. The thickness of the active layer mainly depends on the moisture content and land surface temperature.

Permafrost covers 24% of the land surface of the northern hemisphere and hold around 1700 Gt of organic carbon [4]. In IPCC2013 report, it was found that significant permafrost degradation has occurred in the Russian European North. Over the period 1975–2005, warm permafrost up to 15 m thick completely thawed, the southern limit of discontinuous permafrost moved north by up to 80 km and the boundary of continuous permafrost moved north by up to 50 km [11].

Permafrost degradation is often accompanied by erosion and other physical

changes to the landscape. Ice in permafrost acts like cement to bind soil and rock together such that permafrost is hard, durable and resistant to erosion, so vegetation is restricted to the active layer [12]. But if it warms and thaws, the ice "glues" the soil together softens and makes thawing permafrost extremely vulnerable to erosion or sudden collapse [13]. When it happen, the thermokarst depression will formed in the settlement of the ground following thawing of ice-rich permafrost. The depression will fill with water to form a lake and substantially accelerate thaw of surrounding permafrost if the depression has no outlet [14].

1.1.2 Methane emission in permafrost soil

CH_4 emissions from biogenic sources account for more than 70% of the global total. These sources include wetlands, rice agriculture, livestock, landfills, forests, oceans and termites [6]. Emissions of CH_4 from most of these sources begin with primary fermentation of organic soil in anaerobic (oxygen poor) environments. Followed by secondary fermentation, other carboxylic acids, alcohols, CO_2 and hydrogen (H_2), which are finally converted to CH_4.

$$CH_3COOH \rightarrow CH_4 + CO_2;\ CO_2 + 4H_2 \rightarrow CH_4 + 2H_2O \qquad (1.1)$$

There are three pathway of CH_4 emissions in wetland: diffusion, ebullition and through aerenchyma of plant. Diffusion is movement of methane up through soil or body of water to reach the atmosphere. Ebullition is the sudden release of bubbles of methane into the atmosphere, it is a way of methane releasing from aquatic ecosystem [19]. Plants' arenchyma is methane can transport directly up from the soil into the atmosphere by porous tissue of the plant. Diffusion is a slowly process compare with ebullition. Because of ebullition refers to accumulate and form amount of methane in

the soil over time. The pressure gradually builds up and the part of methane suddenly rising into the air. It was found that after significant rainfall the pressure will increase and suggested that rainfall is directly related to methane emissions in wetlands [15].

1.2. Methane estimation overview

Since the beginning of the Industrial Era, the atmospheric CH_4 concentration increased by a factor of 2.5 (from 722 ppb to 1803 ppb in 2011) [16]. The methane emission is generally estimated from two kinds of measurements: (1) ground based measurement, extrapolation from direct emission measurement or observation sites and process-based modeling; (2) observe atmospheric concentration by satellite, inverse modeling that depends on spatially continuous (aircraft and satellite) observations [17]. Table 1.1 list out the information about ground based measurement and satellite observations include measurement technique and data, resolution, advantage and disadvantage and so on.

Although ground based measurement has high accuracy on time and spatial resolution, it needs many labors and money so that cannot do measurement work all the time. Moreover, it is impossible doing measurement in remote or depopulated area. The satellite observation has its own advantage to fill the weakness of ground −based measurement. It can cover wide range, real-time monitoring, cheap even free of charge. But the limitation is satellite image cannot exactly ensure the reality of the earth. Overall the two approaches are very complementary.

Chamber technique (CT) and micrometeorological technique are commonly used in for measure carbon emission. In micrometeorological technique the eddy covariance (EC) is frequently used. CT is suitable for small-scale monitoring and EC usually apply to landscape scale. EC considered to be the most reliable and practicable for

long-term measurements of carbon emission and are of wide used worldwide [50]. But small-scale chamber measurements can be used to estimate emissiones of CH_4 and CO_2 at landscape scale if emissiones are scaled by different landscape components [47]. CT more relies on land surface condition and EC likely to be affected by environmental variations like wind speed. Therefore these two methods may produce different emission result at same place.

Table 1.1: Information about ground based measurement and satellite observations.

Type	**Ground based measurement**		**Satellite observation**
	In-situ measurement	Inventory data	Atmospheric CH_4 concentration
Measurement technique or data	• Chamber method (closed statistic chamber, closed/open dynamics chamber) • Micrometeorological method (Eddy covariance technique) • Soil profile method		• GOSAT • SCIAMACHY • WDCGG • TCCON
Spatial resolution	<= 600 m	100 ~ 300 m	100 ~ 1000 km
Time resolution	sec./h./d	daily/monthly	Monthly/yearly
Covering period	several months/years	several ~ tens of year (depends on)	several tens of year (depends on)
Advantage	• first hand information in study point • high accuracy	• long time series of statistic data	• continuous data • wide range (remote or depopulated zone) • cheap
Disadvantage	• cannot cover every place especially remote or depopulated zone; • not continuous data; • costly (labor, money and so on)	• data maybe lost because of instrument error or impact of climate	• lower spatial resolution so may cause overestimation of real condition; • data include many noise

Nakano et al. use statistic chamber technique to estimate the rate of methane emission in tundra wetland in Siberia. They found that methane emission from the waterlogged site at Tiksi (71.53N, 130.03E) averaged 46.3 mg CH_4 $m^{-2}d^{-1}$, emission from the waterlogged site at Chersky (68.53N, 161.43E) was much more greater than that at Tiksi and averaged 281.1 mg CH_4 $m^{-2}d^{-1}$ [18]. Sachs et al. reported the first ecosystem-scale methane emission data from a northern Siberian tundra ecosystem by using eddy covariance measurements [20]. Schneider et al. classified the land cover type in Lena Delta based on Landsat images and used it to quantification of methane emissions from the delta ecosystems on the regional scale. They found that the mean daily emission was 10.35 mg CH_4 $m^{-2}d^{-1}$ [21].

The vertically averaged atmospheric CH_4 concentration can be observed by using Fourier Transform Infrared Spectroscopy (FTIR) instruments from the surface [16] and by several satellite instruments from space: Scanning Imaging Spectrometer for Atmospheric Cartography (SCIAMACHY), Thermal And Near infrared Sensor for carbon Observation Fourier-Transform Spectrometer (TANSO-FTS) on board Greenhouse Gases Observing Satellite (GOSAT).

There are several comparisons of CH_4 observed with the GOSAT satellite and FTIR measurements from the TCCON network where located at latitudes lower than 55N, but Gavrilov et al. [22] have done same research in high latitude (~60N) and found substantially lower satellite values compared to those obtained from ground-based observations. Frankenberg et al. [23,24] used CH_4 estimation from SCIAMACHY measurement to compare with model results from the chemistry–transport model TM4 and reported a major revision of SCIAMACHY retrievals due to an update of spectroscopic parameters of water vapor and methane. Bergamaschi [25] analyzed the impact of this revision on global and regional CH_4 concentration

estimates using the TM5-4DVAR inverse modeling system. The satellites offer the unique possibility of sensing methane globally, retrieving methane abundances in remote areas where ground based measurements might be complicated or even impossible due to infrastructural or political obstacles [23]. However, the satellite observation studies usually limited by the number of ground observation site.

A major limitation of present satellite observation is limited number of atmospheric observation sites for calibration and validation of ground based approach. Hence, additional a priori information from ground based measurement is usually required in order to overcome the under determination of the inverse problem. Meanwhile, only satellite observation could cover large-scale region and overcome the weakness of ground-based measurement, which cannot reach to rural or remote area. As a consequence, large uncertainties still exist [23]. In a word, the connection with ground measurement and calibration of top detection are quite difficult but there is a big potential possibility.

1.3. Objectives of this study

This research is focused on five issues that are wetland land cover map, estimation of methane emission, correlation with SCIAMACHY and LSWC，land surface characteristics and validation. Figure 1.1 shows the flowchart of the study. To achieve this, there are five objectives have been followed:

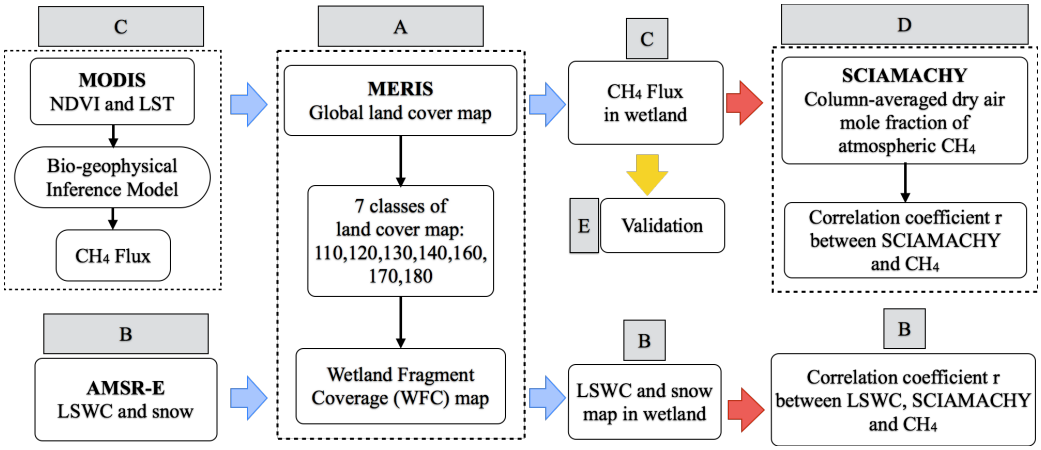

Figure 1.1: Flowchart in this study.

A. Wetland land cover map

- To understand the land cover classification of MERIS land cover data and mapping the wetland fraction coverage (WFC) map in study site.

B. Land surface characterization based on AMSR-E

- To mask out land surface water coverage (LSWC) and snow coverage map in wetland.
- To explore the land surface seasonal dynamics by calculating the coverage area.
- To do correlation analysis between LSWC, SCIAMACHY and methane model estimations.

C. Estimation of methane emission

- To derive the bio-geophysical model by MODIS data.
- To estimate the methane emission in study area.
- To mask out the methane emission map based on WFC map.

D. Comparison analysis between methane estimations and SCIAMACHY

- To compare the modeled methane estimations and SCIAMACHY atmospheric concentration data.

E. To validate the estimation results

1.4. Originality of this research

This study makes several original contributions that improve current methods over Siberian permafrost area.

1. In this study, bio-geophysical models were derived based on in-situ measurement results from Wille et al. [34]. The daily methane emission was obtained from the figure which published on paper [34]. Then collaborated with NDVI and LST data were obtained from MODIS for the same dates to find out the relationship between methane emission with NDVI and LST respectively.
2. To estimate methane emission by these models provided possible method of methane estimation without field survey. This estimation method not only enhanced the advantages of in-situ measurement that have high accuracy but also enhanced satellite observation advantages that can cover huge area.

Chapter 2

NATURAL WETLAND CLASSIFICATION BASED ON MERIS LAND COVER DATA

2.1. Introduction

MERIS is a wide field-of-view push broom imaging spectrometer which measuring the solar radiation reflected by the Earth in 15 spectral bands from 390nm to 1040nm on board ENVISAT launched in 2002 [27]. Table 2.1 shows the each of bands center (nm) and bandwidth (nm).

Table 2.1: The MERIS spectral bands, cited from Rast et al., 1999.

Band	Band center (nm)	Bandwidth (nm)
1	412.50	10.0
2	442.50	10.0
3	490.00	10.0
4	510.00	10.0
5	560.00	10.0
6	620.00	10.0
7	665.00	10.0
8	681.25	7.5
9	705.00	10.0
10	753.75	7.5
11	760.00	2.5
12	775.00	15.0
13	865.00	20.0
14	890.00	10.0
15	900.00	10.0

Global land cover Map has 300m spatial resolution and in WGS 84 map projection. This global Land cover map is derived by an automatic and regionally tuned classification of a MERIS Full Resolution (FR) mosaics (6 products a year, 10 products from December 2004 to June 2006). Its 22 land cover classes are defined with the UN Land-cover Classification System (LCCS), which allows adjusting the detail of the amount of information available to describe each land cover class [28]. Table 2.2 shows the land cover legend and its descriptions, cited from Bicheron et al. [28].

In products validation reports [28], research group used three different steps to accomplish the validation process that are collecting reference data sources, elaborating the sampling strategy and assessing the product's accuracy. This procedure based on the document of the CEOS Land Product Validation subgroup: "Global Land Cover Validation: Recommendations for Evaluation and Accuracy Assessment and of Global Land Cover Maps" [29]. The overall accuracy weighted by the class area reaches 73 % using 3167 points globally distributed and including homogeneous and heterogeneous landscapes [28], therefore this land cover product fit to use for scientific application.

Table 2.2: Legend of the MERIS global land cover classes.

ID	Land cover legend description
11	Post-flooding or irrigated croplands
14	Rainfed croplands
20	Mosaic Cropland (50-70%) / Vegetation (grassland, shrubland, forest) (20-50%)
30	Mosaic Vegetation (grassland, shrubland, forest) (50-70%) / Cropland (20-50%)
40	Closed to open (>15%) broadleaved evergreen and / or semi-deciduous forest (>5m)
50	Closed (>40%) broadleaved deciduous forest (>5m)
60	Open (15-40%) broadleaved deciduous forest (>5m)
70	Closed (>40%) needleleaved evergreen forest (>5m)
90	Open (15-40%) needleleaved deciduous or evergreen forest (>5m)
100	Closed to open (>15%) mixed broadleaved and needleleaved forest (>5m)
110	Mosaic forest or shrubland (50-70%) / grassland (20-50%)
120	Mosaic grassland (50-70%) / forest or shrubland (20-50%)
130	Closed to open (>15%) (broadleaved or needleleaved, evergreen or deciduous) shrubland (<5m)
140	Closed to open (>15%) herbaceous vegetation (grassland, savannas or lichens/mosses)
150	Sparse (<15%) vegetation
160	Closed to open (>15%) broadleaved forest regularly flooded (semi-permanently or temporarily) - Fresh or brackish water
170	Closed (>40%) broadleaved forest or shrubland permanently flooded - Saline or brackish water
180	Closed to open (>15%) grassland or woody vegetation on regularly flooded or waterlogged soil - Fresh, brackish or saline water
190	Artificial surfaces and associated area (urban areas > 50%)
200	Bare areas
210	Water bodies
220	Permanent snow and ice

2.2. Land cover map of the study area

The study area covered whole Siberian permafrost area (42°N~83°N, 27°E~180°E). The north coast of study area has arctic climate, and the southernmost part has cold winters and fairly warm summer lasting at least 4 months. Vegetation has tundra and woody grassland. Tundra vegetation is comprised of lichens, mosses, sedges, grasses, forbs and low shrubs, including heaths, dwarf willows and birches [26]. The study done by Schneider et al. [21] shows, more than 85% of CH_4 emission released from the place where growing sedge, moss and tundra in Siberian natural wetland. So that corresponding the vegetation type in study area, 7 of 22 classes: 110, 120, 130, 140, 160, 170 and 180 were extracted to represent permafrost wetland, noted as Wetland Fraction Coverage (WFC) map hereafter. However, after checking the land cover classes, it was found that two kinds of land cover 160 and 170 do not exist in the study area.

Figure 2.1 is the procedure of masking out WFC map from MERIS land-cover map. According check the existence of all land-cover type, the class 160 and 170 are excluded. Figure 2.2 shows the MERIS land-cover map of study area at 1 km spatial resolution through resized the original map. The map includes all kinds of land-cover types. Figure 2.3 represents the WFC map, which resulted by masking process. The WFC map obtained the wetland classes 110, 120, 130, 140 and 180 from MERIS land-cover. As the result all wetland classes (110, 120, 130, 140 and 180) are merged together and result showed value 0 (no data) and 1. In case of data loss, use stretch processing and pixel aggregate to make sure the WFC map retain as much as information. As a result the data range (0 and 1) change to 0 ~100.

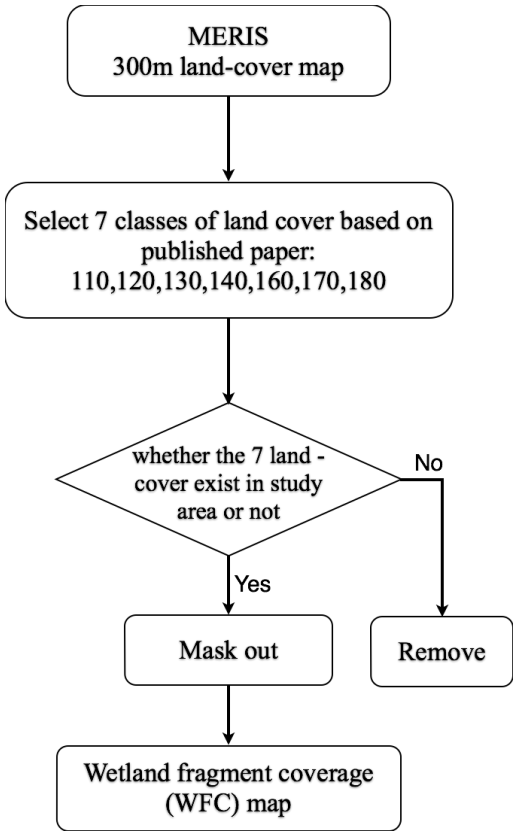

Figure 2.1: Flowchart of masking out Wetland fragment coverage (WFC) map.

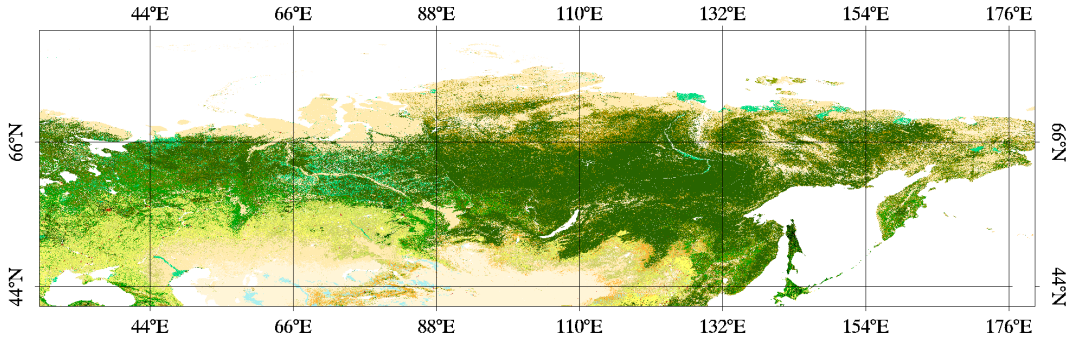

Figure 2.2: MERIS land cover map of study area in 1 km resolution by resize the original land cover map.

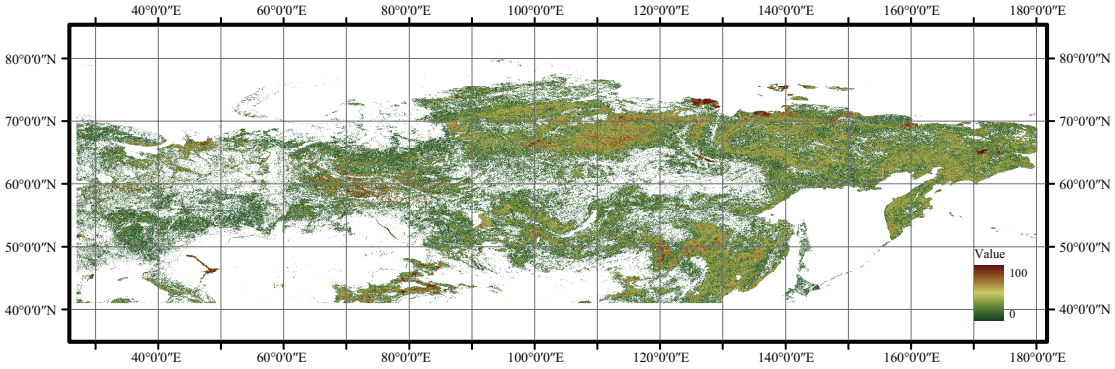

Figure 2.3: Wetland Fraction Coverage (WFC) map of study area. The WFC map obtained through extract the wetland classes from MERIS land cover map and use stretch processing and pixel aggregate to change the value from 0 and 1 to continuous range 0~100. This process is prevent from data loss.

Chapter 3

LAND SURFACE SEASONAL DYNAMICS USING AMSR-E DATA

3.1. LSWC and Snow coverage data

To determine the land surface dynamics in permafrost wetland, the time and area of snow melting and water inundation are the most valuable factors.

The Advanced Microwave Scanning Radiometer-Earth Observing System (AMSR-E) is a sensor on NASA's Aqua satellite (till October in 2011). It is a passive sensor that measures weak microwaves radiated from the Earth at six frequencies in twelve channels.

The LSWC provides the fraction (%) of a land surface covered by water. The normalized difference water index (NDWI) from MODIS 8-day 2km composite data and AMSR-E daily 16km normalized difference polarization index (NDPI) are used to map LSWC [36]. The snow data, from AMSR-E, provides daily at 10km spatial resolution. The time series of data is from 2003 to 2010.

3.2. Land surface dynamics in study area

The land surface water coverage used to represent inundated region in this objective area. Because of water condition in permafrost soil decides the oxidation rate of methane, so that LSWC and snow coverage seasonal variations are the indispensible factor to impact methane production. In this part include two analyses, one is land surface coverage changing and another is correlation analysis between modeled methane emissions and LSWC. Figure 3.1 is a procedure for getting

seasonal dynamics of LSWC and snow coverage.

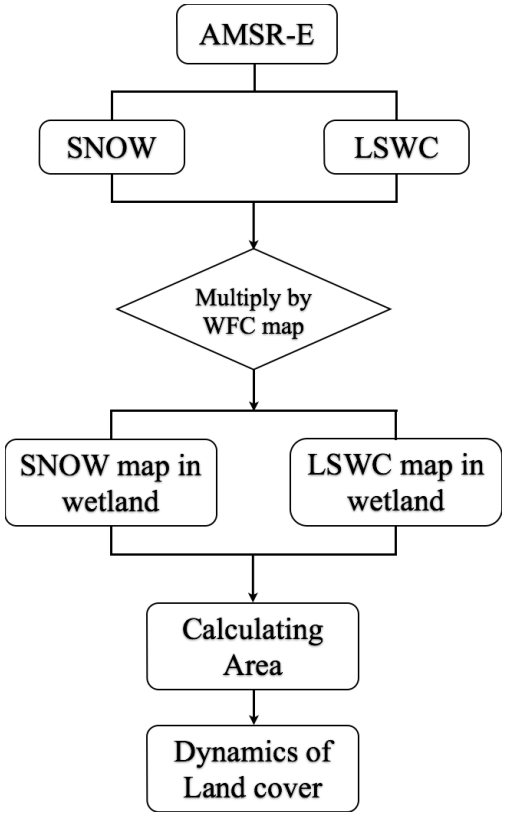

Figure 3.1: Flowchart of evaluates LSWC and snow coverage dynamics.

3.2.1 LSWC and snow coverage seasonal characteristics

1. Figure 3.2 shows the total area of LSWC (red) and snow (black) coverage from 2003 to 2010. From these figures we can know LSWC and snow have a good agreement of seasonal variation in time series. The water inundation comes after snow melting.

   Figure 3.3 and 3.4 illustrate the monthly coverage ratio of LSWC (averaged) map in 2003 and 2010. In order to preserve as much data, here multiply LSWC by 100. The water inundations appeared from May, focused on June to September

showed in Figure 3.3 and Figure 3.4.

Figure 3.5 and 3.6 illustrate the monthly coverage ratio of snow coverage map in 2003 and 2010. In Figure 3.5 and Figure 3.6 the snow coverage starts from October and continue to the next May.

Figure 3.7 illustrates LSWC averaged monthly map of May ((a) and (c)) and October ((b) and (d)) in 2003 and 2010 to compare the area changes in past several years. It is clear that in 2010, the water coverage area is larger than it in 2003 at the same month. Correspondingly, Figure 3.8 illustrates snow coverage monthly map of June ((a) and (c)) and October ((b) and (d)) in 2003 and 2010. Obviously, in 2010 the snow coverage in June is less than it in 2003. It indicates temperature warmer in 2010 at the same month. But winter does not delay in 2010 from Figure 3.8.

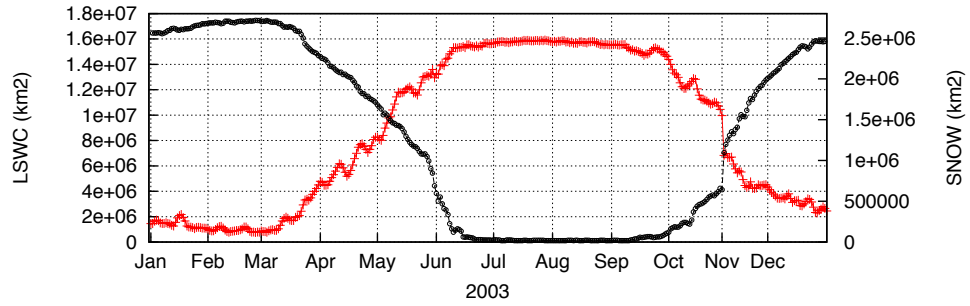
LSWC (km2)
SNOW (km2)
1.8e+07
1.6e+07
1.4e+07
1.2e+07
1e+07
8e+06
6e+06
4e+06
2e+06
0
2.5e+06
2e+06
1.5e+06
1e+06
500000
0
Jan Feb Mar Apr May Jun Jul Aug Sep Oct Nov Dec
2003

(a)

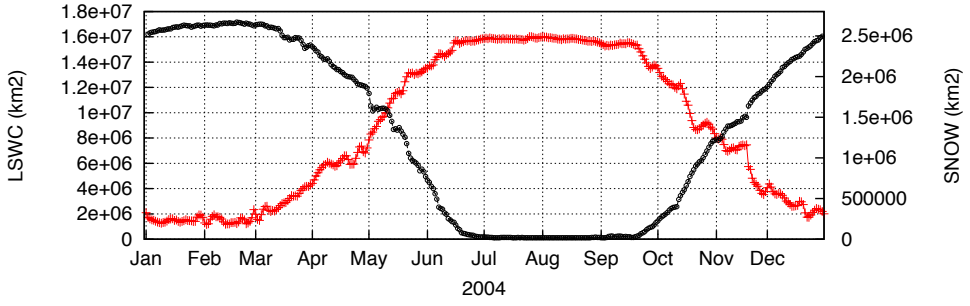
LSWC (km2)
SNOW (km2)
1.8e+07
1.6e+07
1.4e+07
1.2e+07
1e+07
8e+06
6e+06
4e+06
2e+06
0
2.5e+06
2e+06
1.5e+06
1e+06
500000
0
Jan Feb Mar Apr May Jun Jul Aug Sep Oct Nov Dec
2004

(b)

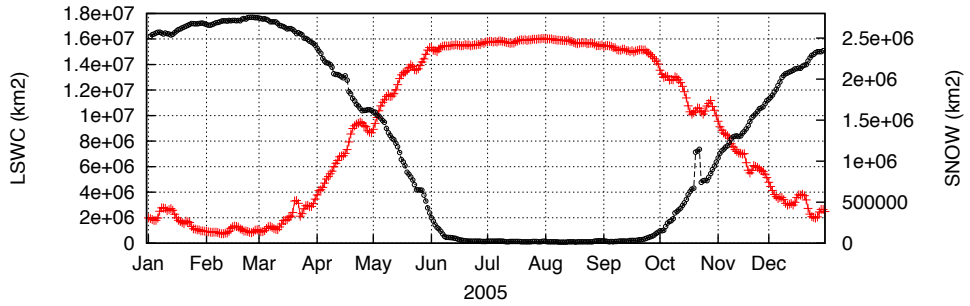
LSWC (km2)
SNOW (km2)
1.8e+07
1.6e+07
1.4e+07
1.2e+07
1e+07
8e+06
6e+06
4e+06
2e+06
0
2.5e+06
2e+06
1.5e+06
1e+06
500000
0
Jan Feb Mar Apr May Jun Jul Aug Sep Oct Nov Dec
2005

(c)

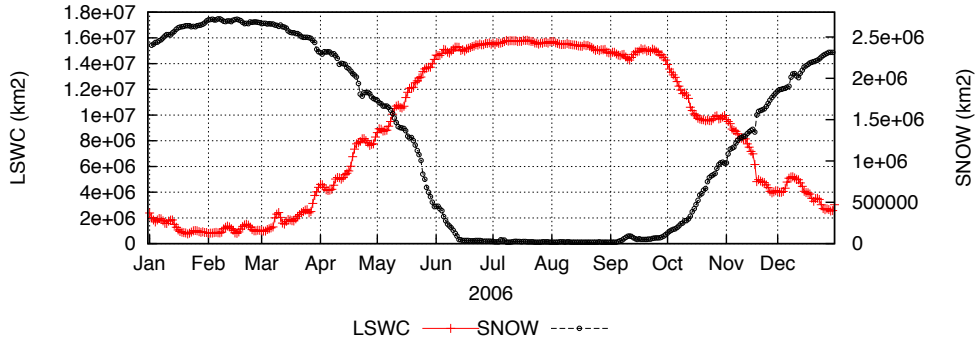
LSWC (km2)
SNOW (km2)
1.8e+07
1.6e+07
1.4e+07
1.2e+07
1e+07
8e+06
6e+06
4e+06
2e+06
0
2.5e+06
2e+06
1.5e+06
1e+06
500000
0
Jan Feb Mar Apr May Jun Jul Aug Sep Oct Nov Dec
2006
LSWC
SNOW

(d)

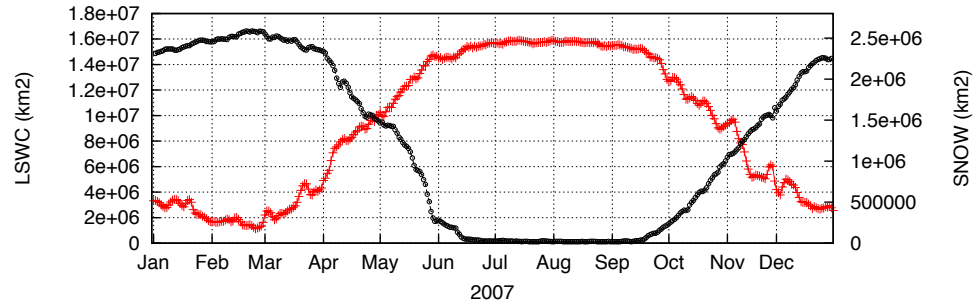

(e)

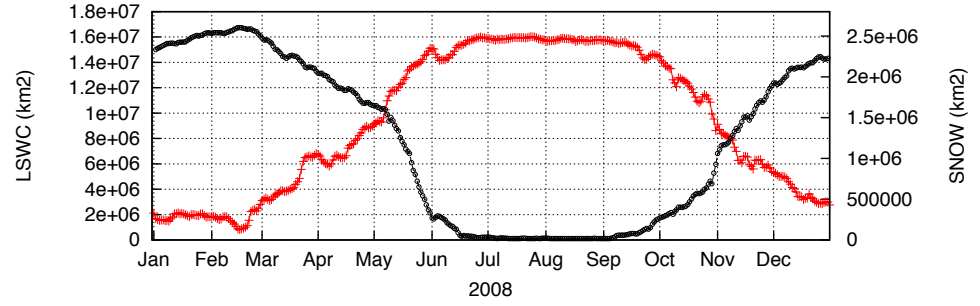

(f)

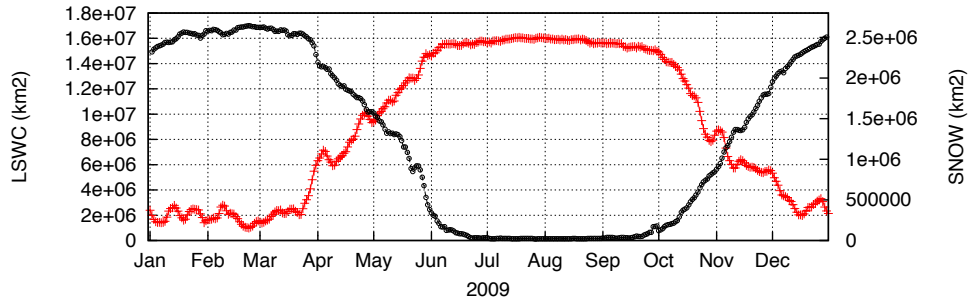

(g)

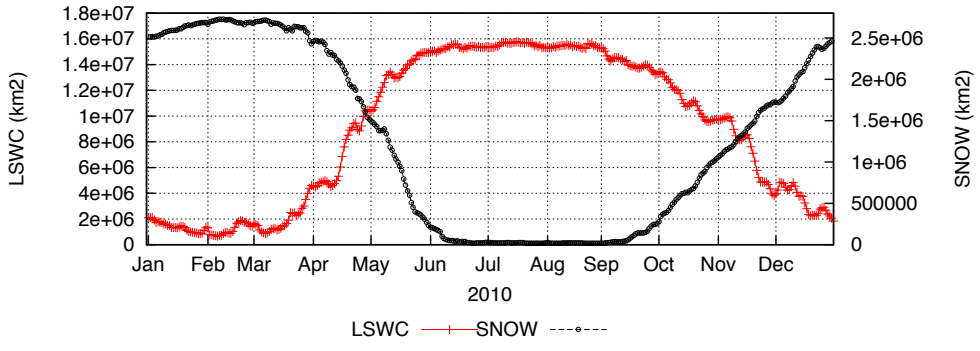

(h)

Figure 3.2: Total area of LSWC (red) and snow (black) coverage in each year from 2003 to 2010 ((a) ~ (h)).

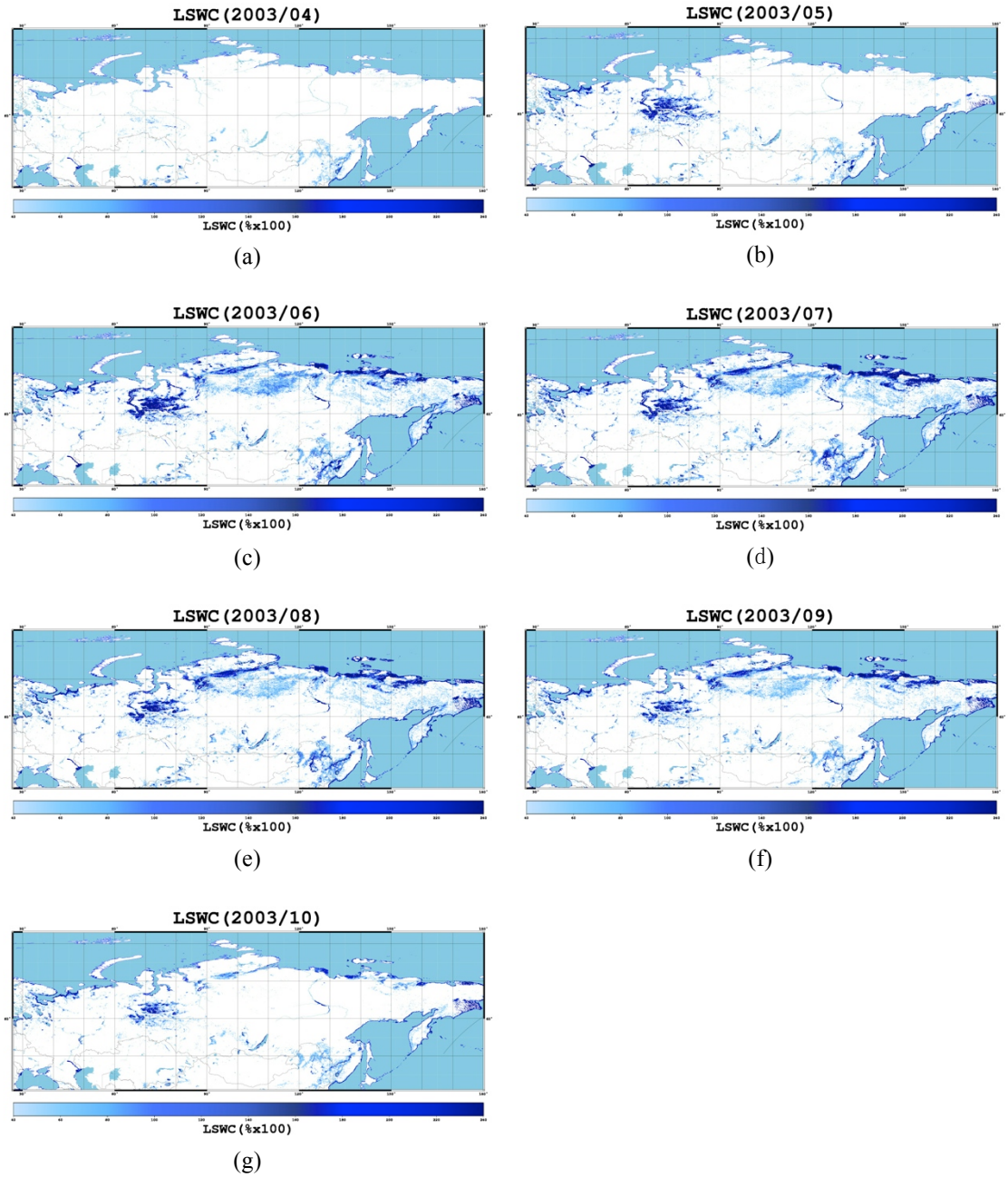

Figure 3.3: Monthly averaged map of LSWC (%) from April to October ((a) ~ (g))in 2003. Large coverage of water continue from June to September.

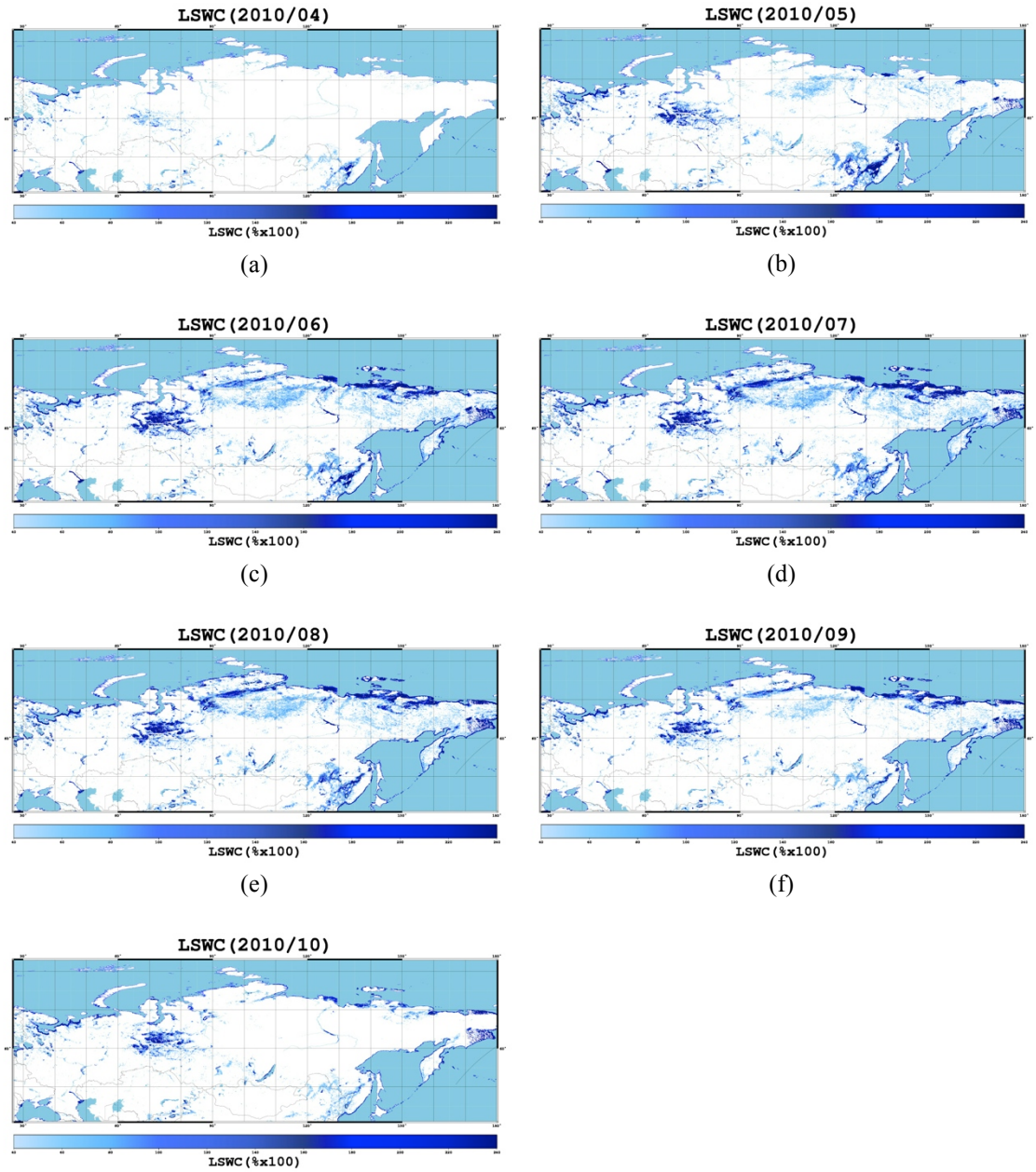

Figure 3.4: Monthly averaged map of LSWC (%) from April to October ((a) ~ (g)) in 2010. Large coverage of water continue from June to September.

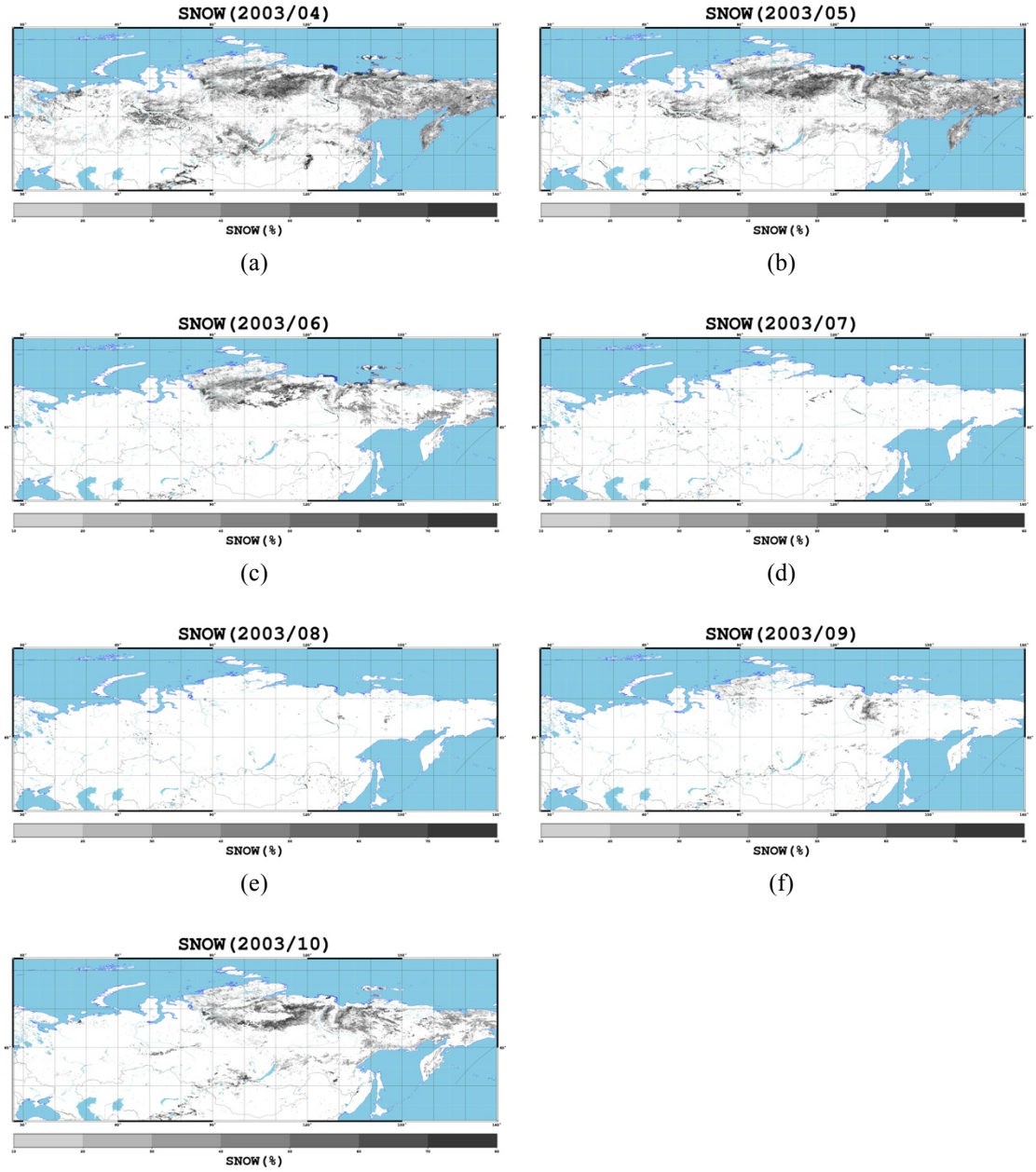

Figure 3.5: Monthly snow coverage (%) map from April to October ((a) ~ (g)) in 2003. Snow free time continue July and August two months.

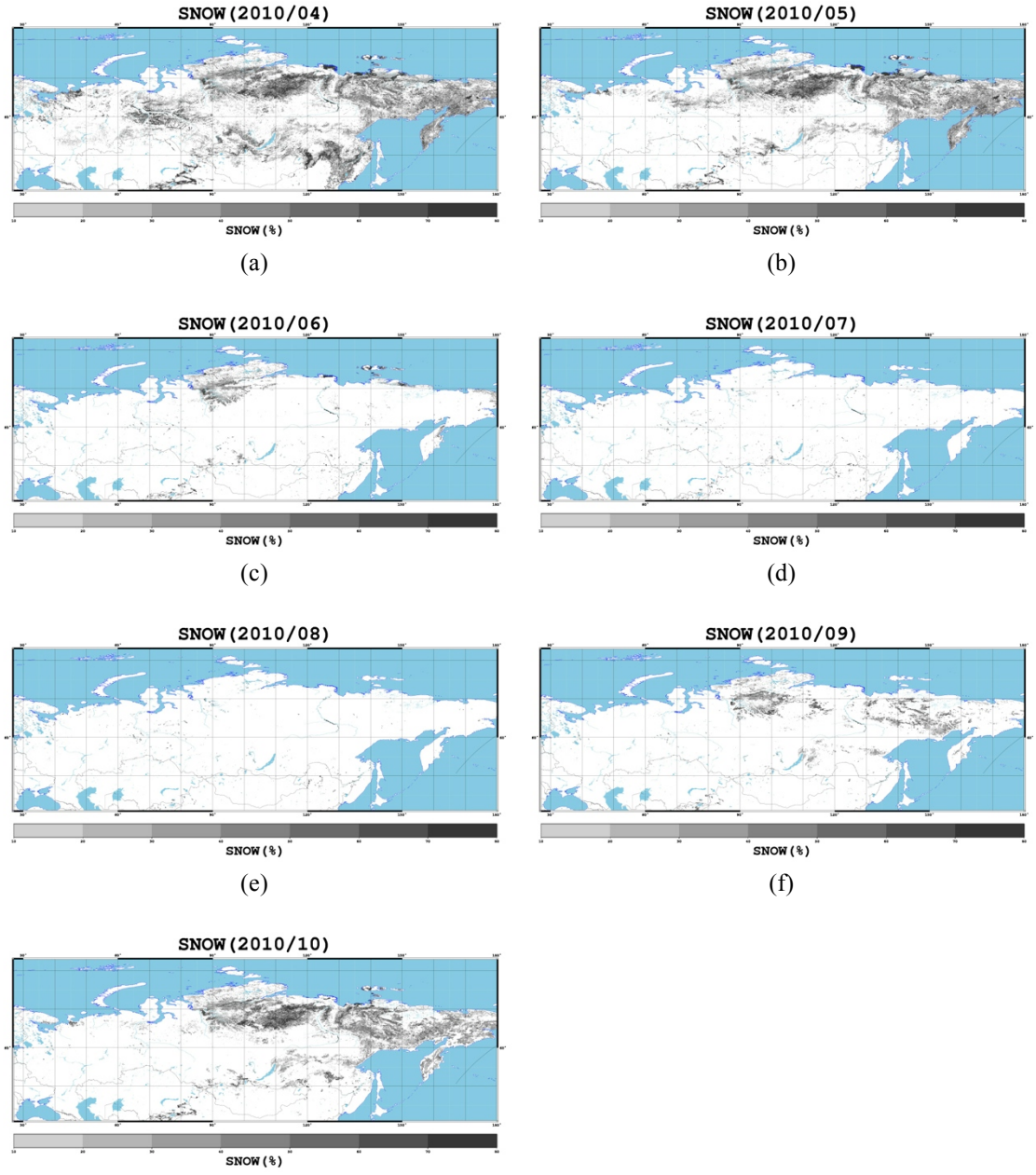

Figure 3.6: Monthly snow coverage (%) map from April to October ((a) ~ (g)) in 2010. Snow free time continue July and August two months.

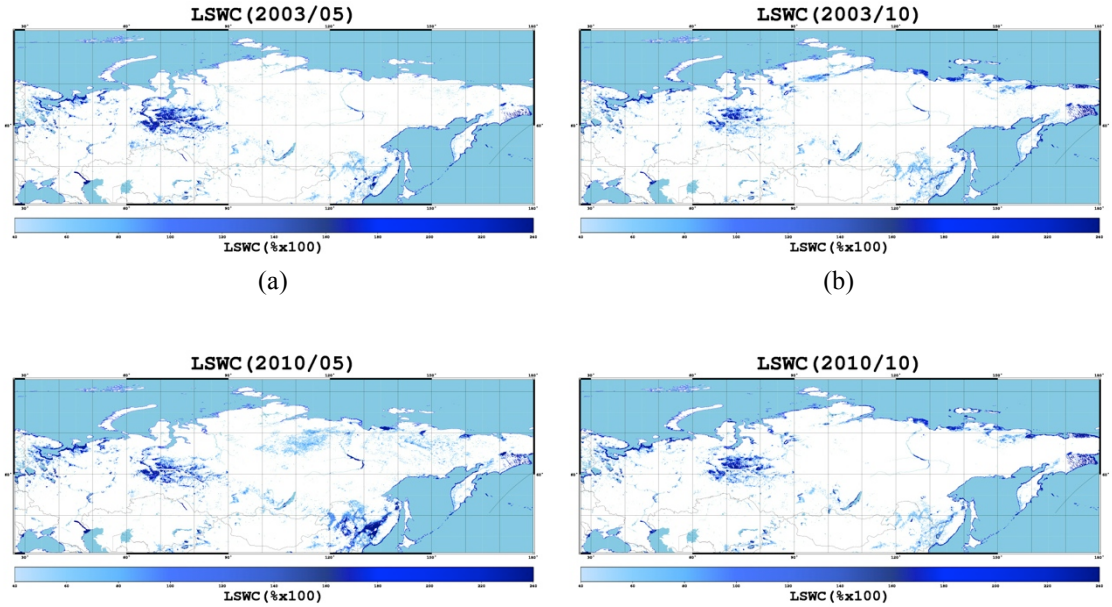

Figure 3.7: Monthly averaged LSWC (%) map of May ((a) and (c)) and October ((b) and (d)) in 2003 and 2010. There are obvious area extention in 2010 compare with 2003, imply the temperature goes warmer and warmer in past several years.

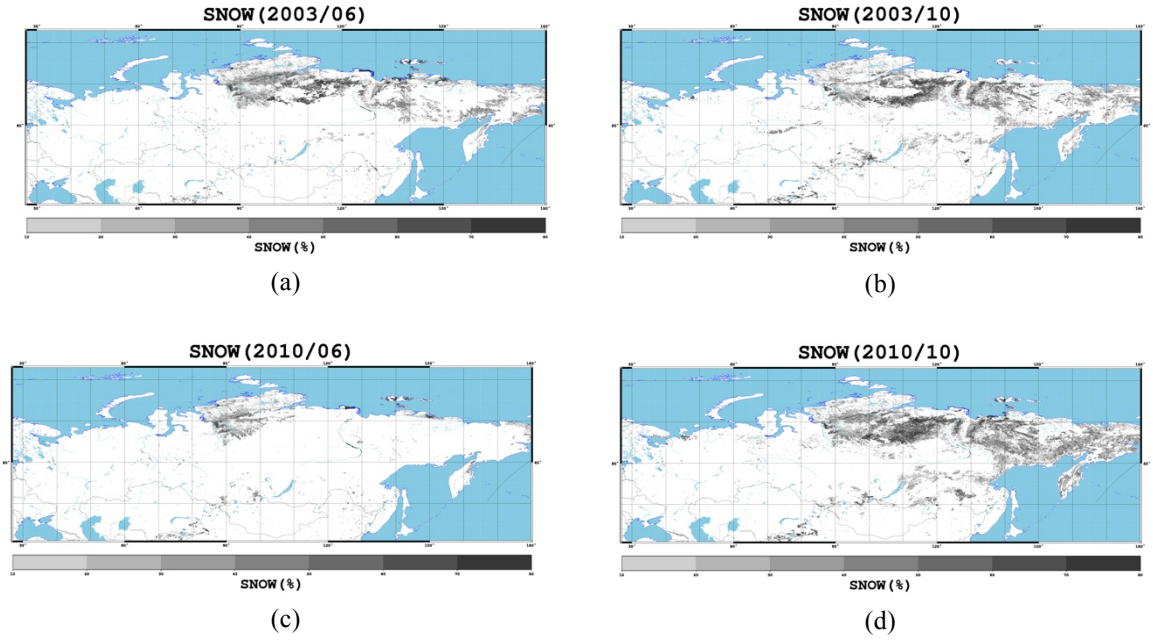

Figure 3.8: Monthly snow map (%) of June ((a) and (c)) and October ((b) and (d)) in 2003 and 2010. It is clearly that the snow melting starts earlier in 2010 than in 2003. But in October there are no winter comes earlier phenomenon.

Figure 3.9 is the mean area of LSWC (a) and snow (b) changes from 2003 to 2010. It is clear that LSWC showed increasing trends and snow coverage showed decreasing trends. Table 3.1 shows the growth rate and annual growth rate of LSWC and snow from 2003 to 2010. LSWC increased 3.31% and at the same time snow coverage decreased 2.11% in 2010 compare with 2003. From this statistic calculation, the changes of LSWC and snow coverage were obvious.

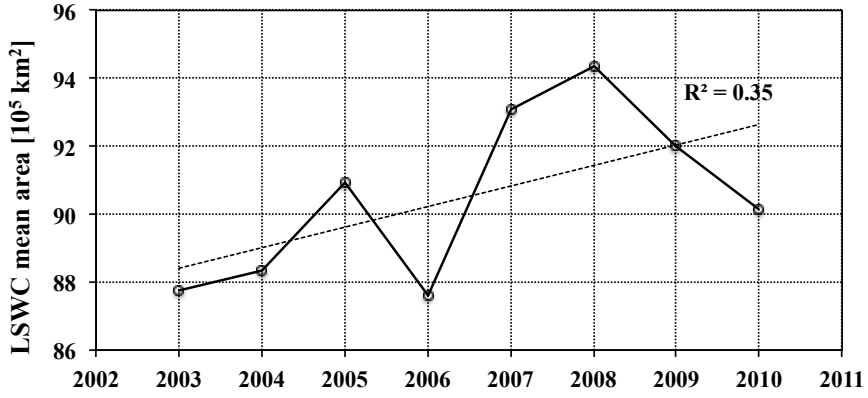

(a)

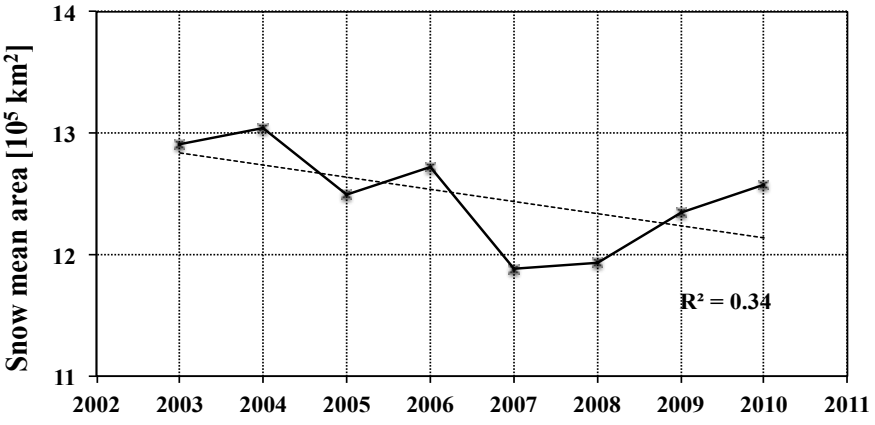

(b)

Figure 3.9: Mean area of LSWC (a) and snow (b) changes from 2003 to 2010.

Table 3.1: Growth rate and annual growth rate of LSWC and snow coverage 2003-2010.

	Growth Rate (%)	Annual growth rate (%)
LSWC	3.31	0.47
Snow coverage	-2.11	-0.30

2. To understand LSWC and snow coverage changing dynamics, except area changes, time and duration variations also indispensable. There are two kinds of definition used to decide the onset-offset date and duration periods. First one is using average (A) value of total area of each year; second one is using half of maximum (HM) value of total area of each year.

   Table 3.2 shows the onset-offset time and duration period of LSWC and snow. Snow duration in this table represents “less snow duration”, means snow free time. In other word it is closer to the duration of LSWC. In A definition, the onset time is in end of March but in HM definition, the onset time starts from end of April. Based on LSWC monthly coverage map (Figure 3.3 and Figure 3.4), the HM definition seems more practical.

   Because of snow time always pass through the New Year and continue to the next spring, therefore, snow time should consider related two years. Table 3.3 shows the onset-offset, snow free duration and snow duration by HM and A definitions respectively. Duration of snow time starts from end of October in previous year and ends in May in the next year. DOY is abbreviation of day of year.

   Depend on these statistic result, Figure 3.10 (a) and (b) showed Onset, offset

and duration of LSWC and snow under A definition. Figure 3.11 (a) and (b) are under HM definition. The order of LSWC from top to down is onset, offset and duration respectively; the order of snow coverage from top to down is offset, onset and duration. The y-axis of duration is number of days. For convenience, the onset plot of LSWC corresponds to the offset plot of snow coverage.

As a result, water coverage started more and more early and ended more and more late both in A and HM definition. The persistent period was longer and longer. Correspondingly, the winter came later and later and continuous time was become shorter.

Consequently, the persistent time of summer season was much more longer than before. The summer season extended phenomenon coincides with the time extension of methane emission.

Table 3.2: Onset, offset and duration of LSWC and snow in HM and A definitions. Duration of snow indicate here is less snow duration, because snow time pass over new year. DOY is abbreviation of day of year.

	LSWC			LSWC		
	Above Average Date	DOY of Average Date	Duration (Days)	Above Half of Max	DOY of Half of Max	Duration (Days)
2003	Mar.30 ~ Nov.20	89 – 324	236	Apr.5 ~ Oct.28	118 – 301	184
2004	Mar.31 ~ Nov.19	90 – 323	234	Apr.30 ~ Nov.1	120 – 305	186
2005	Apr.5 ~ Nov.28	95 – 332	238	Apr.19 ~ Nov.7	109 – 311	203
2006	Mar.31 ~ Dec.11	90 – 345	256	Apr.22 ~ Nov.11	112 – 315	204
2007	Mar.22 ~ Dec.4	81 – 338	258	Apr.11 ~ Nov.7	101 – 311	211
2008	Mar.20 ~ Dec.6	79 – 340	262	Apr.21 ~ Nov.6	111 – 310	200
2009	Mar.29 ~ Dec.3	88 – 337	250	Apr.21 ~ Nov. 5	111 – 309	199
2010	Mar.27 ~ Dec.4	86 – 338	253	Apr.14 ~ Nov.10	104 – 314	211
	SNOW			SNOW		
	Below Average Date	DOY of Average Date	Duration of Less snow (Days)	Below Half of Max	DOY of Half of Max	Duration of Less snow (Days)
2003	May.31 ~ Oct.8	151 – 281	131	May.14 ~ Nov.3	134 – 307	174
2004	Jun.1 ~ Oct.10	152 – 283	132	May.16 ~ Nov.3	136 – 307	172
2005	May.28 ~ Oct.16	148 – 289	142	May.9 ~ Nov.15	129 – 319	191
2006	May.28 ~Oct.19	148 – 292	145	May.17 ~ Nov.16	137 – 320	184
2007	May.27 ~ Oct.16	147 – 289	143	May.11 ~ Nov.10	131 – 314	184
2008	May.24 ~ Oct.22	144 – 295	152	May.13 ~Nov.7	133 – 311	179
2009	May.29 ~ Oct.22	149 – 295	147	May.8 ~ Nov.9	128 – 313	186
2010	May.17 ~ Oct.12	137 – 285	149	May.5 ~ Nov.8	125 – 312	188

Table 3.3: Onset-offset, snow free duration and snow duration by HM and A definitions. Duration of snow time starts from end of October in previous year and ends in May in the next year. DOY is abbreviation of day of year.

SNOW					SNOW			
Year	DOY of Below Average	Duration of less snow (Days)	Year	Duration (Days)	DOY of Below Half of Max	Duration of less snow (Days)	Year	Duration (Days)
2003	134 – 307	174	2003-2004	216	151 – 281	131	2003-2004	194
2004	136 – 307	172	2004-2005	227	152 – 283	132	2004-2005	188
2005	129 – 319	191	2005-2006	224	148 – 289	142	2005-2006	183
2006	137 – 320	184	2006-2007	220	148 – 292	145	2006-2007	176
2007	131 – 314	184	2007-2008	220	147 – 289	143	2007-2008	184
2008	133 – 311	179	2008-2009	219	144 – 295	152	2008-2009	183
2009	128 – 313	186	2009-2010	207	149 – 295	147	2009-2010	177
2010	125 – 312	188			137 – 285	149		

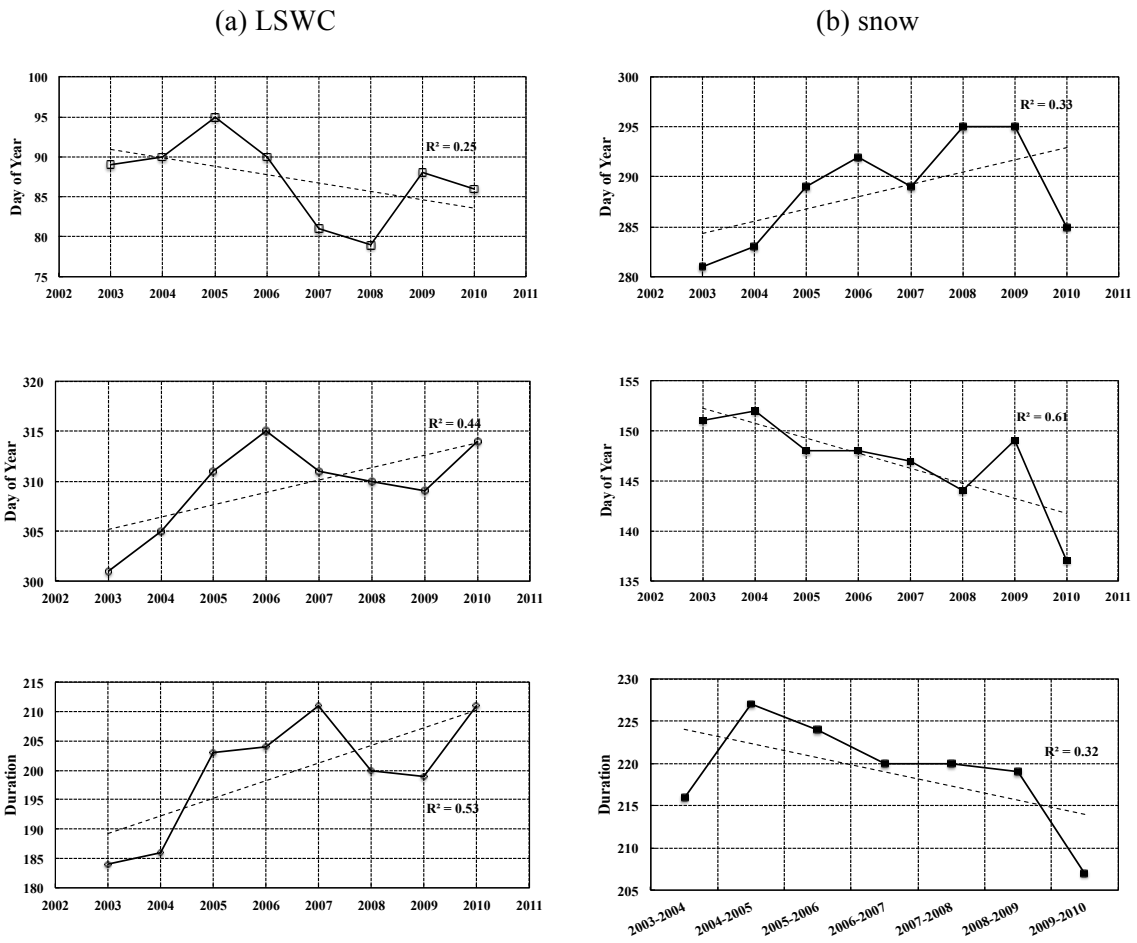

Figure 3.10: (a) and (b): Onset, offset and duration of LSWC and snow by A definition. The order of LSWC from top to down is onset, offset and duration respectively; the order of snow from top to down is offset, onset and duration. The y-axis of duration is number of days.

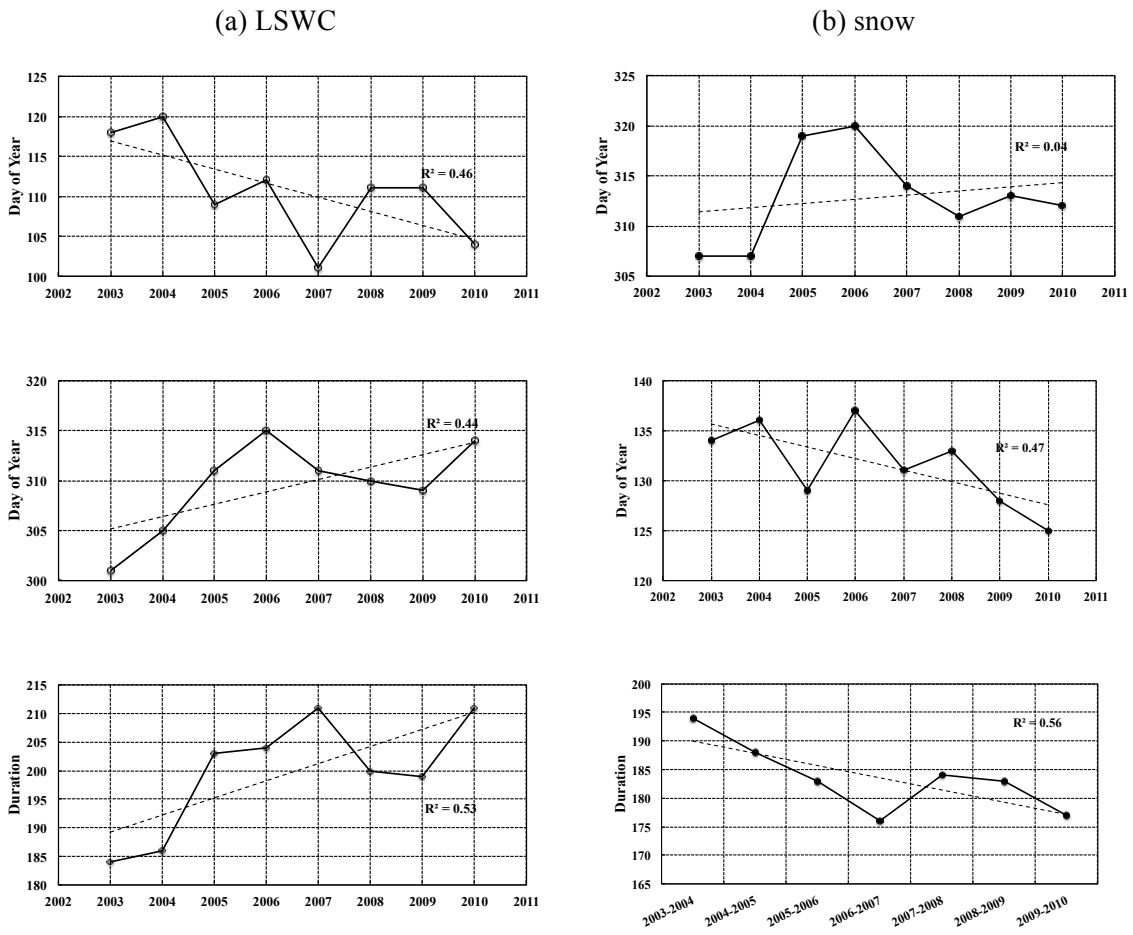

Figure 3.11: (a) and (b): Onset, offset and duration of LSWC and snow by HM definition. The order of LSWC from top to down is onset, offset and duration respectively; the order of snow from top to down is offset, onset and duration. The y-axis of duration is number of days.

3.2.2 LSWC with methane emissions and concentration

Table 3.4 shows the Pearson's correlation coefficient (r) between LSWC, modeled methane emissions (Chapter 4) and atmospheric methane concentration. All of them show good correlation (> 0.8), especially CH4_ndvi has better correlation with LSWC than others. It means variation of LSWC could directly impact vegetation growth. At the last column in Table 3.4 is Pearson's correlation coefficient (r) between LSWC and SCIAMACHY concentration data. The values show good correlations (> 0.6), but a bit lower than that observed with model estimations. A possible explanation is that atmospheric concentration methane is affected by many kinds of impact factors, not only water condition.

Table 3.4: the Pearson's correlation (r) between LSWC, methane estimations and concentration.

	LSWC & CH4_lst	LSWC & CH4_ndvi	LSWC & CH4_Ndl	LSWC & SCIAMACHY
2003	0.877	0.911	0.895	0.819
2004	0.863	0.901	0.881	0.677
2005	0.857	0.893	0.875	0.745
2006	0.836	0.885	0.854	0.682
2007	0.856	0.900	0.874	0.762
2008	0.832	0.877	0.851	0.721
2009	0.832	0.886	0.850	0.746
2010	0.821	0.855	0.835	0.629

3.3. Discussion and Conclusion

In this chapter, analyzed the land surface water coverage and snow coverage seasonal dynamics and its correlation with methane emissions by model estimation. The results were very positive. Under global warming environment, the snow coverage indicated early melting phenomenon and LSWC appeared rising and area extension characteristic at the same time. Accordingly, the climate warming, snow cover melting and methane emissions have interaction relationship. The warming temperature caused huge amount of upper permafrost melting and make active layer thicker and thicker. Iijima et al. [37] found, reduction in ground freezing due to changes in hydrothermal properties within the active layer and upper part of permafrost in eastern Siberia. Changes in snow cover conditions have been described as factor affecting shorter time scale variations in both active-layer thickness and soil as observed in this study.

High Pearson's correlations were showed between LSWC with methane estimations and LSWC with SCIAMACHY. The results indicate water condition is a crucial factor that will affect methane emission and atmospheric concentration. It also emphasizes the interaction effect of climate change and greenhouse effect.

Chapter 4

BIO-GEOPHYSICAL MODELING USING MODIS DATA

4.1. Review of literature

There are many researches focused on methane emission changes associate with land surface temperature and water condition. Zhuang et al. [30] used the Terrestrial Ecosystem Model (TEM) to estimate how rates of methane emissions in high latitude soils of the northern hemisphere had changed over the past century in response to climate change. They found Russia, Canada and Alaska are the major methane regional sources to the atmosphere and especially Russia responsible for 64% of their estimation results. They also suggested future global warming will enhance methane emission from the Pan-Arctic region. They estimated that average net methane emissions increased by 0.08Tg per year over the 20th century. Christensen et al. [31] report the temperature sensitivity of the methane emissions showed a suggestion about feedback mechanism on climate change.

According Anisimov modeling [7], by mid-21st century the annual emission of methane from Russian permafrost regions may increase by 6–8 Mt. If other sinks and sources of methane remain unchanged, the atmospheric methane increase by approximately 100 Mt and lead to 0.012℃ global temperature rise. The 22.2 Mt of methane emission comes from West Siberia compare with it in Russian northern wetlands around 24-33 Mt and it may increase by 25% by the mid 21st century.

Dramatic changes in the distribution of permafrost and vegetation caused by climate warming observed recent decades. Christensen et al. [33] reported the changes of permafrost and vegetation associated with increases in methane emissions

in a range of 22-66% over the period 1970 to 2000. A model simulation by Cao et al. [32] shows estimation of global emission was 145 Tg per year, of which 92 Tg per year came from natural wetlands in high latitude wetland area. They also found a 19% emission increase under a uniform temperature increase 2℃. But when increases in both temperature (by 2℃) and precipitation (by 10%) the methane emission from northern wetlands would increase by 21%. In Nakano et al. result [18], the methane emission from wet (waterlogged) sites is higher than that from dry (moist, mesic) sites. All above scientific results indicate every physical parameter such as surface temperature, soil, vegetation and water condition have interaction with methane emission increasing.

4.2. Bio-geophysical model derived from NDVI and LST

4.2.1 Mechanism of methane production in anaerobic soil

Methane from anaerobic soil has three ways to go into the atmosphere: diffusion, ebullition and plant-mediate transport. Figure 4.1 shows the mechanism of methane procedure in anaerobic soil (active layer). In growing season, climate warmed up and soil organic matter (SOM) is decomposed by a sequence of microbial processes to methane under anaerobic conditions. The methane was released to the atmosphere by diffusion and ebullition. Furthermore, vegetation is another important factor for methane except temperature. It occupied not only in transport of methane but also in microbial processes [9]. Thus temperature and vegetation condition are crucial for methane production and emission. Increasing of methane in the atmosphere will caused surface temperature increasing then make active layer deepens. As a result, more permafrost was thawing and more methane emitted into the atmosphere.

4.2.2 NDVI and LST from MODIS data

In this study, used Normalized Difference Vegetation Index (NDVI) and Land Surface Temperature (LST) to derive a biophysical inference model to estimate methane emission by MODIS.

1. NDVI is an index of plant greenness; it is an estimate of the photosynthetically absorbed radiation over the land surfaces, in other word, gives a measure of the vegetation cover on the earth. Vegetation tends to absorb strongly the red wavelengths (550-700 nm) of sunlight and high reflect in the near-infrared (NIR) wavelengths (730-1000 nm).

$$\mathrm{NDVI} = \frac{\mathrm{NIR} - \mathrm{VIS}}{\mathrm{NIR} + \mathrm{VIS}} \qquad (4.1)$$

From Equation 4.1 we can know, if there is much more reflected radiation in NIR wavelengths than in red wavelengths (visible wavelength, VIS), then in that pixel imply the vegetation is healthy and density. If there is very little difference in the intensity of VIS and NIR wavelengths reflected, then the vegetation is probably unhealthy or sparse or consists of shrubland and tundra.

The MODIS NDVI complements NOAA AVHRR products and provides continuity for time series historical applications. Global MODIS vegetation indices are designed to provide consistent spatial and temporal comparisons of vegetation conditions. NDVI itself varies between -1.0 and +1.0, it derived from infrared and red spectral reflectance ratio.

The MOD13A2 and MOD13A3 at 1km spatial resolution products used in this study. Global MOD13A2 are provided every 16 days and MOD13A3 are provided monthly. Both of them are in the Sinusoidal projection.

2. LST data used MOD11C1, abbreviation of MODIS/Terra V4 LST/E L3 Global CMG (climate modeling grid). It includes daytime and nighttime product at around 4km spatial resolution. But only daytime product used in this study.

4.2.3 Bio-geophysical model

Depend on analyzing the relationship between specific point of methane emission results [20 and 34] and corresponding date of NDVI and LST, created several linear relationships to compare. As a result, one couple of linear correlation was decided for methane emission estimation. Figure 4.2 shows the flowchart of methane emission estimation in this chapter.

1. Figure 4.3 shows the linear correlation between methane emissions [34] and LST (MODIS). In Wille et al. [34] study, the methane estimations focused on the date from July 19th to October 22nd in 2003 and June 1st to July 21st in 2004. That means they did methane measurement only in summer season. Therefore, the figure shows increasing linear trend.

Figure 4.4 shows the linear correlation between methane emissions [34] and NDVI (MODIS). For convenience to processing data the NDVI multiplied by 100 in this study. Likewise, this figure shows increasing trend as well.

According the methane estimation in referenced paper, combine with Figure 4.3 and Figure 4.4, two models (4.2) and (4.3) were derived. These two used for first step of methane estimation in this study at a point in RespublikaSakha (72.37°N, 126.50°E), Russia.

$$\mathbf{YCH4_{lst} = 0.4181 \times LST + 37.102} \qquad (\mathbf{4.2})$$

$$\mathbf{YCH4_{ndvi} = 0.1505 \times NDVI + 33.371} \qquad (\mathbf{4.3})$$

Where $YCH4_{lst}$= CH_4 emission in LST function (mg $m^{-2}day^{-1}$); $YCH4_{ndvi}$ = CH_4 emission in NDVI function (mg $m^{-2}day^{-1}$);

2. When land surface temperature goes to minus the ground will frozen and there is no methane emission. Therefore in Figure 4.3 the parts of methane emission correspond to negative LST should be neglected. In a similar way, there are some emissions occurred where NDVI around 0 in Figure 4.4. If only consider of methane emission in growing season, the emission values should not be considered when NDVI smaller than or equal to zero.

The models' thresholds depend on the results of CH_4 emission [20 and 34], NDVI and LST. Figure 4.5 indicates the changing characteristics of NDVI and LST value, which corresponding to the methane emission [34] date in 2003. It was found that, vegetation index will go down significantly and tends to zero when temperature equal or lower than 0, and vegetation index was around 0.4 at a same time. It means 0.4 of NDVI value is a critical value of plant growing in study area. Hence, updating Equation (4.2) and (4.3) got new equations as followed (Equation (4.4) and (4.5)). In convenient named as CH4_lst and CH4_ndvi respectively hereafter.

Equation (4.4) is taking LST as impact factor to estimate methane emission. The physical meaning is methane releasing only in positive surface temperature condition. Equation (4.5) is taking NDVI as impact factor to estimate methane emission in growing season. The threshold of NDVI explained by Figure 4.5. Equation (4.6) is

based on Equation (4.4) and (4.5), considers NDVI and LST both. It used to estimate methane emission on vegetation model (Equation (4.5)) when LST higher than 0 no matter whether NDVI value higher or lower than 0.4, called CH4_Ndl hereafter. These three models used to estimate methane emissions in this study area.

$$\mathbf{YCH4_{lst}} = \begin{cases} \mathbf{0.4181 * LST + 37.102}, & \mathbf{LST > 0} \\ \mathbf{0}, & \mathbf{LST \leq 0} \end{cases} \quad (\mathbf{4.4})$$

$$\mathbf{YCH4_{ndvi}} = \begin{cases} \mathbf{0.1505 * NDVI + 33.371}, & \mathbf{NDVI \geq 40} \\ \mathbf{0}, & \mathbf{NDVI < 40} \end{cases} \quad (\mathbf{4.5})$$

$$\mathbf{YCH4_{Ndl}} = \begin{cases} \mathbf{0.1505 * NDVI + 33.371}, & \mathbf{LST > 0} \\ \mathbf{0}, & \mathbf{LST \leq 0} \end{cases} \quad (\mathbf{4.6})$$

Where $YCH4_{lst}$= CH_4 emission in LST function (mg $m^{-2}day^{-1}$); $YCH4_{ndvi}$ = CH_4 emission in NDVI function (mg $m^{-2}day^{-1}$); $YCH4_{Ndl}$ = CH_4 emission, combine LST and NDVI function (mg $m^{-2}day^{-1}$), NDVI = original NDVI * 100.

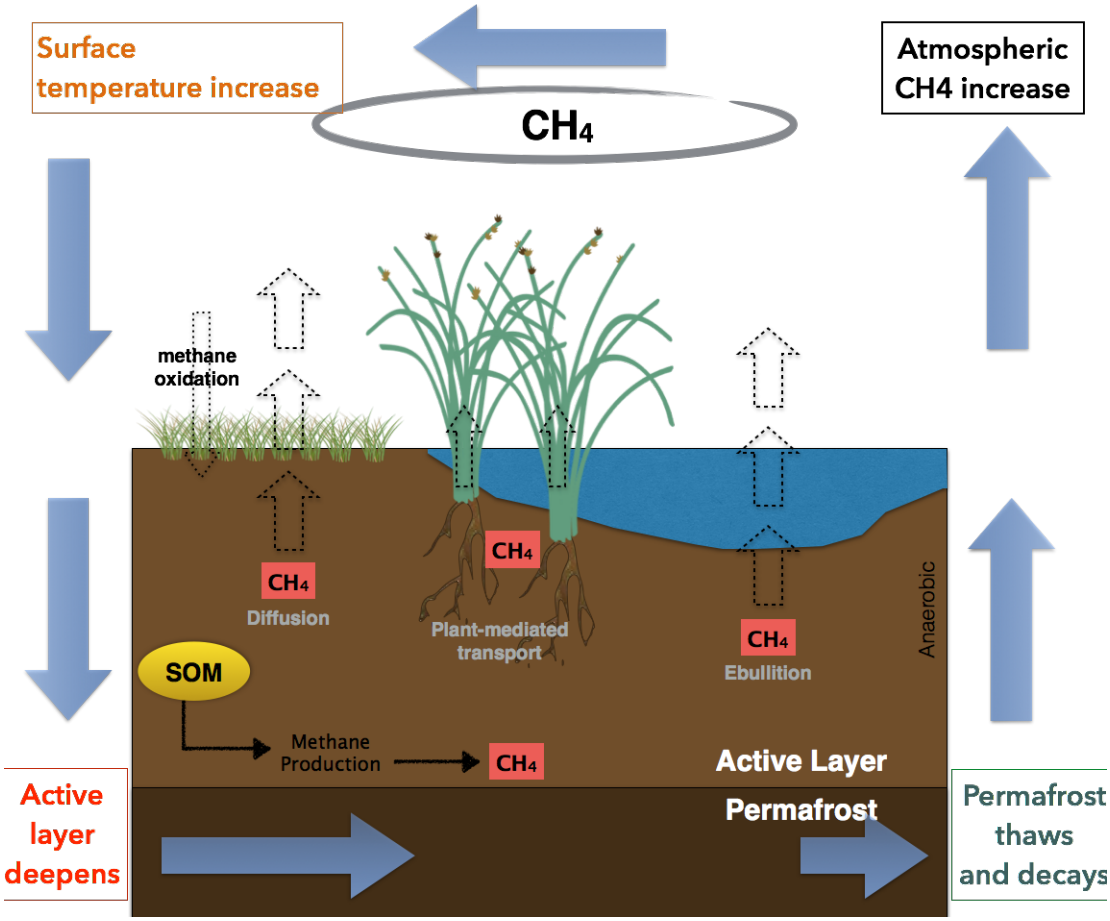

Figure 4.1: Mechanism of methane production in anaerobic soil.

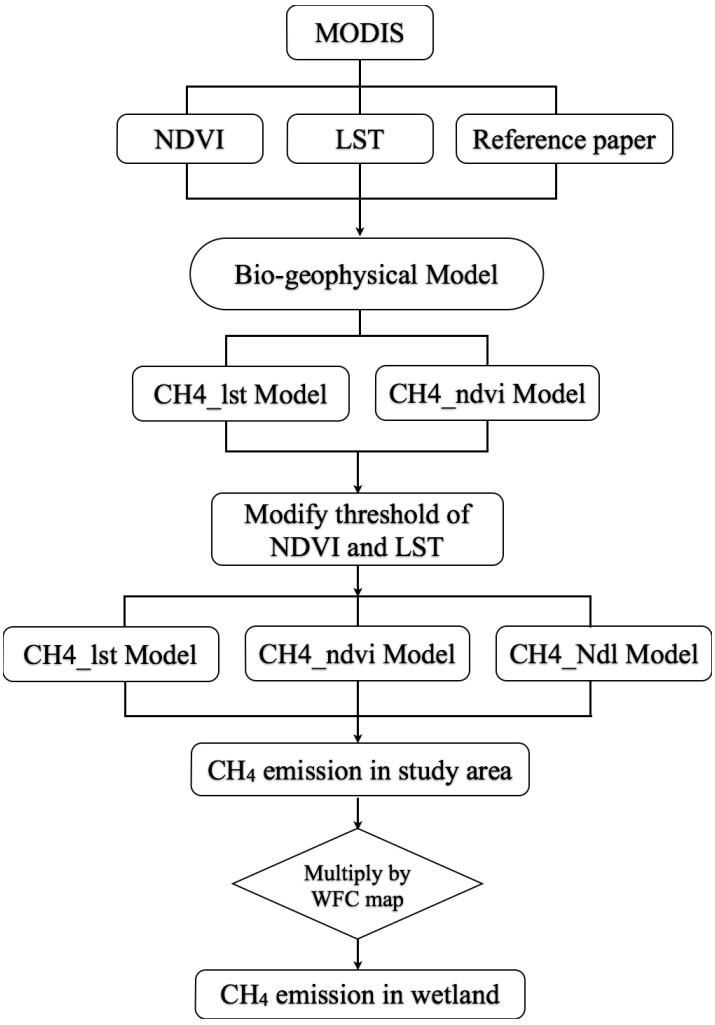

Figure 4.2: Flowchart of CH4 emission estimation in permafrost wetland area by MODIS in this study.

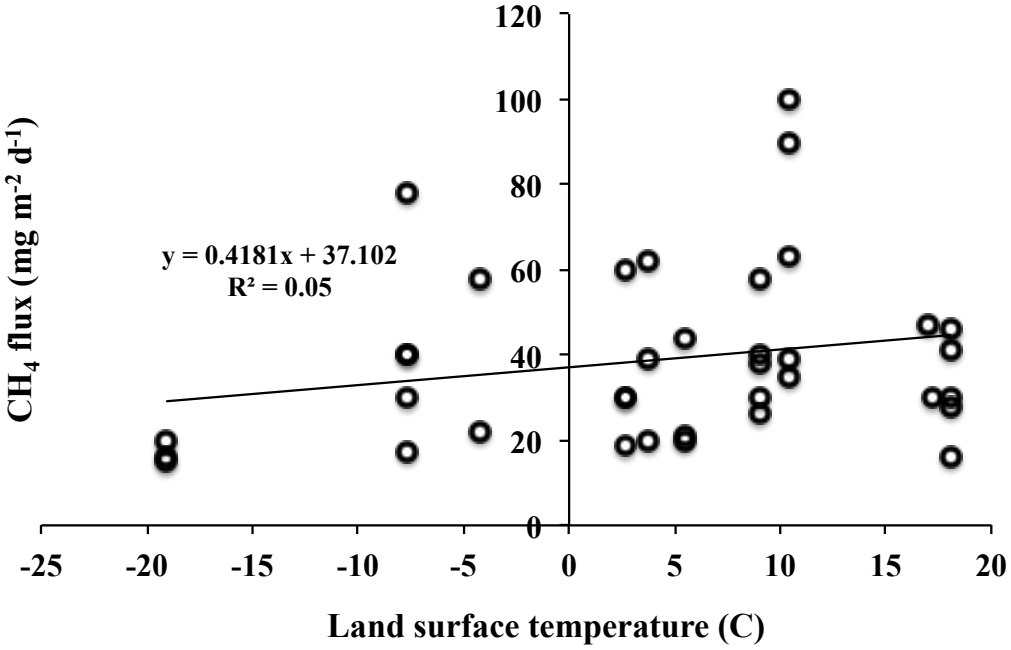

Figure 4.3: Linear correlation between CH_4 estimation [34] and LST. The estimation date [34] was in summer season. The methane emissions in the left part of y-axis are not realistic because when temperature goes to minus the ground will freeze and no methane emissions.

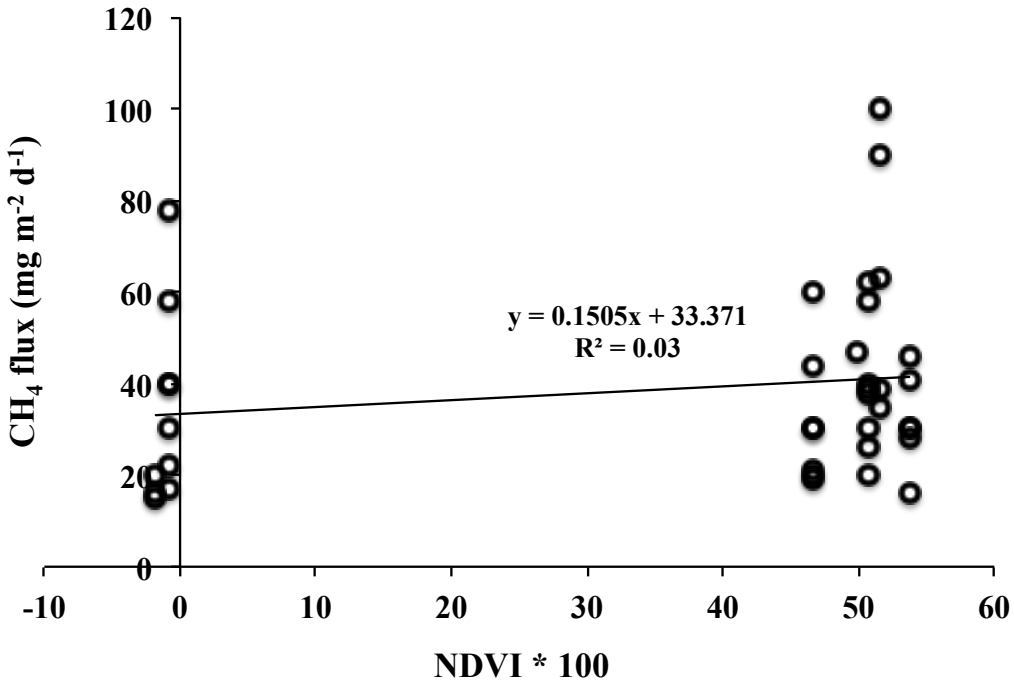

Figure 4.4: Linear correlation between CH4 estimation [34] and NDVI. There are some emissions occurred where NDVI around 0. The estimation date [34] was in summer season. If only consider the emissions in growing season, the values should not be considered where less than or equal to NDIV.

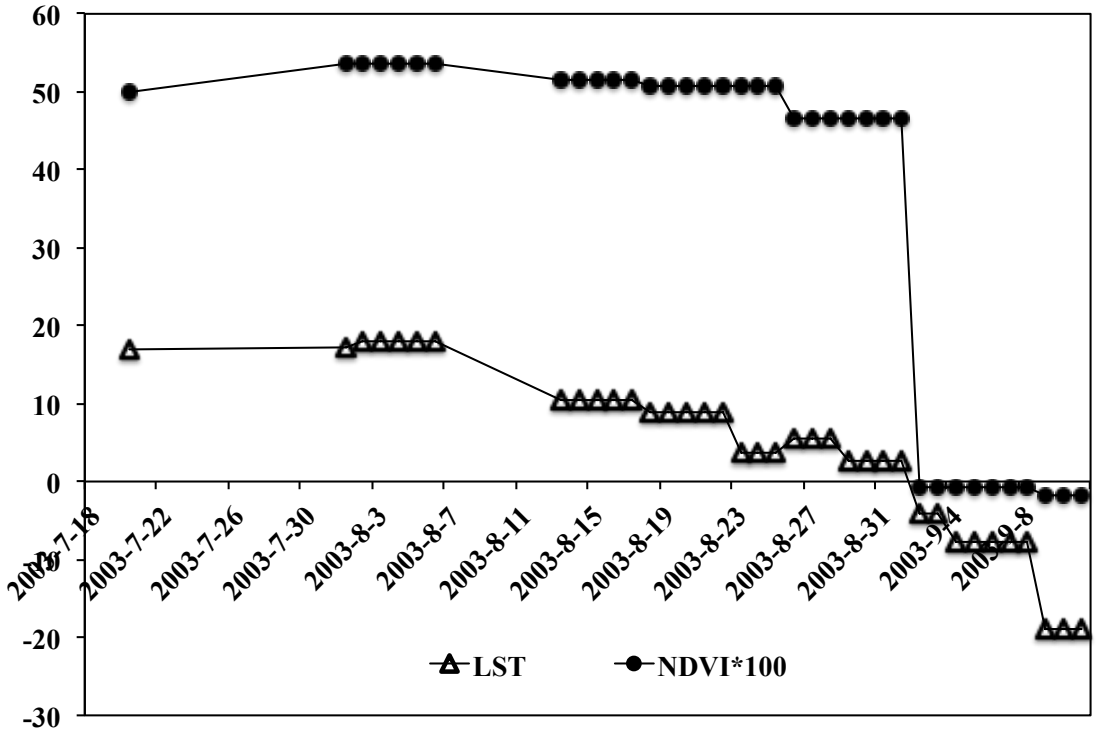

Figure 4.5: The changing characteristics of NDVI and LST value, which corresponding to the methane emission [34] date in 2003. When LST goes to minus in early winter, the vegetation will die and the ground will frozen. At the same time, the NDVI suddenly dropped to 0 from 40 (NDVI * 100). Indicate a critical value of vegetation index and ground frozen.

4.3. Methane estimation in wetland

4.3.1 Methane estimation in RespublikaSakha

The study site is located in Lena River Delta (72°~73.8°N, 122°~129.5°E) of eastern Siberia at a point 72.37°N, 126.50°E, named RespublikaSakha. Lena Delta Wildlife Reserve is in the far north of eastern Siberia, Russia. It has a total land area of 61,000 km^2, making it the largest protected area in Russia. The delta itself has a size of about 30,000 km^2, making it one of the largest of the world [35].

Figure 4.6 cited from paper Hubberten et al. [35]. The research point in this study selected exactly the same place as Wille et al. [34] and Hubberten et al. [35]. In this estimation, calculate annual emission from 2003 to 2010. In order to make sure results more realistic, some of data were abandoned.

For Equation (4.2), based on Wille et al. [34] measurement period in 2003 (~ day of year 202-297, 95 days), corresponding maximum and minimum value of LST and its fluctuation period were determinate for each year from 2003 to 2010. Figure 4.7 shows the methane emission in every fluctuation period at daily scale. For Equation (4.3) get rid of all negative NDVI values from this application, shown in Figure 4.8. The curves in Figure 4.7 and Figure 4.8 show a similar methane emission dynamics in growing season. From early June (around the 161st day), the methane emission gradually increased and the peak value concentrated in July.

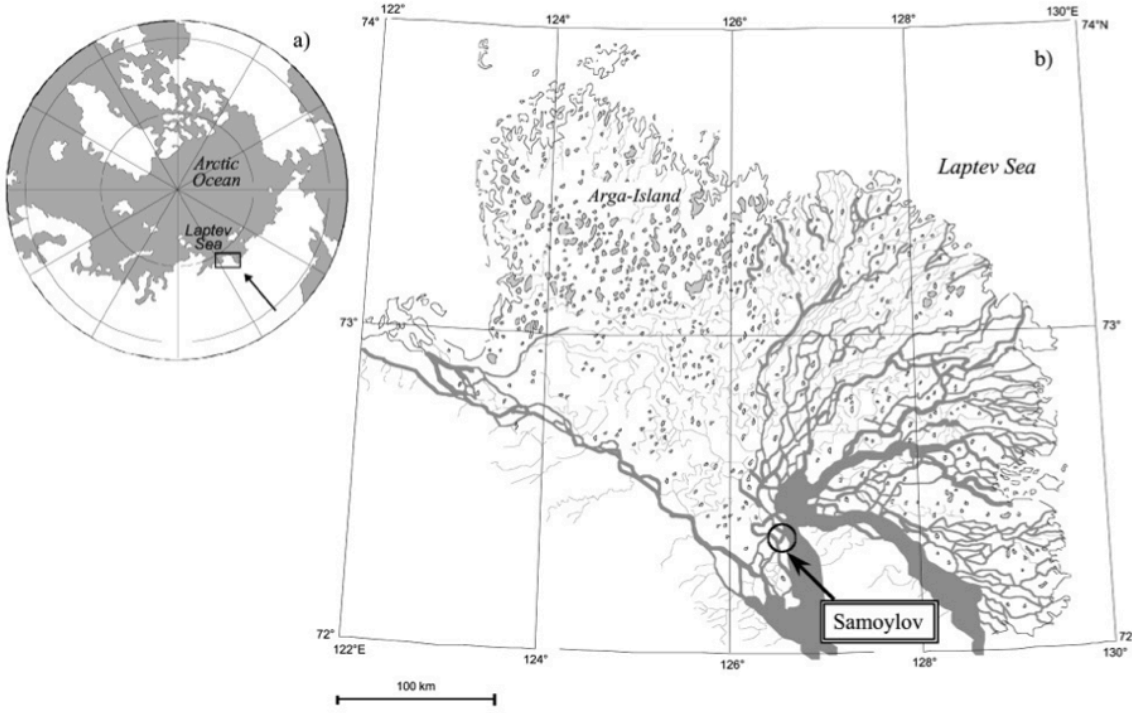

Figure 4.6: Cited from Hubberten et al. [35] study. Position of the Lena Delta region on the coast of the Laptev Sea, Arctic Ocean (a) and location of Samoylov Station on Samoylov Island (72°22'N, 126°28'E) within the active and central part of the delta (b).

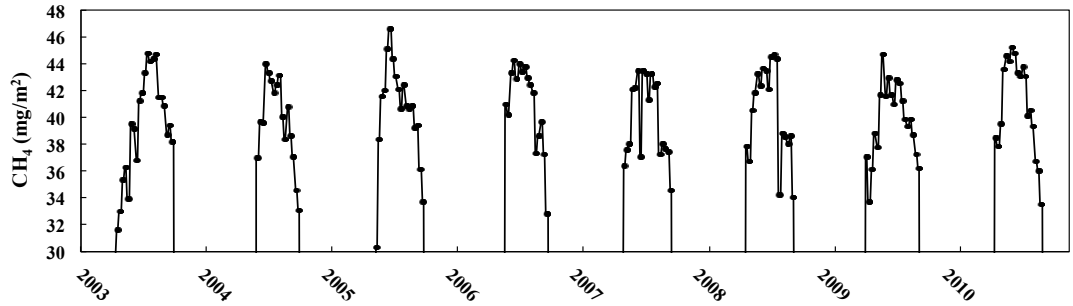

Figure 4.7: Methane estimation from Equation (3.2) from 2003 to 2010. The estimation based on daily application. The plot focused on LST maximum and minimum fluctuation period determined by Wille et al. [34] measurement time.

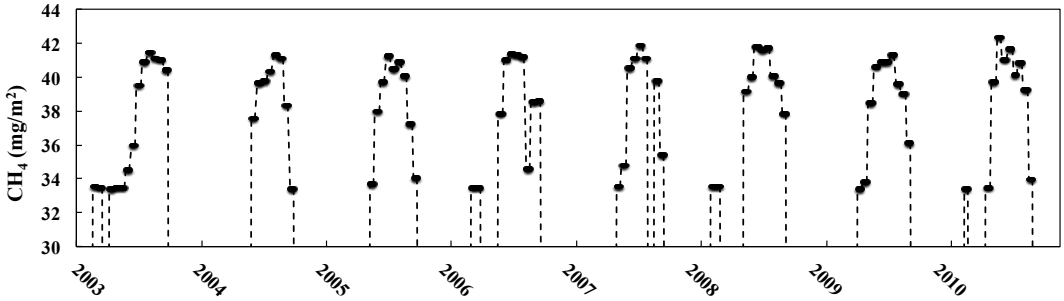

Figure 4.8: Methane estimation from Equation (3.3) from 2003 to 2010. The estimation based on 16-days application. The plot focused on positive NDVI value.

Table 4.1: Statistic value of CH_4 emission from 2003 to 2011.

Year		2003	2004	2005	2006	2007	2008	2009	2010	2011	Average ($mg/m^2/yr$)
CH4_lst Eq. (3.2)	Emission ($mg/m^2/yr$)	1345.68	949.93	1501.84	1054.15	833.16	998.95	1028.97	1097.90	1141.76	1105.81
	Duration(day)	176	128	144	128	144	144	160	141	161	
CH4_ndvi Eq. (3.3)	Emission ($mg/m^2/yr$)	2010.26	1975.08	1955.26	1990.8	2125.68	2101.83	1971.37	2257.08	2304.57	2076.91
	Duration(day)	208	128	144	160	128	160	160	157	161	
CH_4 (*Reference value)	Emission ($mg/m^2/yr$)	1737	-	-	1458	-	-	-	-	-	-
	Duration(day)	95	-	-	70	-	-	-	-	-	-

*: [34] Christian Wille, etc. 2008, Global Change Biology (2008) 14, 1395–1408;

[20] Torsten Sachs, etc. 2010, Global Change Biology (2010) 16, 3096–3110.

In Table 4.1 the Equation (4.2) (CH4_lst) result shows 1105.81 mg $m^{-2}yr^{-1}$ in average 147 days, which is half of the Equation (4.3) (CH4_ndvi) application. CH4_ndvi has 2076.91 mg $m^{-2}yr^{-1}$ in average 156 days. This phenomenon could be explained that in early winter the land surface temperature nearly zero and appeared very stable condition and this condition could sustain around 1 month. At the same time, the vegetation almost died of old age and the soil become freezing. Result of this reason, there is a hypothesis that the methane emission still happened released from the soil because of physical mechanical effects in cold weather condition even there is no vegetation.

Compare with reference value, the result of Equation (4.3) was overestimated and from Equation (4.2) was underestimated. This could be result from two reasons: (a) the simple linear regression analysis cannot express comprehensive effects of all parameters and (b) in reference paper it has some peak values which are abnormal because of specific factors influence the model. Fortunately, there are not so much differences between estimation results and measurement data [20 and 34].

4.3.2 Methane estimation in separate land-cover

In Chapter 2, five land-cover types used to create WFC map (Figure 2.3). The WFC map consist of 110, 120, 130, 140, and 180, see Table 4.2. The three models (CH4_lst, CH4_ndvi and CH4_Ndl) applied on each of land cover type at daily scale. The result figures shown in Figure 4.8.

Figure 4.9 shows the methane emission estimation from 2001 to 2012 in separate land cover type in daily process. All three sub-figure (a), (b) and (c) indicate a similar appearance. Consider amount of methane emissions, ID 110 occupied the largest ratio. Then is ID 120, around half of ID110. ID140 and ID180 have almost similar emissions in the third. ID130 has a few contributions for methane emission in study area. Consider the methane emitting time, generally speaking ID 110 still has the longest period than others. By the way, ID140 has the nearest and sometimes even longer emission time compare with ID110. ID120 and ID180 emission days are quite closer.

Figure 4.10, Figure 4.11 and Figure 4.12 show two kinds of pie chart to indicate the contribution ratio of each land cover class by three CH4 modeling (CH4_lst, CH4_ndvi and CH4_Ndl). (a) represents averaged methane emission ratio of each class in 11 years (2001 to 2012); (b) represents mean area ratio of each class in 11

years (2001-2012). In the pie charts, around 40 ~ 50 percentage of methane emission released from ID110 and it is also have the largest distribution in study area. ID120 is in the next place, followed by ID140 and 180.

Table 4.2: Land cover type in WFC map and its description.

ID	Land cover legend description
110	Mosaic forest or shrubland (50-70%) / grassland (20-50%)
120	Mosaic grassland (50-70%) / forest or shrubland (20-50%)
130	Closed to open (>15%) (broadleaved or needleleaved, evergreen or deciduous) shrubland (<5m)
140	Closed to open (>15%) herbaceous vegetation (grassland, savannas or lichens/mosses)
180	Closed to open (>15%) grassland or woody vegetation on regularly flooded or waterlogged soil - Fresh, brackish or saline water

(a)

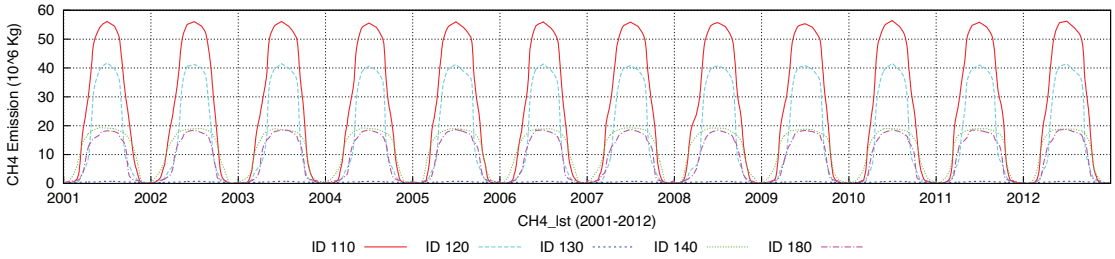

(b)

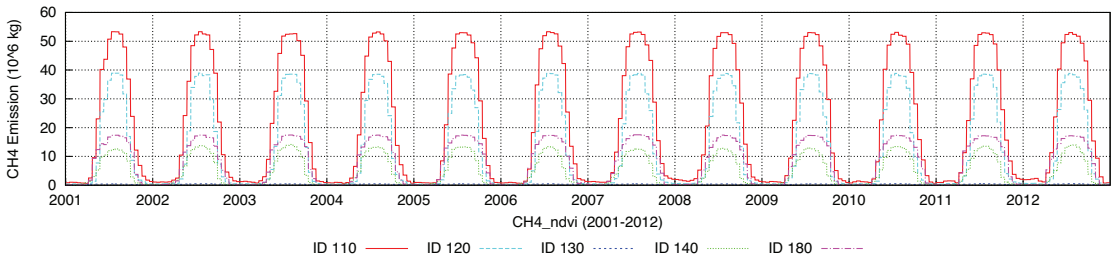

(c)

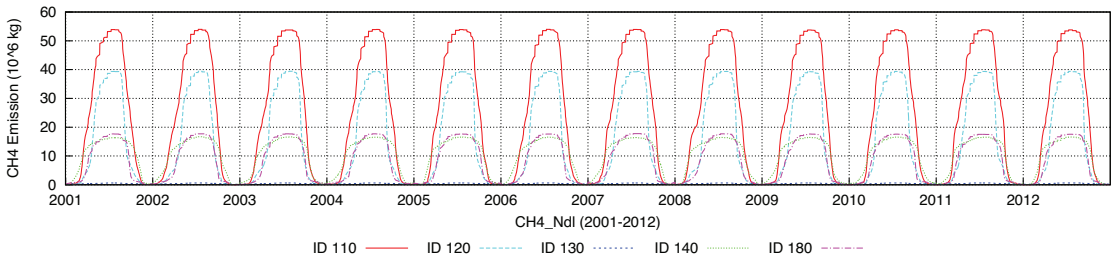

Figure 4.9: Methane emission estimation from 2001 to 2012 in separate land cover type in daily scale. (a), (b) and (c) are the amount of methane emission from CH4_lst, CH4_ndvi and CH4_Ndl model respectively.

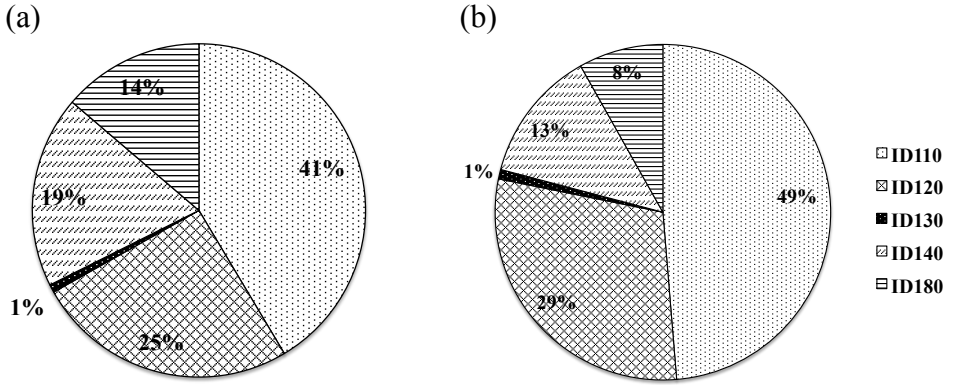

Figure 4.10: Pie chart of mean methane emission ratio (a) and mean area ratio (b) of each land cover class by CH4_lst model from 2001 to 2012.

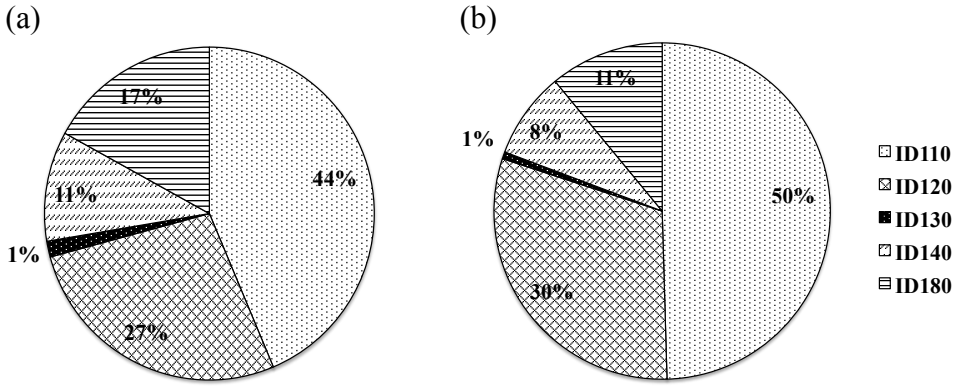

Figure 4.11: Pie chart of mean methane emission ratio (a) and mean area ratio (b) of each land cover class by CH4_ndvi model from 2001 to 2012.

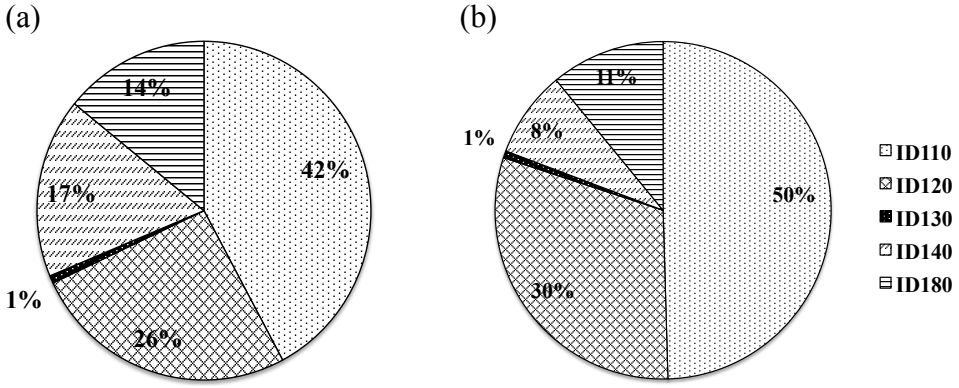

Figure 4.12: Pie chart of mean methane emission ratio (a) and mean area ratio (b) of each land cover class by CH4_ndl model from 2001 to 2012.

4.3.3 Methane estimation in all land-cover

From March the land surface temperature rises to positive value (LST > 0℃) and continue to end of September. The methane emission starts from April spread from south to north following LST becomes positive. CH4_lst (Equation (4.4)) is estimation depends on LST dynamics. When temperature is above zero, the calculation will be applied on temperature data. CH4_ndvi (Equation (4.5)) is estimation on the basis of vegetation growing characteristic. When NDVI is equal or greater than 0.4, the equation will be applied on vegetation data. CH4_Ndl (Equation (4.6)) is estimation synthesizes LST and NDVI both. The calculation will be applied on vegetation data when corresponding LST pixel value greater than zero. All three models applied on study area in regional scale.

Figure 4.13 illustrates total methane emission from 2003 to 2010. The estimation based on daily process and shows in monthly basis. The three curves (pink, green and blue) represent CH4_lst, CH4_ndvi and CH4_Ndl modeling respectively. There are good agreements in all estimations. All peak value happened in July, formed "one-peak" pattern in three estimations. But green (CH4_ndvi) line explored a delay phenomenon on onset time compare with others, while offset time fitted very well. It probably because plant growing usually starts when temperature risen to specified value.

To understand whether methane emission variation greatly affected by climate change, there are two factors considered. One is whether methane emission increased or not, another is how emission time and duration changed. To know methane emission increased or not, the emitting area and amount can provide evidences.

1. Figure 4.14 and Figure 4.15 show methane emission map modeled by CH4_lst. They are derived from CH4_lst model on LST daily image processing. Figure

4.16 and Figure 4.17 are from CH4_Ndl model, which consider LST and NDVI both. In this evaluation because of NDVI data has 16 days time resolution, therefore when apply CH4_Ndl we used same NDVI image in every 16 day correspondingly. Figure 4.18 and Figure 4.19 are derived from CH4_ndvi model by monthly NDVI image (MOD13A3), because of 16 days NDVI images difficult to represent monthly variations. The values in color table from Figure 4.14 to Figure 4.17 are on behalf of monthly total emission (10^{-4}mg m^{-2}) and color table of Figure 4.18 and Figure 4.19 represent averaged monthly emission (10^{-4}mg m^{-2}).

Figure 4.20 and Figure 4.21 show the comparison map of methane emission in April and October in 2003 and 2010 by the three modeling. Figure 4.20 indicates the methane emitting area in April extend in 2010 (right column) than in 2003 (left column). It means during several years methane emission starts earlier in 2010 than in 2003. In summer growing season continuous CH_4 emissions has been increased till temperature goes minus. Figure 4.21 shows the methane emission area of October in 2003 and 2010. It shows area extension phenomenon as well as in April, implies the methane ends later and summer time last longer in past several years.

Figure 4.22 illustrates mean LST changes of April and October from 2003 to 2010. The curves show rising trends both in April and October, indicate temperature growing up gradually in past several years. Also means the climate warmer in the same month of the year, and it could be a proper reason why methane emissions starts earlier and continue much longer time (Figure 4.21).

Figure 4.23 (a), (b) and (c) show the averaged methane emission from 2003 to 2012 by CH4_lst, CH4_ndvi and CH4_Ndl model. It is clear that methane

emissions have significant increasing tendency during past decade.

Through analysis above, the methane emitting area extended and methane increased annually. In general, climate variation greatly affect to methane emissions.

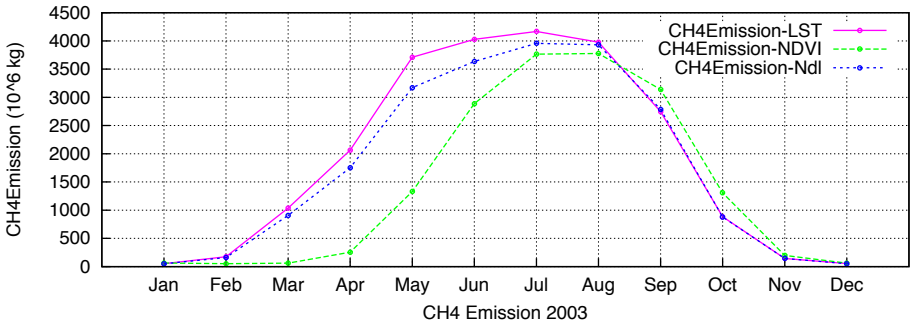
CH4Emission-LST
CH4Emission-NDVI
CH4Emission-Ndl
CH4Emission (10^6 kg)
4500
4000
3500
3000
2500
2000
1500
1000
500
0
Jan Feb Mar Apr May Jun Jul Aug Sep Oct Nov Dec
CH4 Emission 2003

(a)

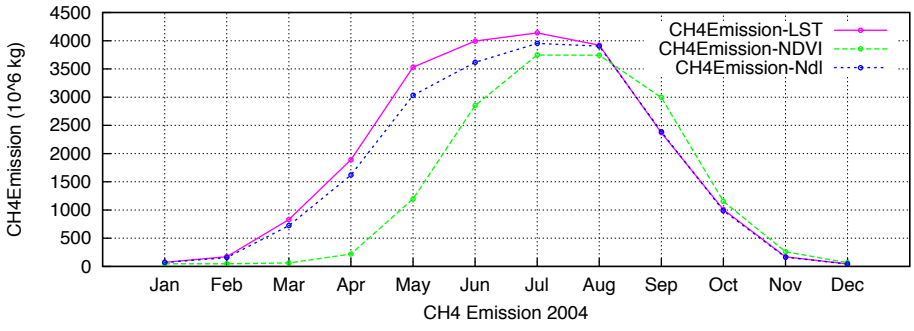
CH4Emission-LST
CH4Emission-NDVI
CH4Emission-Ndl
CH4Emission (10^6 kg)
4500
4000
3500
3000
2500
2000
1500
1000
500
0
Jan Feb Mar Apr May Jun Jul Aug Sep Oct Nov Dec
CH4 Emission 2004

(b)

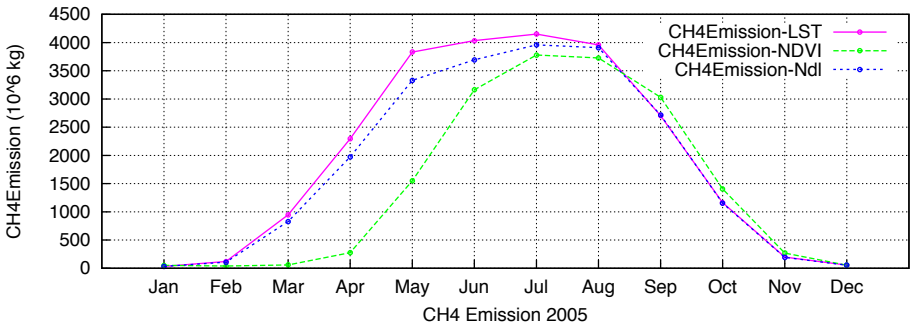
CH4Emission-LST
CH4Emission-NDVI
CH4Emission-Ndl
CH4Emission (10^6 kg)
4500
4000
3500
3000
2500
2000
1500
1000
500
0
Jan Feb Mar Apr May Jun Jul Aug Sep Oct Nov Dec
CH4 Emission 2005

(c)

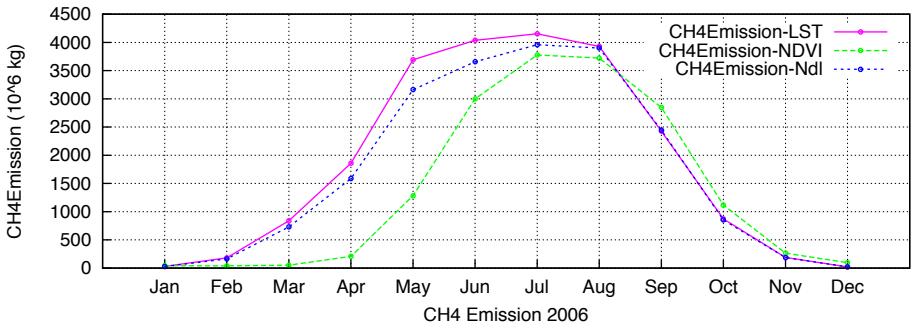
CH4Emission-LST
CH4Emission-NDVI
CH4Emission-Ndl
CH4Emission (10^6 kg)
4500
4000
3500
3000
2500
2000
1500
1000
500
0
Jan Feb Mar Apr May Jun Jul Aug Sep Oct Nov Dec
CH4 Emission 2006

(d)

(e)

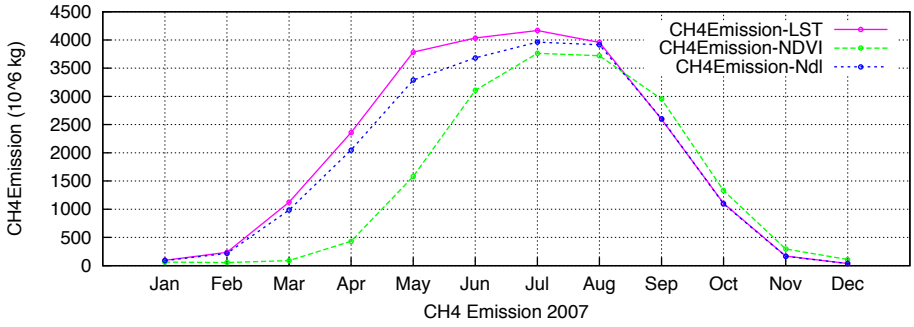

(f)

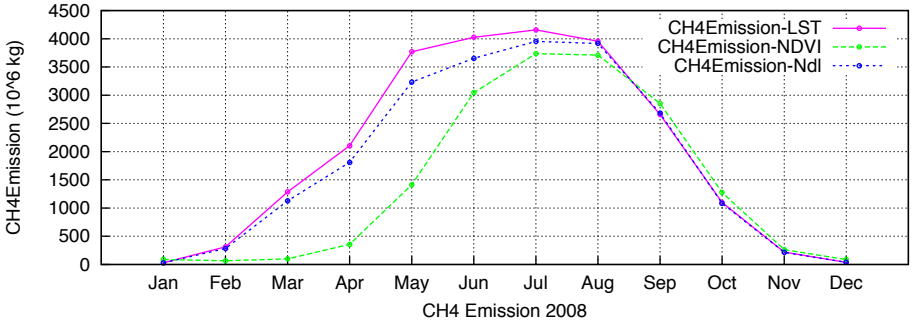

(g)

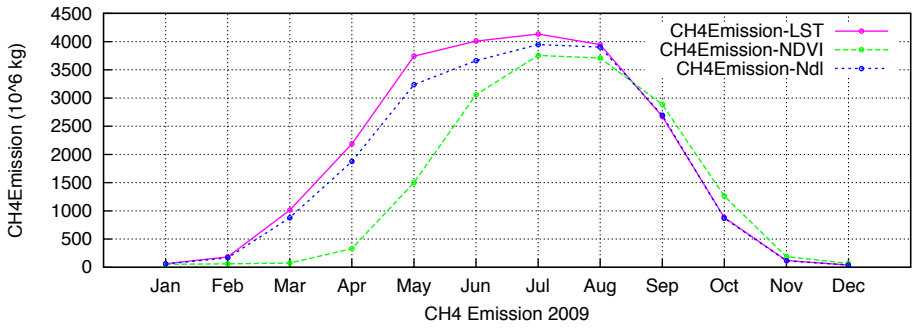

(h)

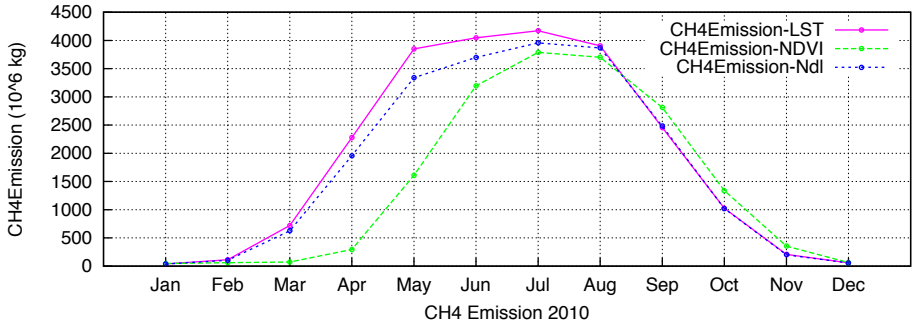

Figure 4.13: Methane emission estimations curves in each year from 2003 to 2010 ((a) ~ (h)).

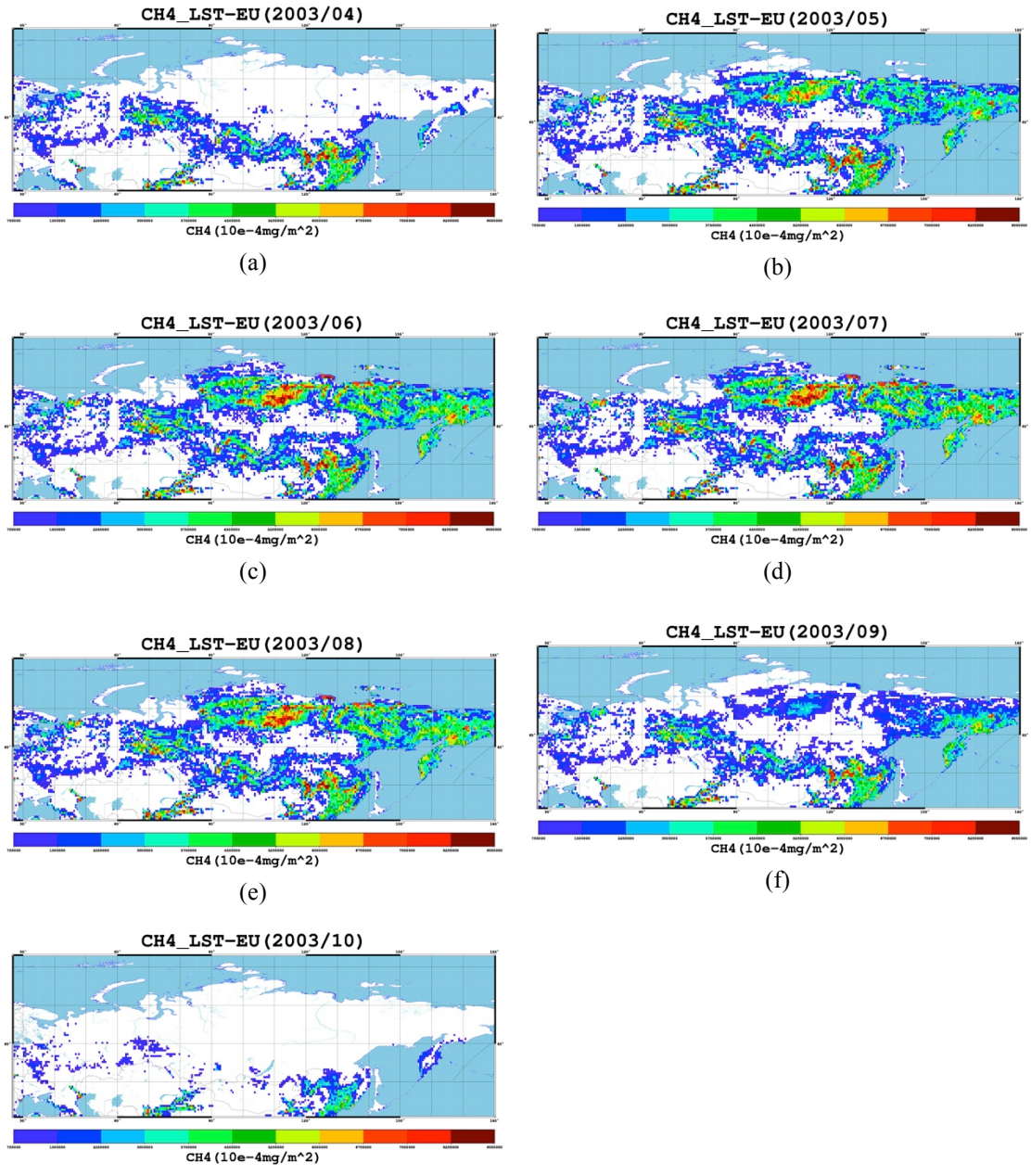

Figure 4.14: Monthly methane emission map from CH4_lst modeling from April to October ((a) ~ (g)) in 2003. Large amount of methane emissions starts from May and continue to August.

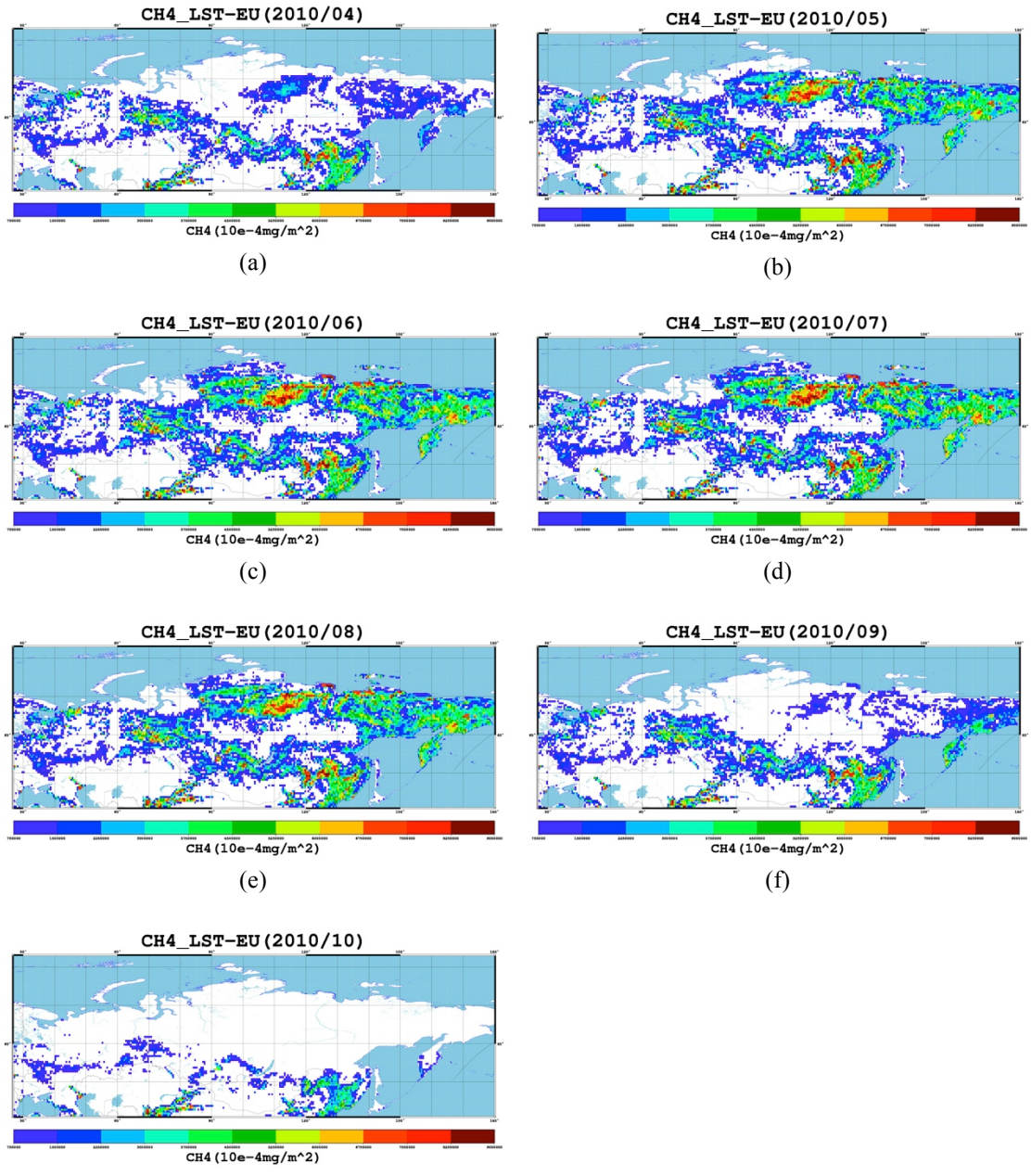

Figure 4.15: Monthly methane emission map from CH4_lst modeling from April to October ((a) ~ (g)) in 2010. Large amount of methane emissions starts from May and continue to August.

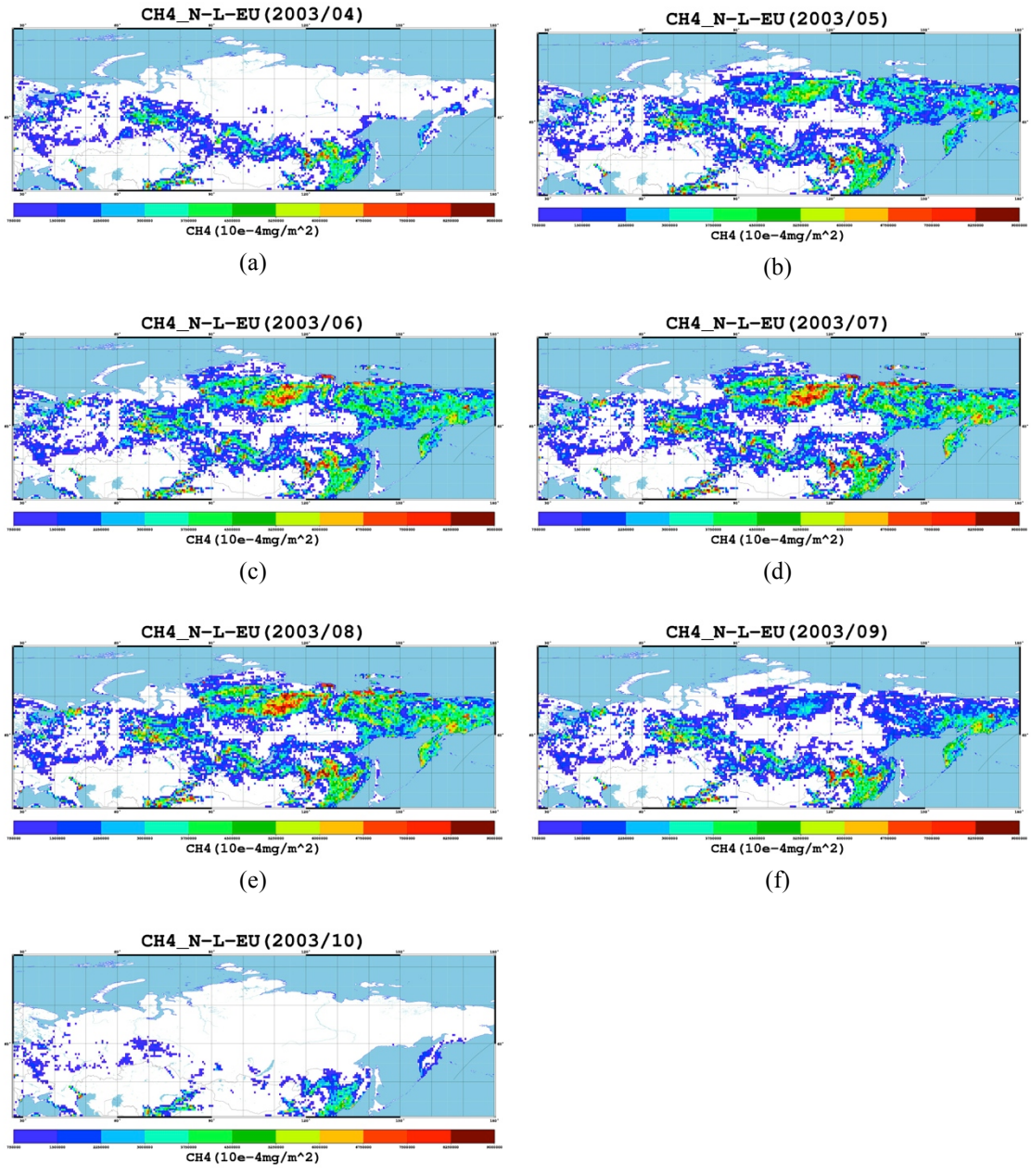

Figure 4.16: Monthly methane emission map from CH4_Ndl modeling from April to October ((a) ~ (g)) in 2003. Large amount of methane emissions starts from May and continue to August.

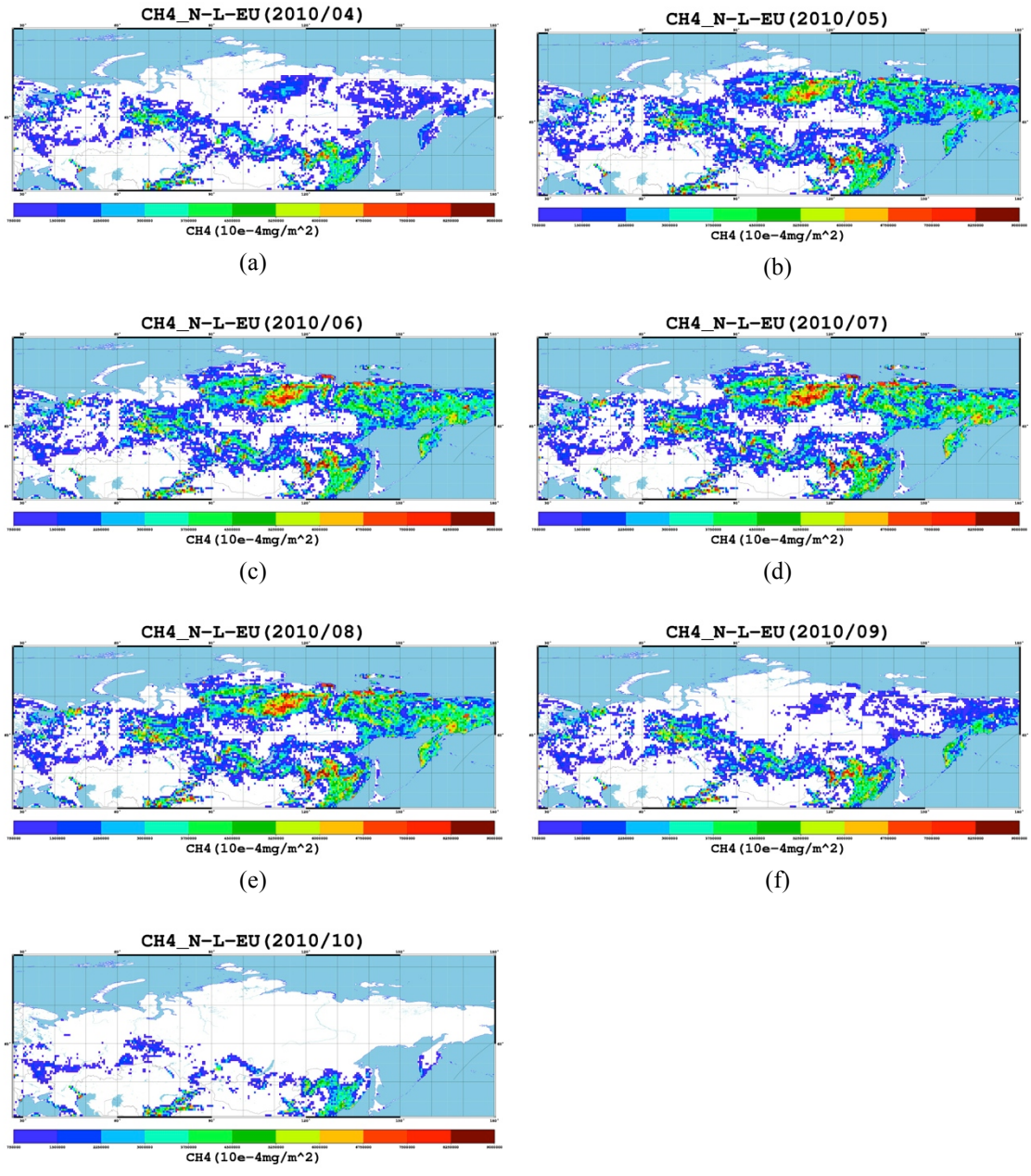

Figure 4.17: Monthly methane emission map from CH4_Ndl modeling from April to October ((a) ~ (g)) in 2010. Large amount of methane emissions starts from May and continue to August.

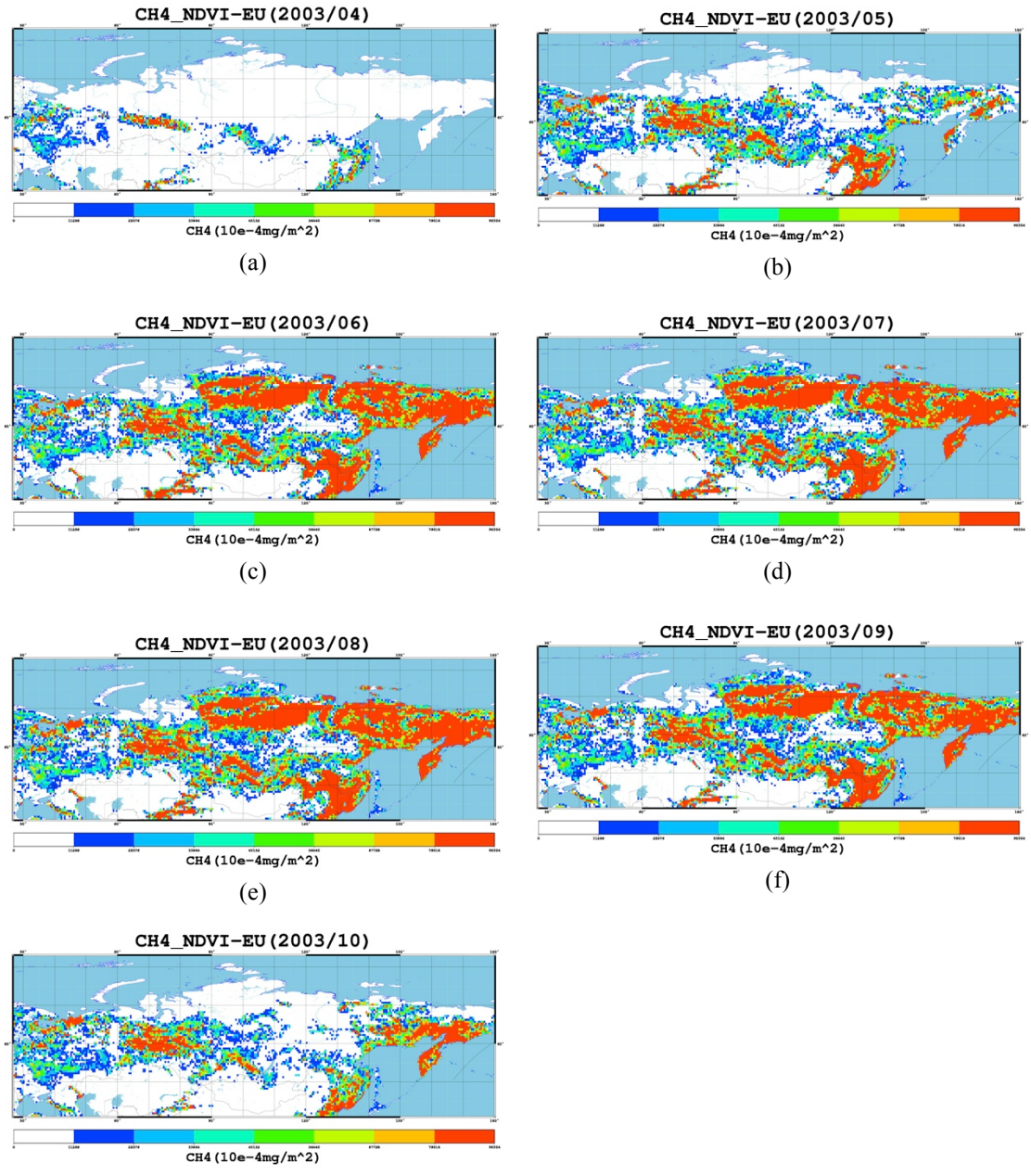

Figure 4.18: Monthly mean methane emission map from CH4_ndvi modeling from April to October ((a) ~ (g)) in 2003. Large amount of methane emissions starts from May and continue to September.

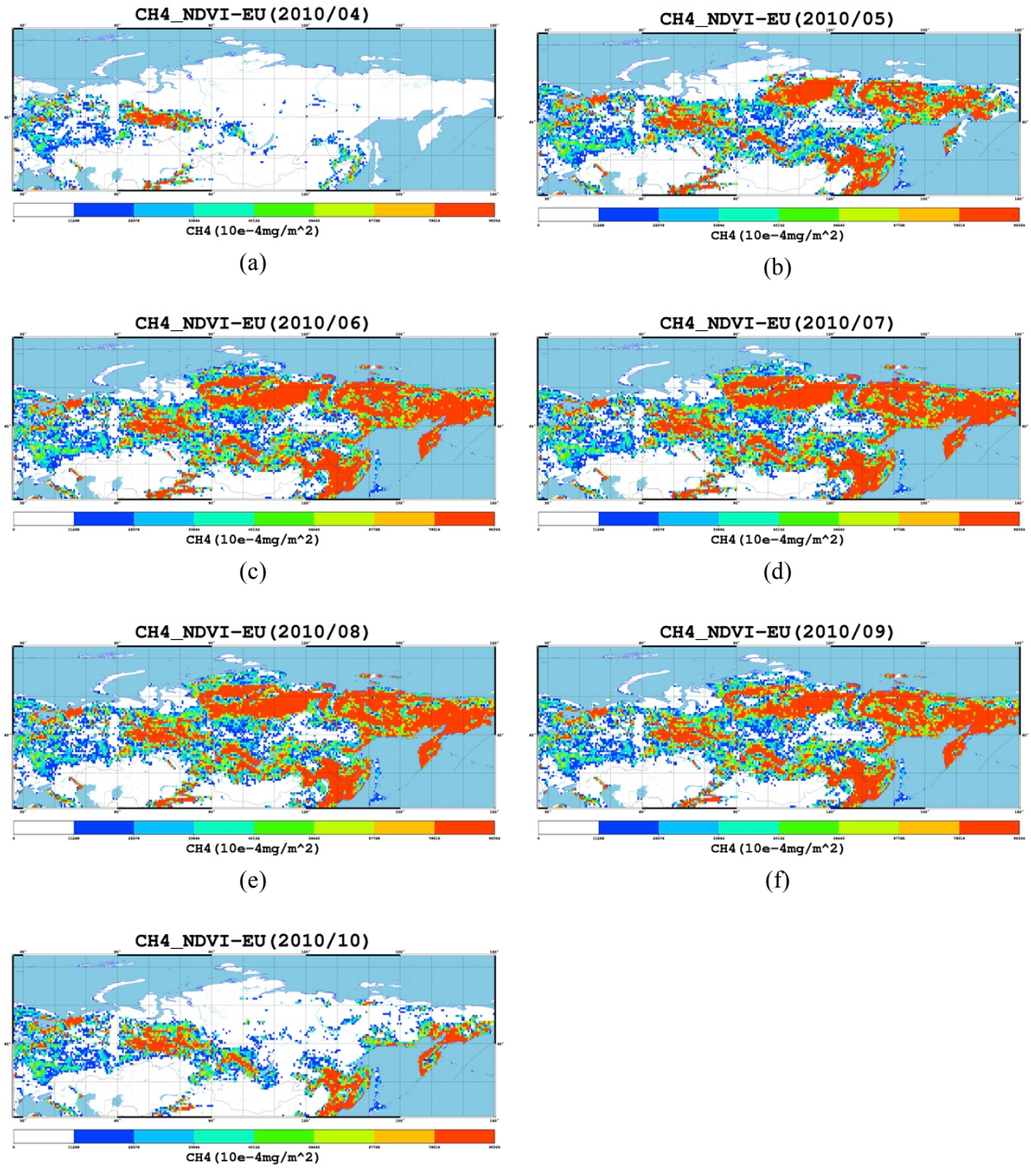

Figure 4.19: Monthly mean methane emission map from CH4_ndvi modeling from April to October ((a) ~ (g)) in 2010. Large amount of methane emissions starts from May and continue to September.

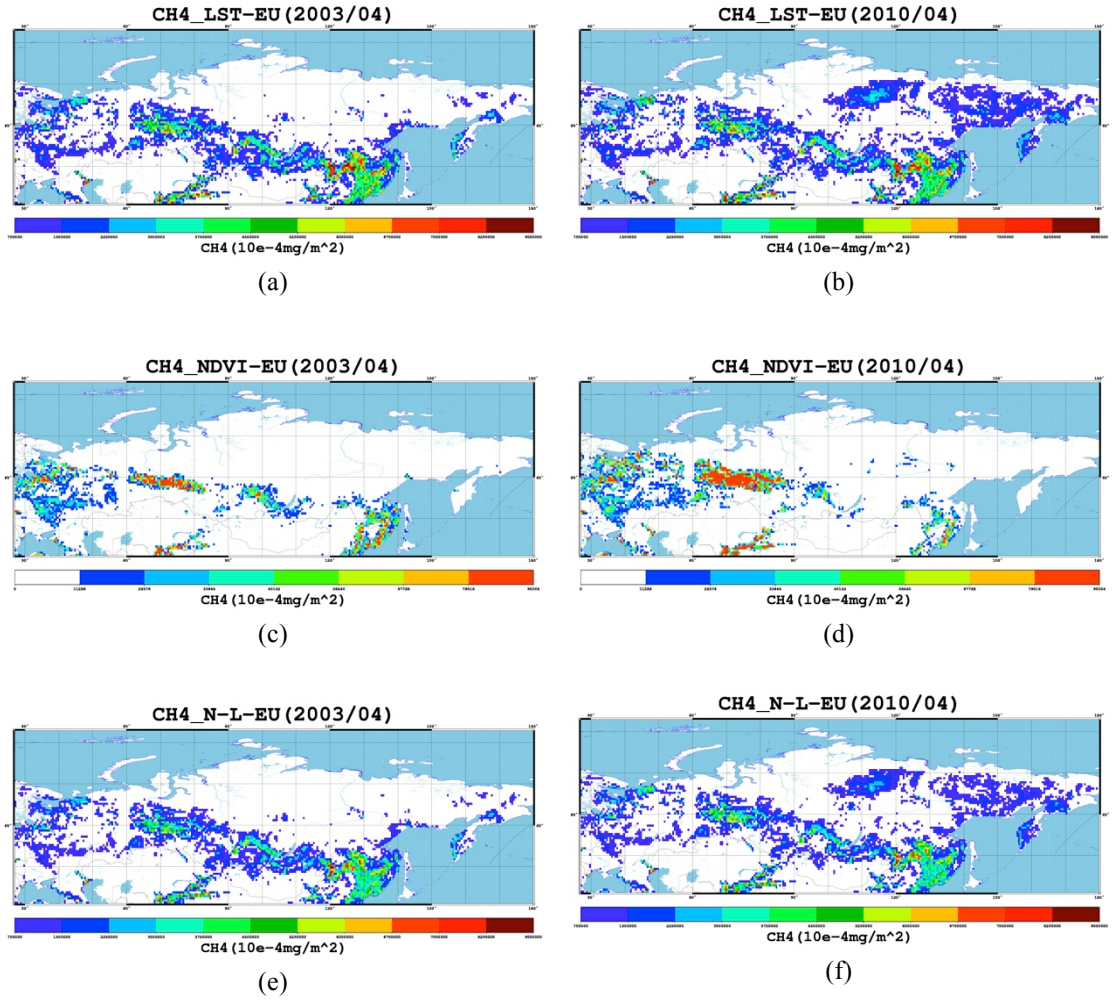

Figure 4.20: Monthly methane emission map of April in 2003 and 2010 by CH4_lst ((a) and (b)), CH4_ndvi ((c) and (d)) and CH4_Ndl ((e) and (f) modeling respectively. There are obvious area extention in 2010 compare with 2003, imply the methane starts more and more early in past several years.

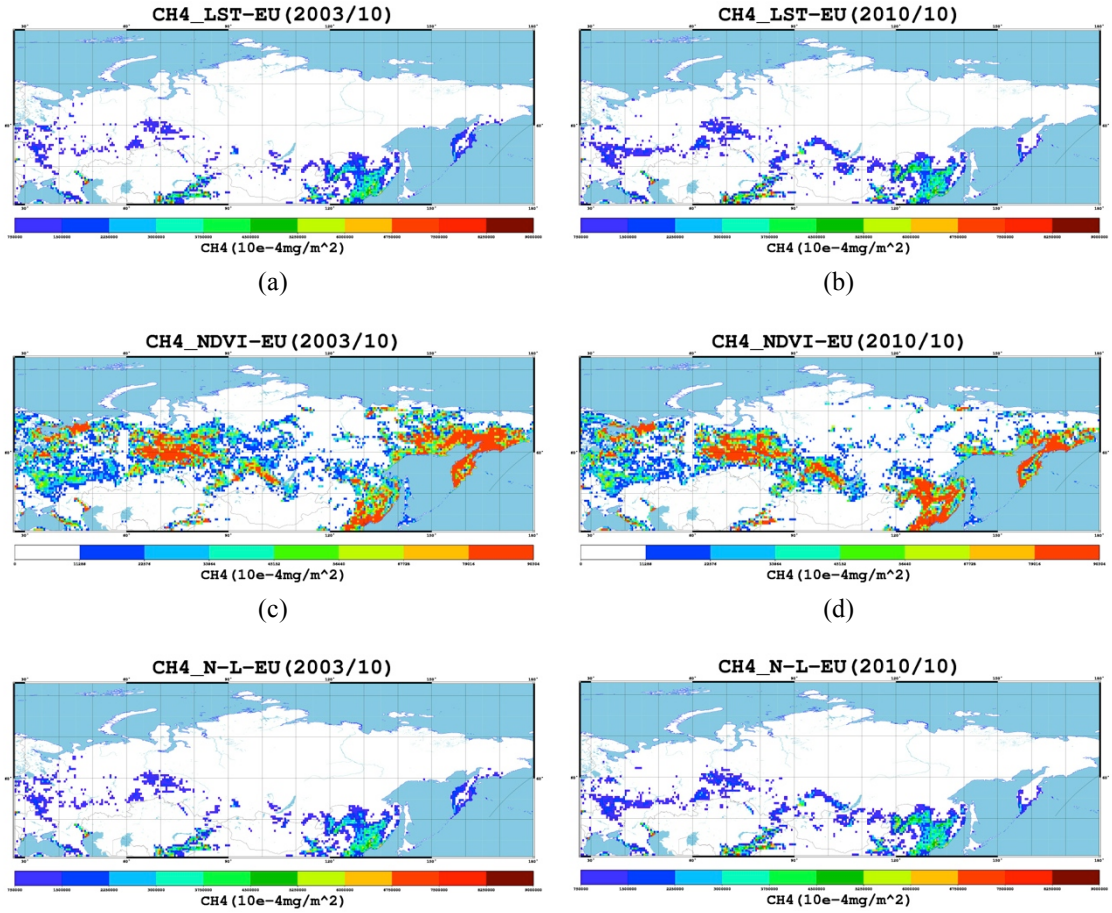

Figure 4.21: Monthly methane emission map of October in 2003 and 2010 by CH4_lst ((a) and (b)), CH4_ndvi ((c) and (d)) and CH4_Ndl ((e) and (f)) modeling respectively. There are obvious area extention in 2010 compare with 2003, imply the methane ends more and more late in past several years and winter comes later.

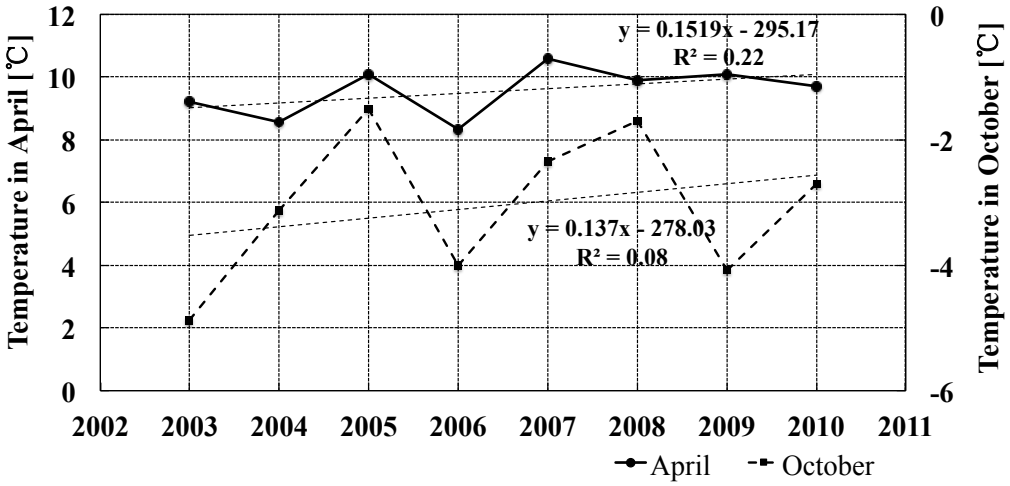

Figure 4.22: Mean LST changes of April and October from 2003 to 2010. This figure indicates rising trends in time series. It means the temperature is more and more higher in the same month of year.

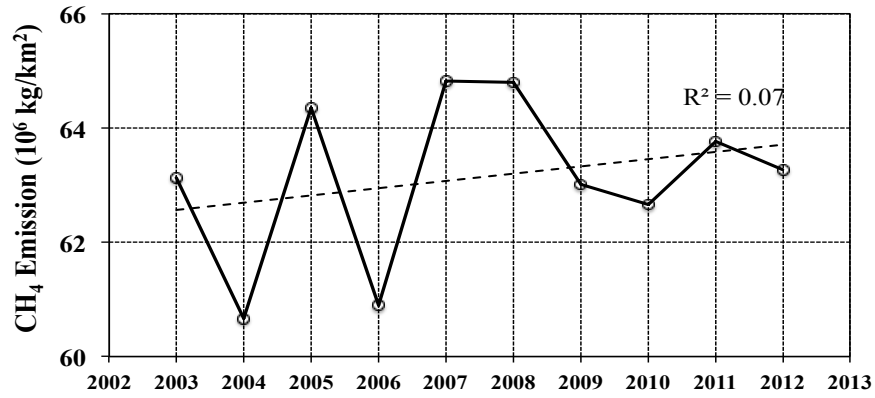

(a)

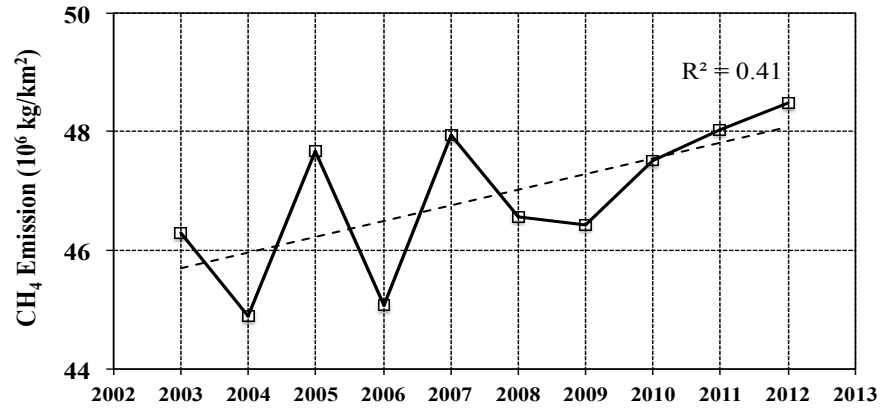

(b)

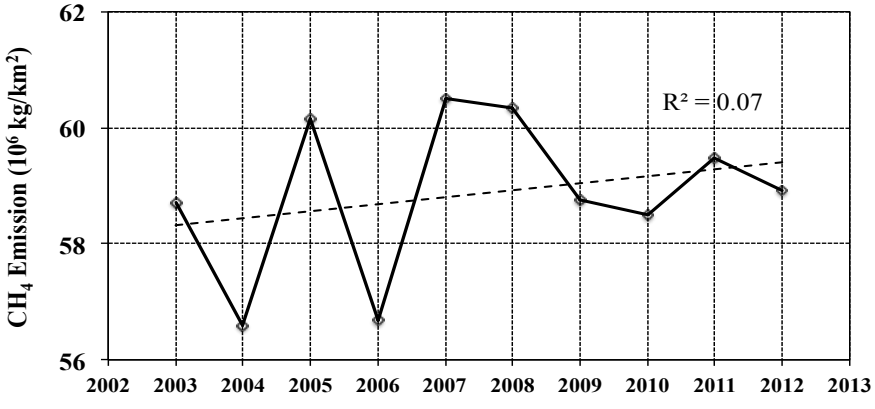

(c)

Figure 4.23: (a), (b) and (c): The averaged methane emission in study area from 2003 to 2012. Represent the result from model CH4_lst, CH4_ndvi and CH4_Ndl respectively. It is obvious that methane emissions are increasing gradually in past decade.

2. To define the methane emission time and duration, there are two kinds of definition used in this study are half of maximum (HM) and average (A). HM means use half of maximum value of total methane emission of each year to define the onset-offset date; A is using average value of total methane emission of each year to define the time and duration.

Figure 4.24 and Figure 4.26 illustrate the onset-offset and duration of methane estimations modeled by CH4_lst and CH4_Ndl in the two definitions (HM and A). The left columns (a) in solid line represent HM definition results and the right columns (b) in dashed line represent A definition results. The order from top to down is the onset, offset and duration respectively. The y axis of onset and offset is DOY, abbreviation of day of year; y axis of duration is number of days. Figure 4.25 illustrates the duration of methane estimation by CH4_ndvi model. Caused by the NDVI data used for CH4_ndvi estimation was 16-days time resolution data, cannot identify the onset and offset date in daily scale. Therefore, only durations show in that figure.

All figures (4.24, 4.25 and 4.26) indicated same changing phenomenon in onset, offset and duration. Onset means the day of emission start and offset is the day of emission end. All onset plots show decreasing trends both in HM and A, indicated emission starting date more and more early in time series; all offset plots show increasing trends both in HM and A, means emission ending date more and more late in time series. The methane continuous emitting period are in rising trends, so that emission time last much longer during past ten years. From Figure 4.24 and 4.26, it was found that the onset date is fluctuate within a range of 4/8~4/21 (DOY 98±3 ~ 111±5) and offset date is around 9/21~9/28 (DOY 264±4 ~ 271±3). Duration is fluctuate within a range of 155±6 ~ 176±2

days.

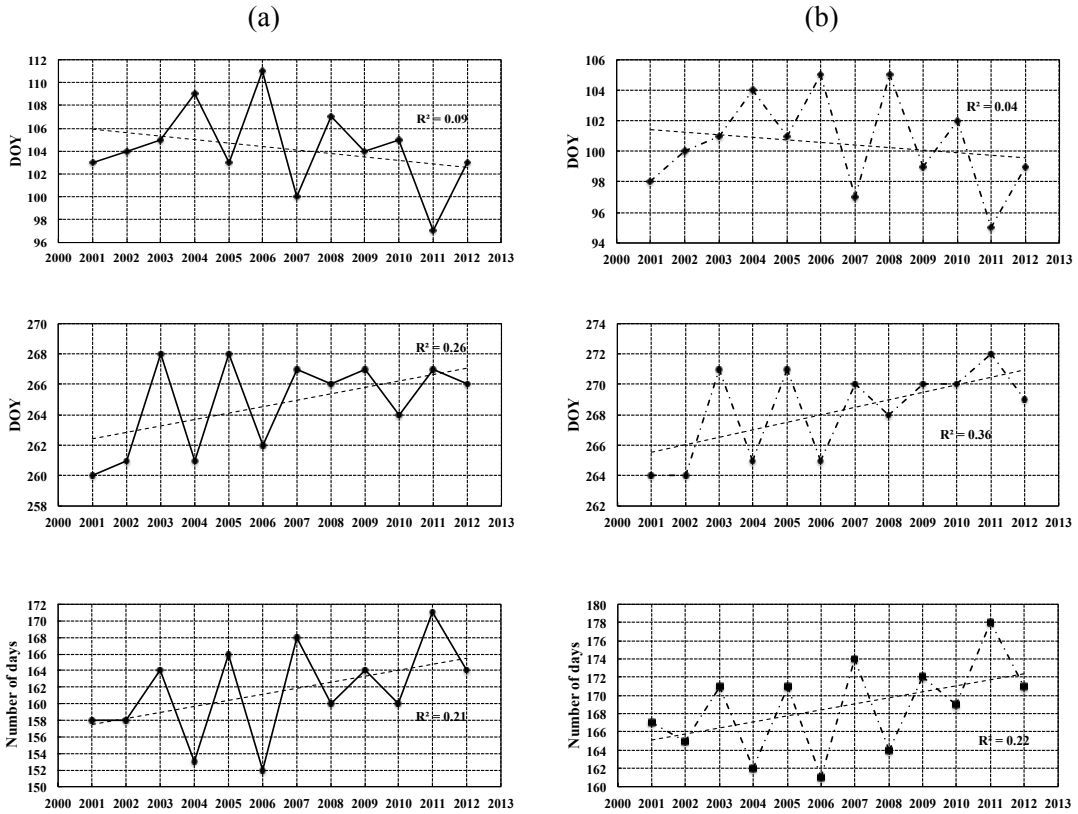

Figure 4.24: (a) and (b): Onset, offset and duration of HM definition by CH4_lst model. Solid line represents "HM" definition and dashed line presents "A" definition. The order from top to down is onset, offset and duration plot respectively. The y-axis of onset and offset is DOY, abbreviation of Day Of Year, and the y-axis of duration is number of days.

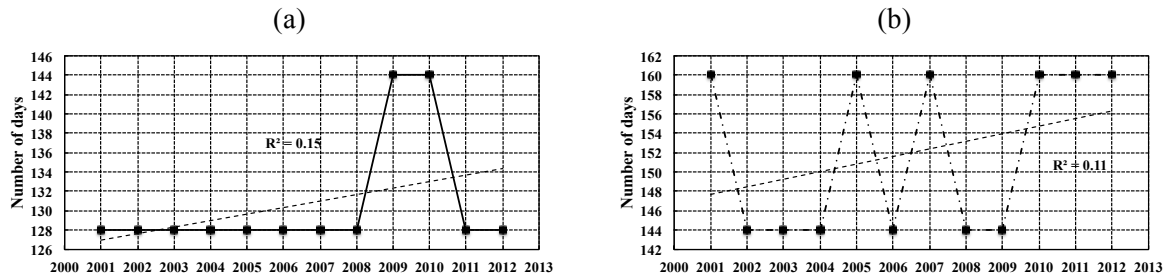

Figure 4.25: (a) and (b): Onset, offset and duration of HM definition by CH4_ndvi model. Solid line represents "HM" definition and dashed line presents "A" definition. The y-axis of duration is number of days. Because the NDVI data used for methane estimation was 16-days time resolution data, so that it cannot identify the onset and offset date in daily scale. Therefore, only durations show in this figure. In HM, the duration fluctuates within the range of 128-144 days and in A 144-160 as well.

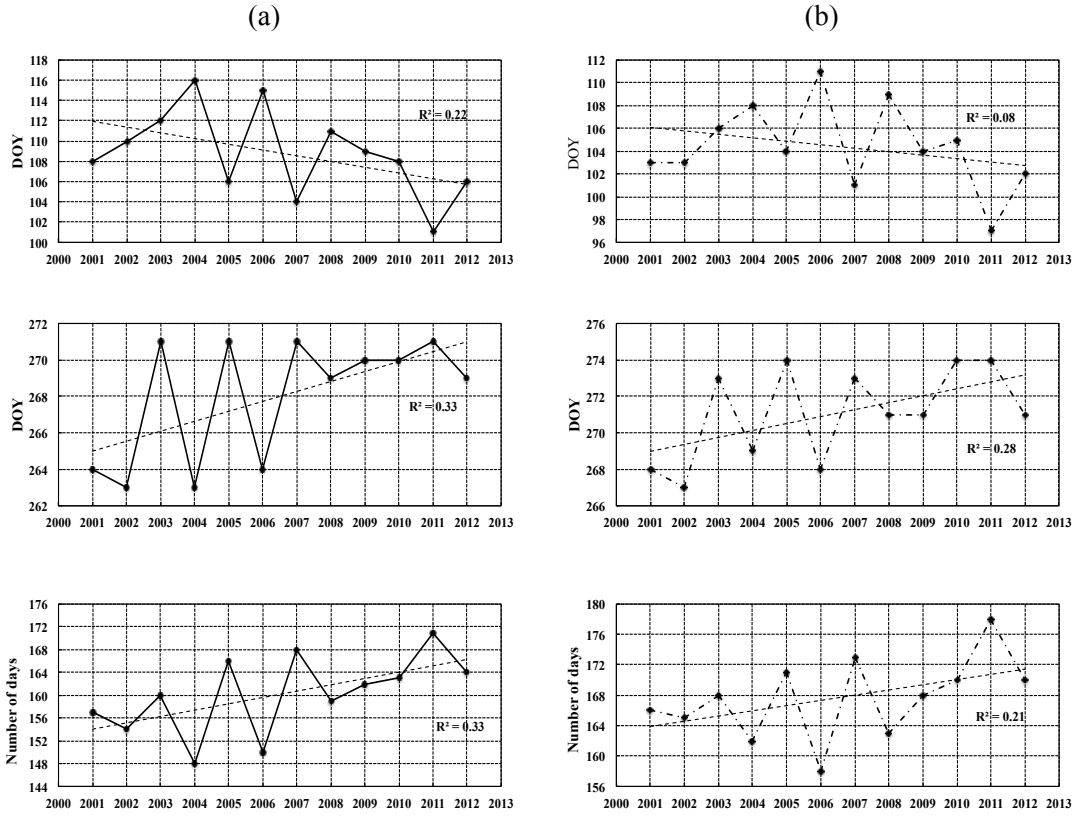

Figure 4.26: (a) and (b): Onset, offset and duration of HM definition by CH4_Ndl model. Solid line represents "HM" definition and dashed line presents "A" definition. The order from top to down is onset, offset and duration plot respectively. The y-axis of onset and offset is DOY, abbreviation of Day Of Year, and the y-axis of duration is number of days.

Till now, there are some special appearances show in Figure 4.24 and 4.26 that are all plots have “up and down” potential changing role even their overall trend are very clear and obvious. To explain this phenomenon, the temperature anomalies analyzed in this part.

According onset and offset analysis, it was found onset starts in April and offset appeared in September usually. Figure 4.27 shows Land surface temperature anomalies of April and September 2001-2012. Negative value means the temperature in that year cooler than from 2001 to 2012 average temperature. Positive value means the temperature in that year warmer than average temperature from 2001 to 2012.

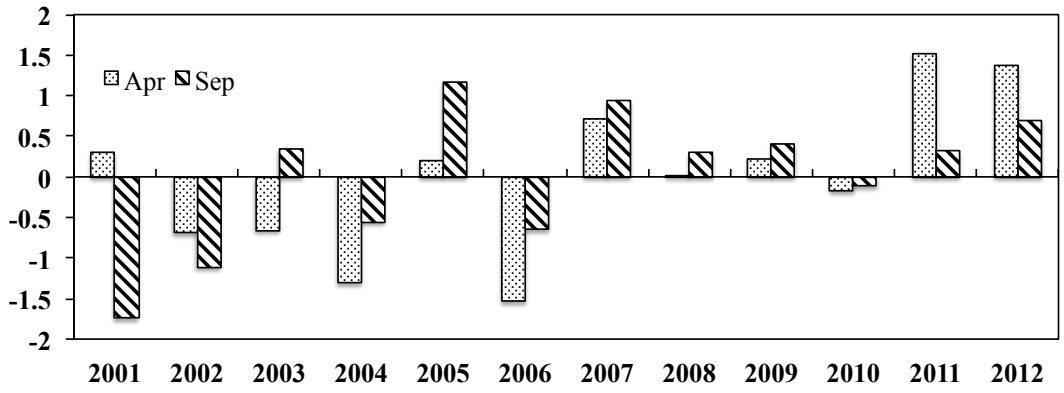

Figure 4.27: Land surface temperature anomalies of April and September 2001-2012. Negative value means the temperature in that year cooler than from 2001 to 2012 average temperature. Positive value means the temperature in that year warmer than average temperature from 2001 to 2012.

See April histogram in Figure 4.27, and then look at the plots of onset in Figure 4.24 or 4.26. Take Figure 4.24 (a) as an example. When temperature anomaly is minus in 2004 the onset date is the 109th day of year; in 2005 temperature anomaly goes to positive value, the onset date is the 103rd day of year; in 2006 again goes to minus and this anomaly much bigger than in 2004, corresponding the onset date is the 111th day of year, which date is later than in 2004. At the same time, histogram on behalf of September shows when anomaly is minus in 2004, the offset date is the 261st day of year; in 2005 anomaly goes to positive value, the offset date is the 268th day of year; in 2006 when anomaly goes to minus again, the offset date is the 262nd day of year. Therefore, the "up and down" appearance found in onset and offset plot is directly related with temperature anomalies. As a consequence, for onset, positive anomalies lead ahead of time of DOY; minus anomalies lead delay of DOY. For offset just a reverse, positive anomalies lead delay of DOY and minus anomalies lead ahead of time of DOY.

4.3.4 Warmest anomalies in 2010

The GISS Surface Temperature Analysis figured out, the two warmest anomalies on the planet in 2010 were Eastern Europe and the Antarctic Peninsula [48]. The multiple natural hazards: drought in the southern part of Russia, and raging fires in western Russia and eastern Siberia occurred in Russian Federation against the backdrop of unusual warmth. Bloomberg reported that temperatures in parts of the country soared to 42 degrees Celsius [49]. A large expanse of northern central Russia exhibits below-average temperatures. Eastern Siberia toward the southwest appears above-average temperature phenomenon, but the most obvious area of temperature

anomaly occurs north and northwest of the Caspian Sea, southeast of Moscow.

Section 3.3.3 indicated the temperature is the most important impact factor to methane emission. Hence, based on the temperature anomaly on July 2010, whether the methane emission situation appears anomaly or not seems quite interesting. Figure 4.28 shows temperature anomaly map from 20-27 July 2001-2012, compared to temperatures for the same dates from 2000 to 2008. It is obvious that the biggest anomaly happen in 2010, same as GISS report.

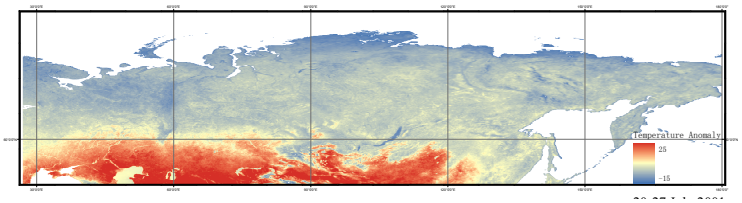

(a) 20-27 July 2001

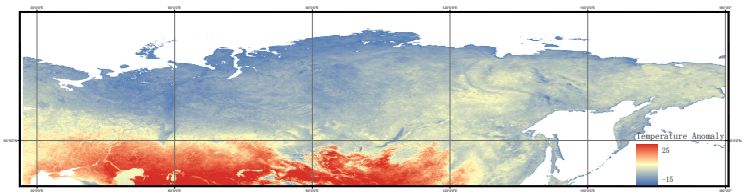

(b) 20-27 July 2002

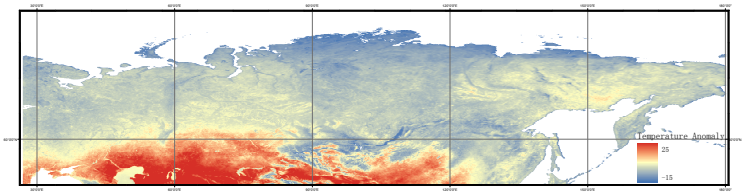

(c) 20-27 July 2003

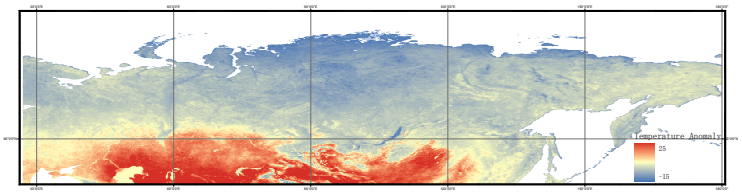

(d) 20-27 July 2004

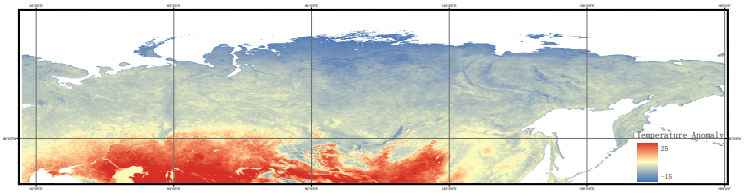

(e) 20-27 July 2005

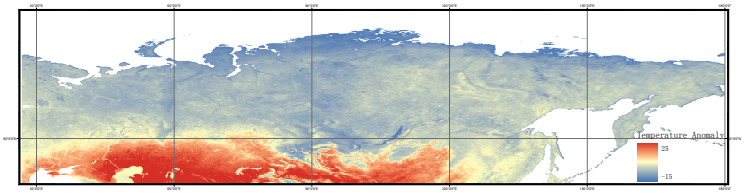

(f) 20-27 July 2006

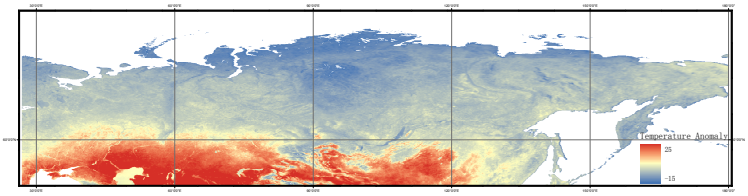

(g) 20-27 July 2007

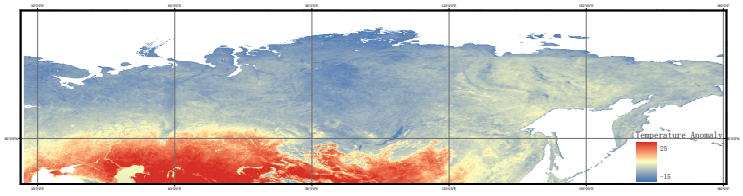

(h) 20-27 July 2008

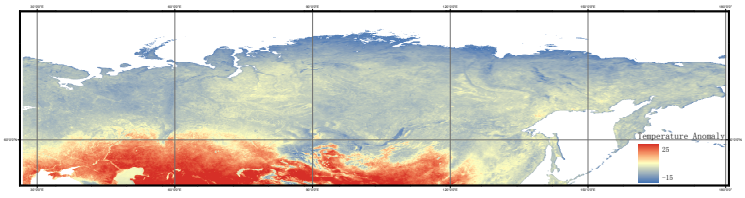

(i) 20-27 July 2009

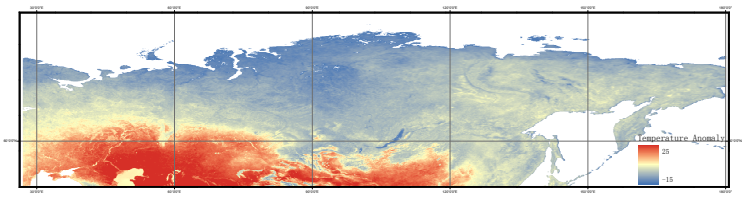

(j) 20-27 July 2010

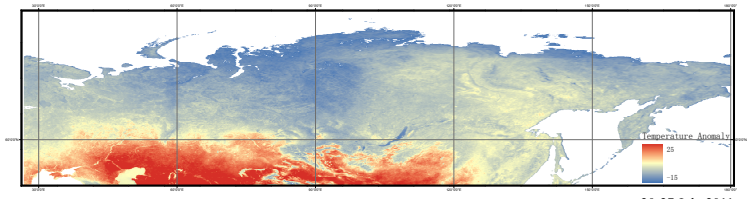

(k) 20-27 July 2011

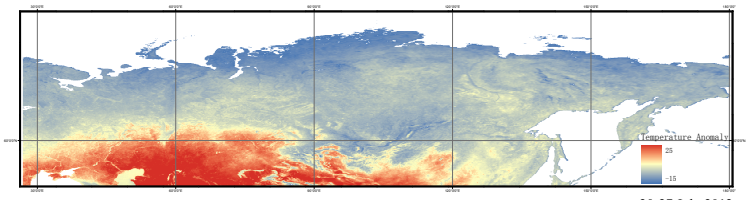

(l) 20-27 July 2012

Figure 4.28: Temperature anomaly from 20-27 July 2001-2012 ((a) ~ (l)), compared to average temperature for the same dates from 2000-2008.

Figure 4.29 and Figure 4.30 are the methane emission from CH4 modeling (CH4_lst and CH4_Ndl) from 2003 to 2012 respectively. Because of NDVI data used in model CH4_ndvi has 16 days time resolution so that could not represent weekly phenomenon. Methane emission map, which modeled by CH4_lst shows in Figure 4.29. The highest methane emission appears in Caspian Sea, southeast of Moscow in 2010. But Figure 4.30 exhibits opposite results that no highest CH_4 emission appeared in that place. From CH4_Ndl modeling results could not find any significant methane anomalies from 20-27 July in time period of 2003-2012. That is because model CH4_lst is as a function of LST, therefore the changes of LST will directly influence methane emission amount. Correspondingly, model CH4_Ndl is as a function of LST and NDVI, so that shown different emission value.

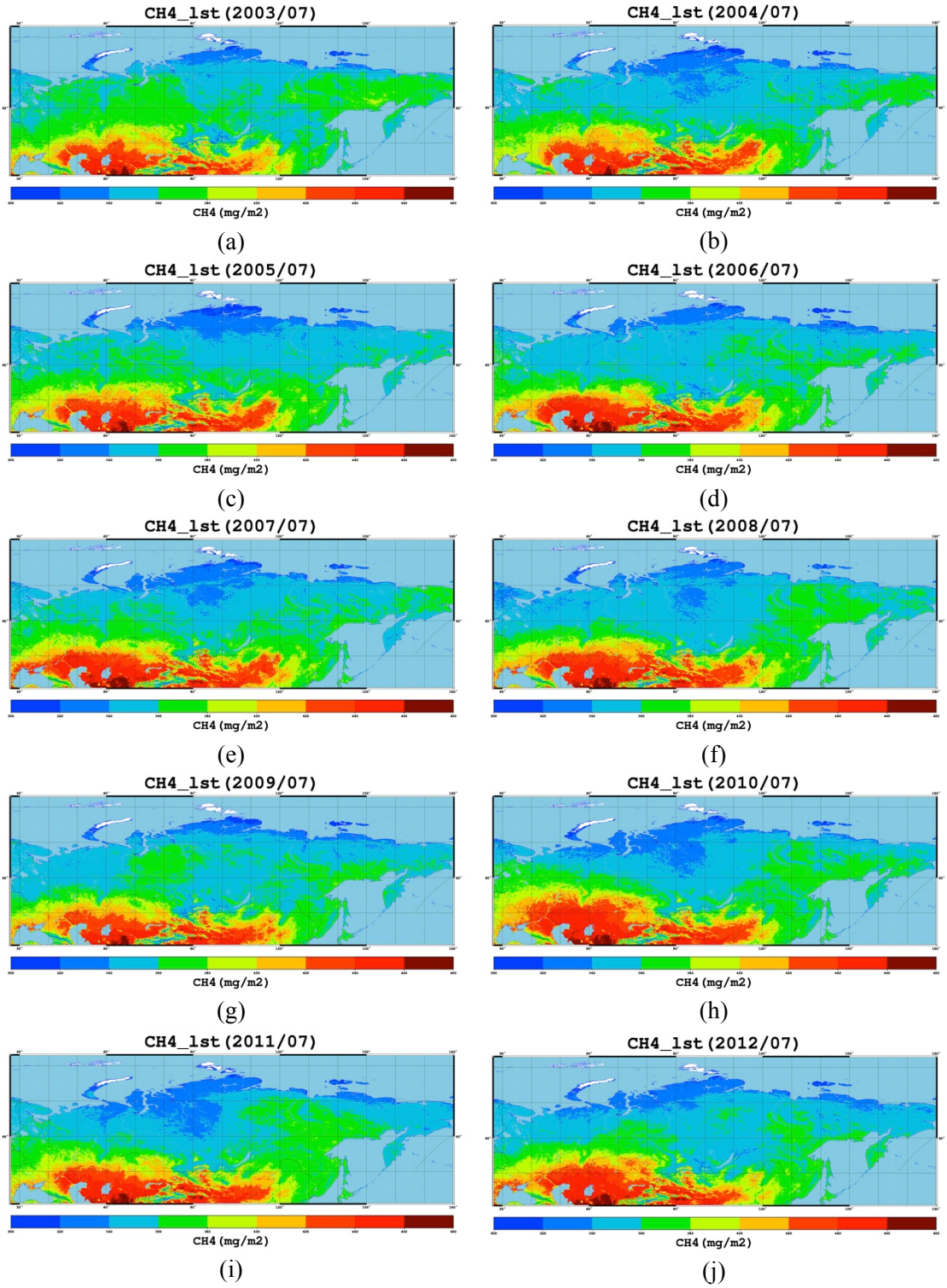

Figure 4.29: Methane emission map from CH4_lst model from 20-27 July 2003-2012 ((a) ~ (j)).

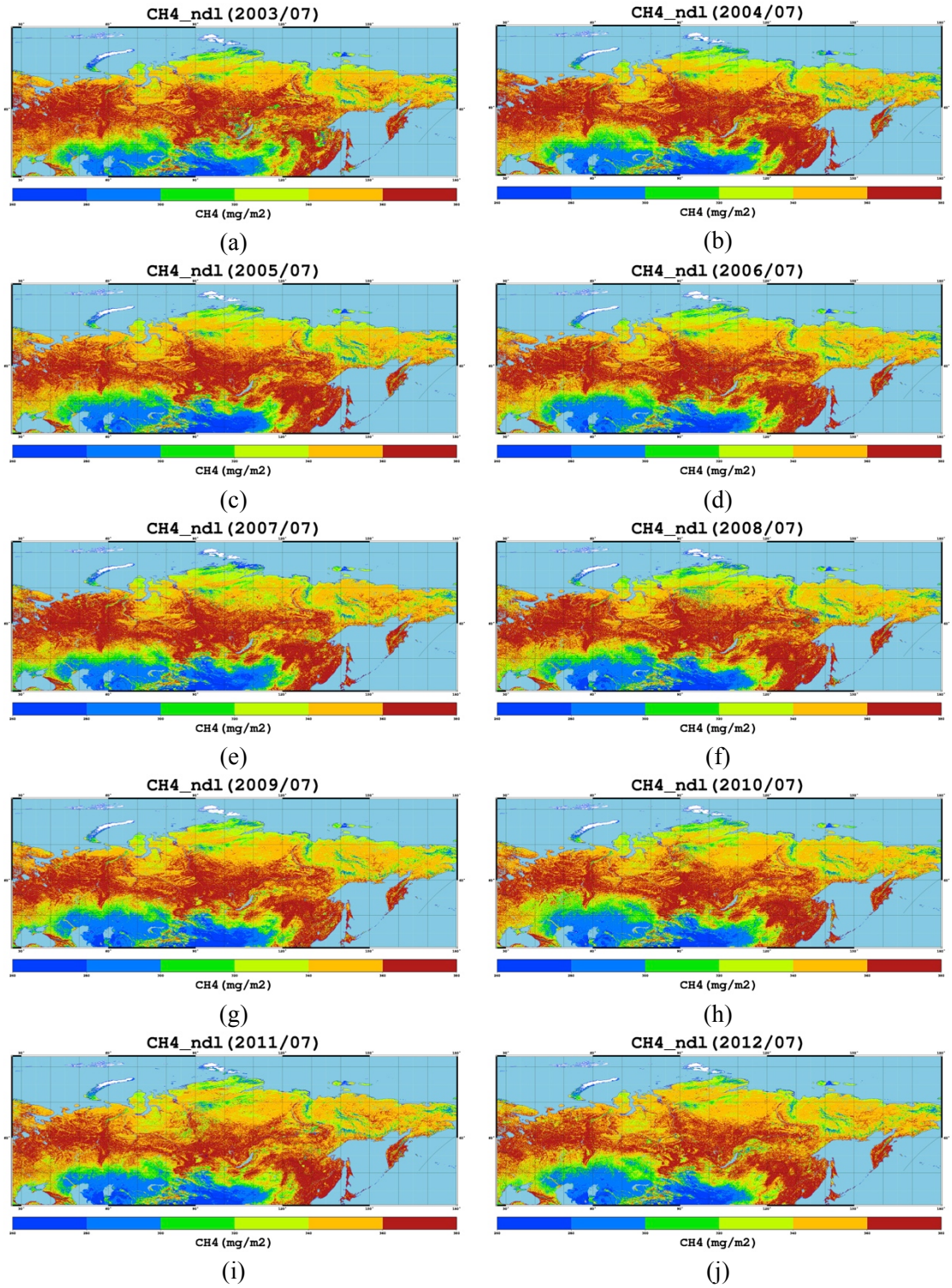

Figure 4.30: Methane emission map from CH4_Ndl model from 20-27 July 2003-2012 ((a) ~ (j)).

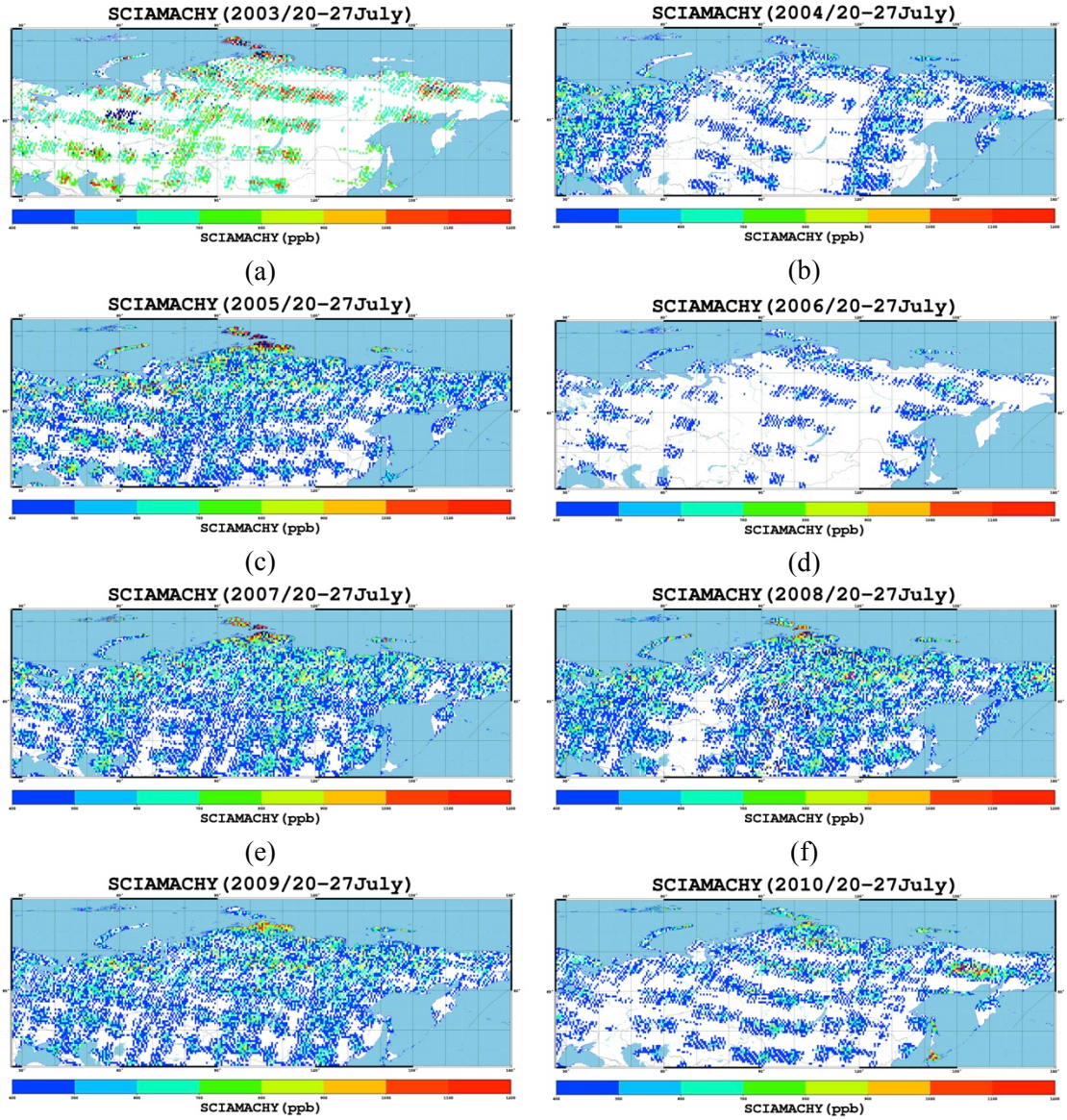

Figure 4.31: Methane concentration map of SCIAMACHY from 20-27 July 2003-2010 ((a) ~ (h)).

Figure 4.32 shows temperature anomaly bar graph correspond to Figure 4.28. The bar graph shows obvious temperature anomaly in 2010 compare with other years. Figure 4.33 shows average methane concentrations of SCIAMACHY in the same dates correspond to Figure 4.31. The highest emission did not appeared in 2010, same as indicated in Figure 4.30.

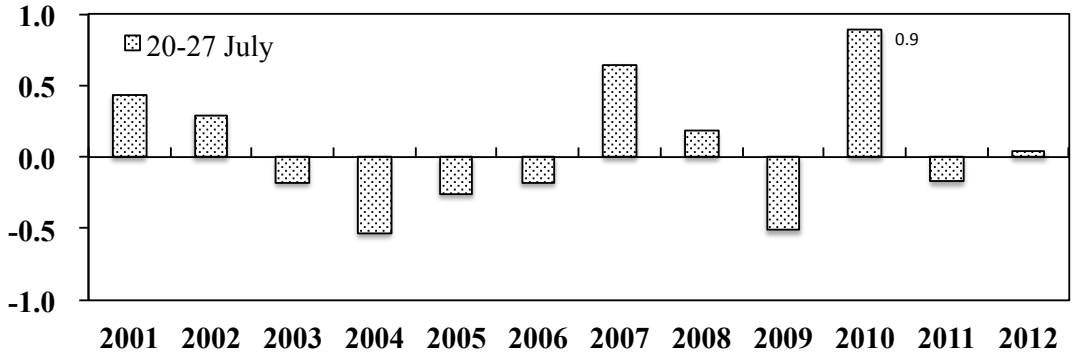

Figure 4.32: Temperature anomaly from 20-27 July 2001-2012, compared to average temperature of same dates from 2000 to 2008.

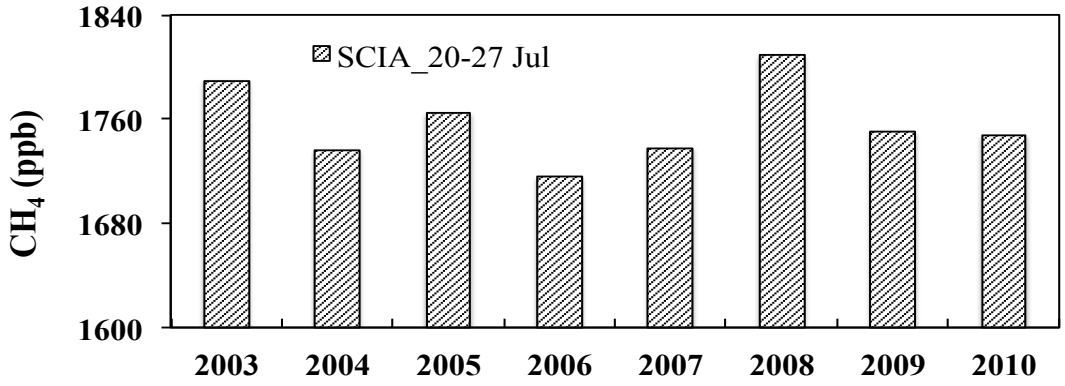

Figure 4.33: Methane emission of SCIAMACHY from 20-27 July 2003-2010. The highest value appeared in 2003 and 2008.

4.2. Discussion and Conclusion

There are a lot of estimation methods for green house gas including in-site measurement using statistic chamber technique, eddy covariance, process-based modeling and inverse modeling and so on. No matter what kind of method used for research, the crucial point is all necessary requirements can be easily available and work for the mission.

In this chapter, a method how to estimate methane emission by bio-geophysical models were shown. The estimation applied on one study point and whole study area respectively. The models used to estimate regional scale emission were updated from point estimation models.

It was found that methane emission from northern hemisphere permafrost region was increasing significantly and affected by temperature variation very much. This assumption proved by two analyses: methane emission amount and its seasonal emitting time. The results indicated increasing methane emission from 2003 to 2012. The results also proved the land surface temperature not only affect amount of methane emissions but also impact the onset and offset of methane emissions. Along with rising up of land surface temperature and its consecutive positive anomalies in recent years, the climate exactly goes warmer. Under this changes, more permafrost area would melt and provided more anaerobic environment and carbon source to produce methane and release to the atmosphere.

Global temperature anomaly frequently happened in recent years. But this kind of extremely climate event usually continues very short time compare with many years' simulation. Therefore a certain period of one-week temperature anomaly in urban area cannot interference methane emission in wetland.

Chapter 5

CORRELATION BETWEEN METHANE ESTIMATION AND SCIAMACHY DATA

5.1. SCIAMACHY measurement data

The SCanning Imaging Absorption spectroMeter for Atmospheric CHartographY (SCIAMACHY) sensor on board on ENVISAT provides the information of methane distribution at lower altitude down to the surface. It is an eight-channel grating spectrometer that takes measurements in the ultraviolet, visible, and near-infrared wavelengths, its objective is the global measurement of various trace gases in the troposphere and stratosphere including CH_4, CO_2, NO_2, H_2O, SO_2 and O_3. SCIAMACHY retrievals are based on absorption spectra of solar radiation in the near infrared [23]. The CH_4 data used in this study are retrieved from the nadir spectra in a micro-window of Channel 6 ranging from 1640 to 1670 nm [38]. SCIAMACHY measurement data provides the information of methane distribution at lower altitude down to the surface. The data are retrieved from (IMAP) DOAS algorithm [23], which defined as column-averaged dry air mole fraction of atmospheric methane. The total columns of CH_4 (VCD(CH_4)) and CO_2 (VCD(CO_2)) are retrieved from the observed spectra (Channel 6), and then the volume mixing ratio of CH_4 (VMR(CO_2)) is obtained by (Equation 5.1). in the equation unit is parts per billion in volume (ppbv), indicated as xCH4.

$$\mathrm{x}CH_4 = \frac{\mathrm{V_{means}(CH_4)}}{\mathrm{V_{means}(CO_2)}} \cdot \overline{\mathrm{VMR}}(\mathrm{CO_2}) \qquad (5.1)$$

where $\overline{\mathrm{VMR}}(\mathrm{CO_2})$ is the modeled column averaged mixing ratio of CO_2, obtained from the model field calculated by CarbonTracker [38 and 39].

5.2. SCIAMACHY and analysis

SCIAMACHY measurement data has daily time resolution. Atmospheric methane concentration is the result from all sources of methane in the atmosphere. The study has been done under monthly basis. Figure 5.1 and Figure 5.2 illustrate the monthly averaged SCIAMACHY maps from April to October in 2003 and 2010. When we compare these two figures, it is evident that in 2010 the average concentration value is much higher than that in 2003 in the same month of year, which means methane concentration reached higher value earlier and earlier in in early summer during past 8 years.

Figure 5.3 shows overlay of methane concentration of SCIAMACHY and the methane emission estimation derived in Chapter 4 from 2003 to 2010. All emission curves generally fitted and appear same seasonal variations in time series. But some differences were found:

1. Range of seasonality of SCIAMACHY measurement data shows different features from those of emissions in every year. That is possibly because SCIAMACHY atmospheric concentration methane comes from all sources such as fossil fuel, biomass burning and rice paddy and so on. Not only that, the atmospheric concentration trace gas also affected by atmospheric transport processes.
2. Some anomalies found in SCIAMACHY curve that are peak value in 2003 and 2009. The peak happened in September, which is different from normal emission. To understand this phenomenon, the monthly mean LST in September of those

years should be explored in more detail.

Figure 5.4 shows the mean temperature of September and October of each year from 2003 to 2010 with mean temperatures of those 8 years (2003-2010). In this figure, it was found that the difference between September and October in 2003 and 2009 are much bigger than other years'. As we already described, higher temperature leads more emissions, thus the difference of temperatures show in Figure 5.4 is consistent with Figure 5.3.

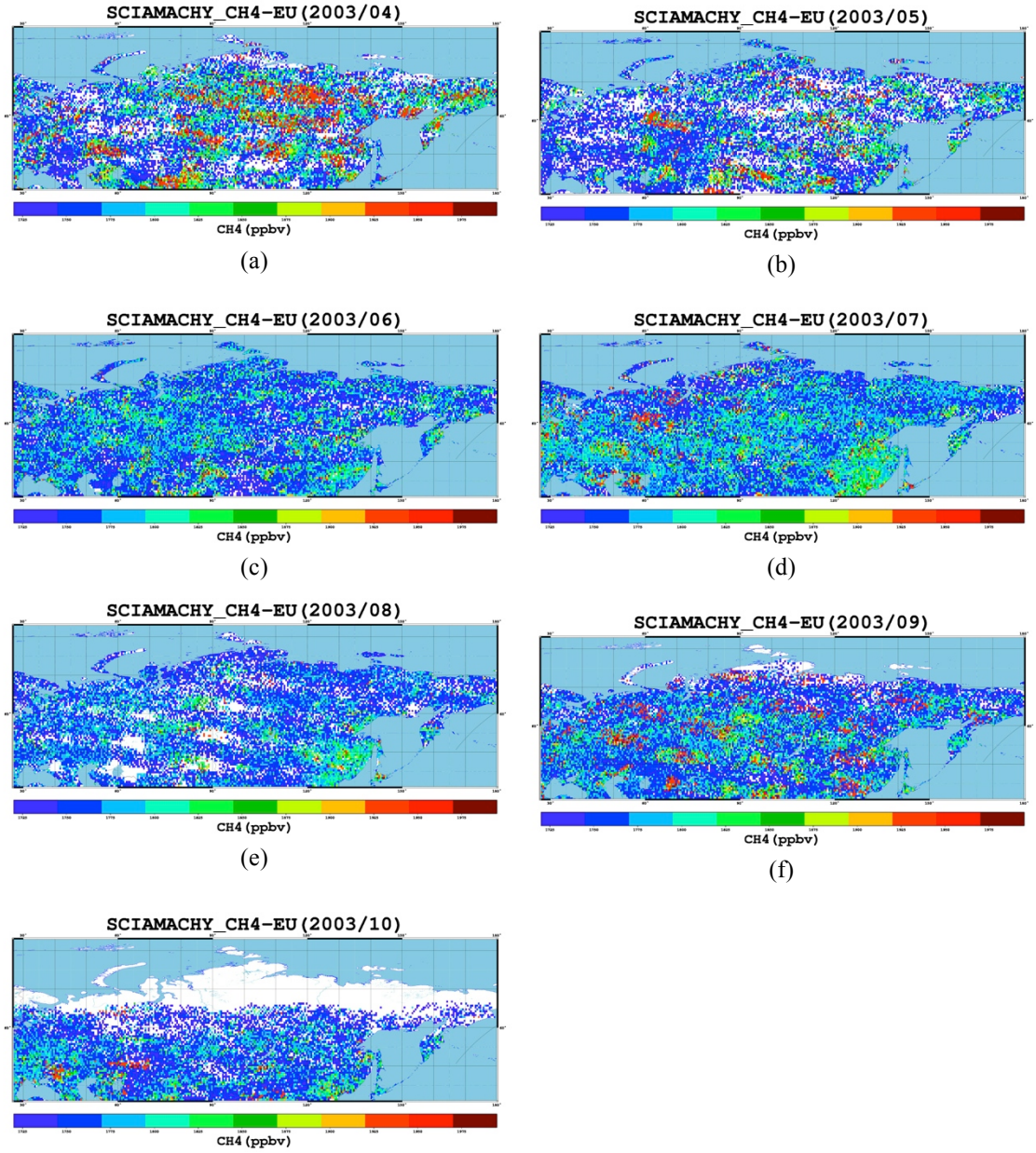

Figure 5.1: Monthly averaged map of SCIAMACHY from April to October ((a) ~ (g)) in 2003.

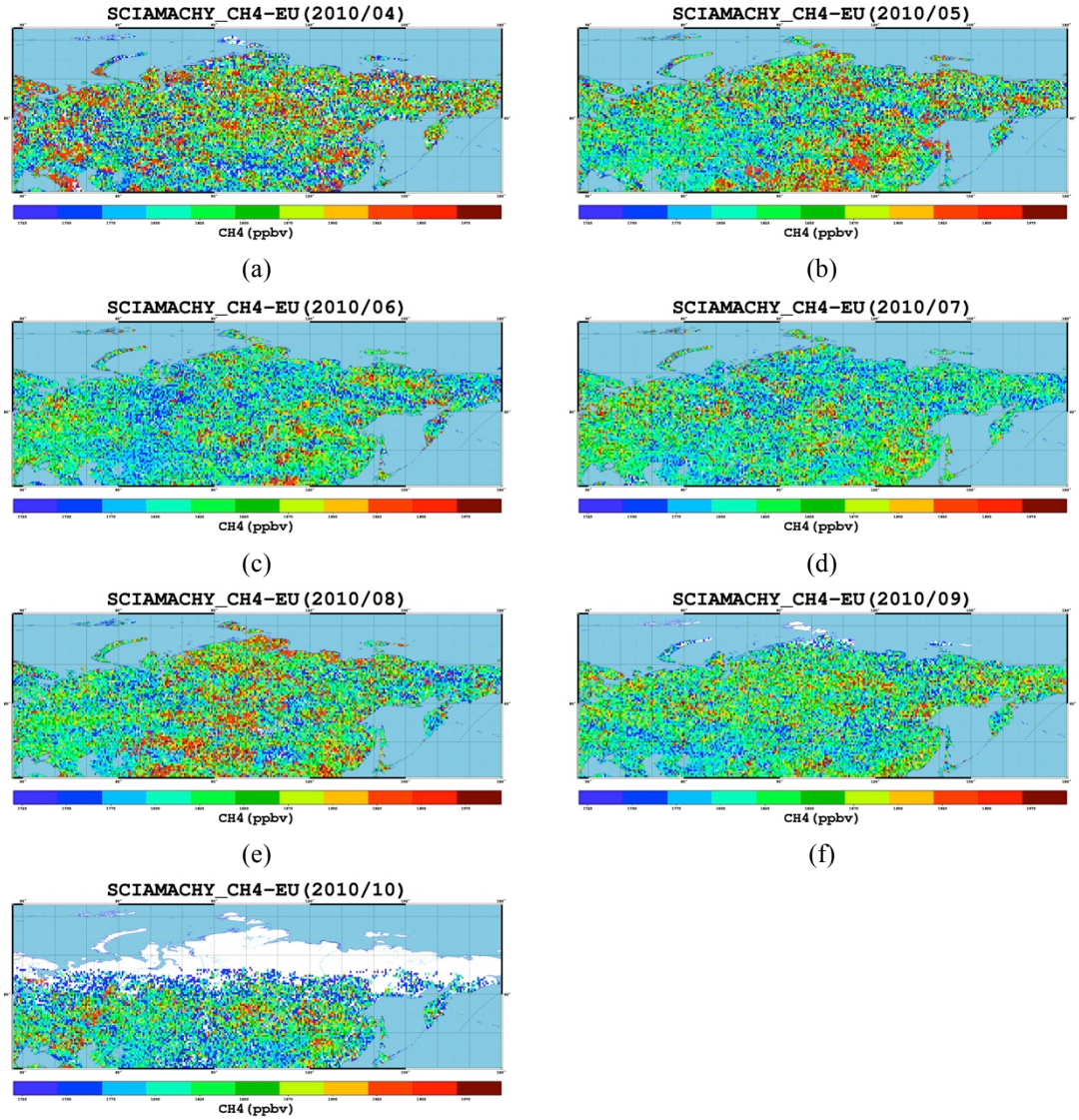

Figure 5.2: Monthly averaged map of SCIAMACHY from April to October ((a) ~ (g)) in 2010.

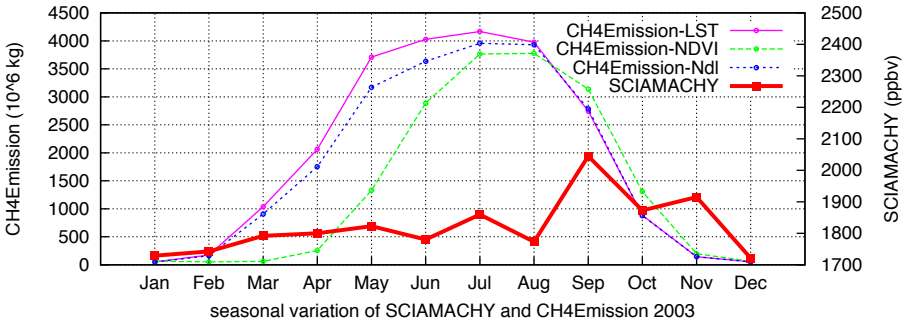
CH4Emission (10^6 kg)
SCIAMACHY (ppbv)
CH4Emission-LST
CH4Emission-NDVI
CH4Emission-Ndl
SCIAMACHY
Jan Feb Mar Apr May Jun Jul Aug Sep Oct Nov Dec
seasonal variation of SCIAMACHY and CH4Emission 2003

(a)

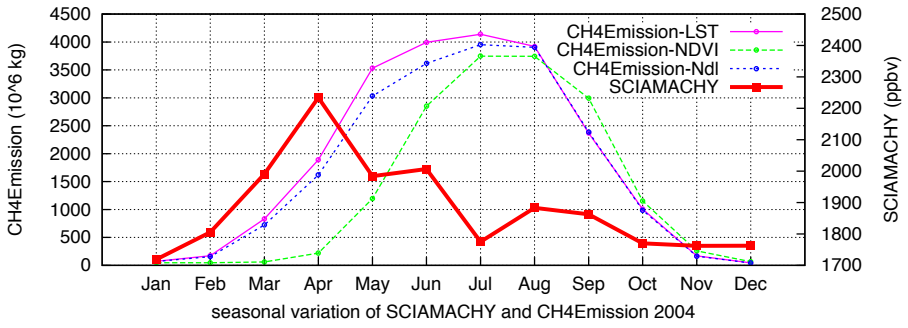
CH4Emission (10^6 kg)
SCIAMACHY (ppbv)
CH4Emission-LST
CH4Emission-NDVI
CH4Emission-Ndl
SCIAMACHY
Jan Feb Mar Apr May Jun Jul Aug Sep Oct Nov Dec
seasonal variation of SCIAMACHY and CH4Emission 2004

(b)

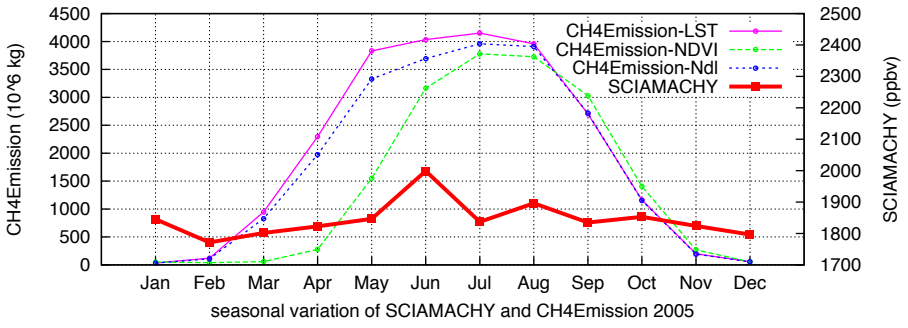
CH4Emission (10^6 kg)
SCIAMACHY (ppbv)
CH4Emission-LST
CH4Emission-NDVI
CH4Emission-Ndl
SCIAMACHY
Jan Feb Mar Apr May Jun Jul Aug Sep Oct Nov Dec
seasonal variation of SCIAMACHY and CH4Emission 2005

(c)

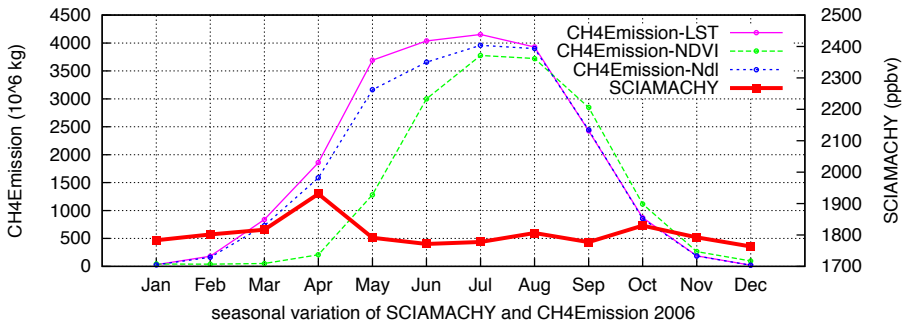
CH4Emission (10^6 kg)
SCIAMACHY (ppbv)
CH4Emission-LST
CH4Emission-NDVI
CH4Emission-Ndl
SCIAMACHY
Jan Feb Mar Apr May Jun Jul Aug Sep Oct Nov Dec
seasonal variation of SCIAMACHY and CH4Emission 2006

(d)

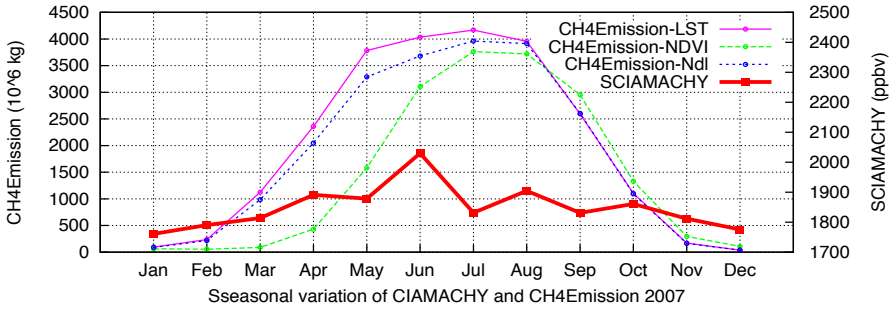

(e)

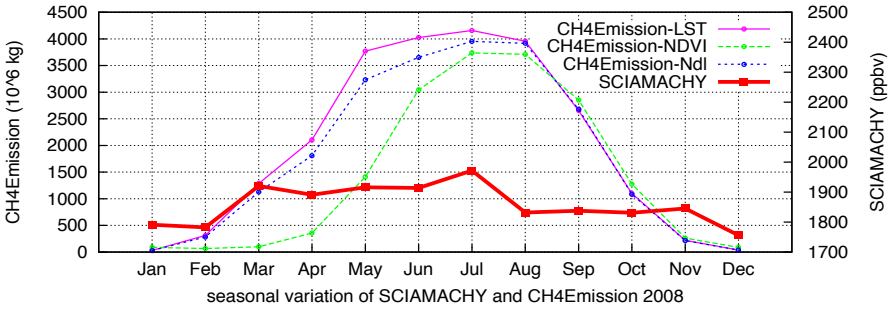

(f)

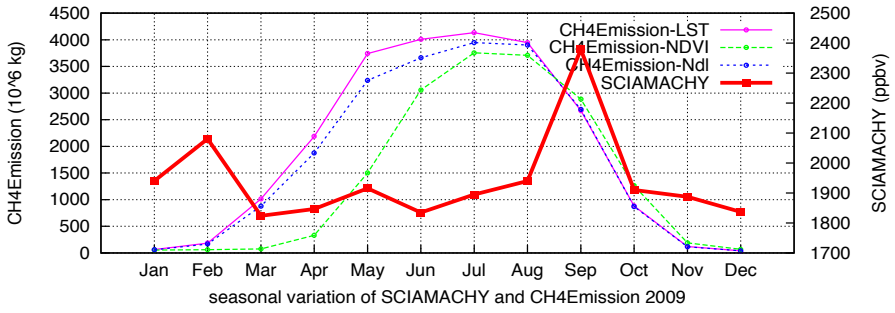

(g)

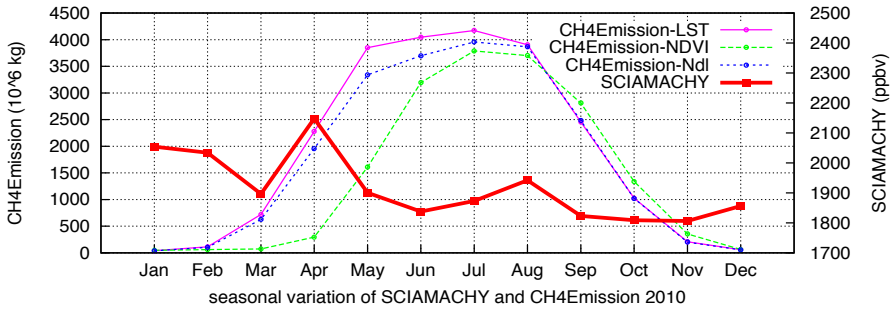

(h)

Figure 5.3: Curves of methane concentration by SCIAMACHY measurement and model estimation of methane emission in each year from 2003 to 2010 ((a)~(h)). Right scale used to read methane concentration and left scale used to read methane emission.

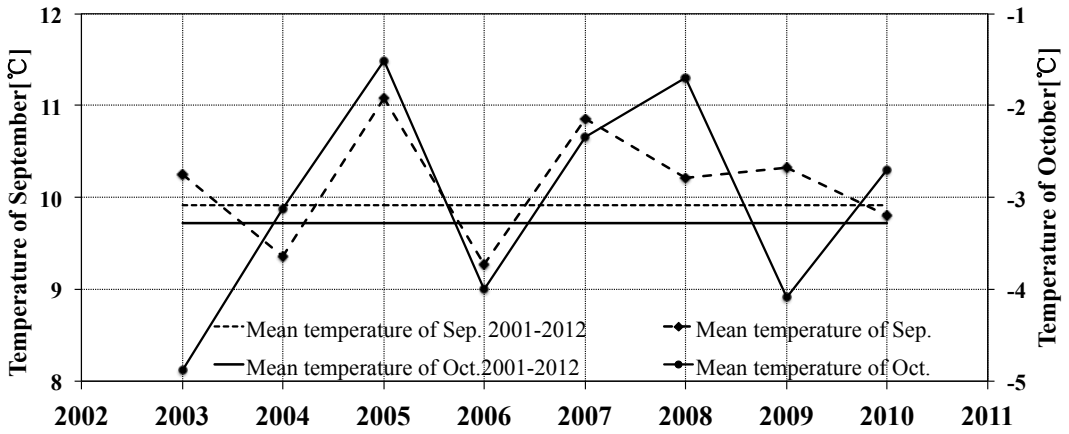

Figure 5.4: Mean temperature of September and October of each year from 2003 to 2010 respectively. The solid and dashed lines represent the mean temperature of October and September respectively. The transverse lines are the mean temperature during the periods from 2003-2010.

Table 5.1: Proximity Matrix of SCIAMACHY and methane estimations.

Proximity Matrix				
	Correlation between the value of the vector			
	SCIAMACHY	CH4_lst estimation	CH4_ndvi estimation	CH4_Ndl estimation
SCIAMACHY	1.000	.854	.673	.845
CH4_lst estimation	.854	1.000	.868	.996
CH4_ndvi estimation	.673	.868	1.000	.904
CH4_Ndl estimation	.845	.996	.904	1.000

Table 5.2: Growth rate and annual growth rate of SCIAMACHY and methane estimations. In this table, calculation period of methane estimation is from 2003 to 2012 and of SCIAMACHY is from 2003 to 2010 because of data shortage.

	Growth rate (%)	Annual growth rate (%)
SCIAMACHY	12.68	1.72
CH4_lst estimation	0.24	0.03
CH4_ndvi estimation	4.74	0.52
CH4_Ndl estimation	0.36	0.04

Table 5.1 shows a proximity matrix of the Pearson's correlation coefficients (r). From this table we could understand SCIAMACHY data has a good correlation with CH4_lst model estimation, r=0.854 and secondly with CH4_Ndl model estimation, r=0.845. Table 5.2 shows the growth rate and annual growth rate of SCIAMACHY and methane emissions by model estimations. In this table, calculation period of methane estimation is from 2003 to 2012 and of SCIAMACHY is from 2003 to 2010 because of data shortage. The methane growth rates appear positive value no matter for SCIAMACHY measurement or model estimation. It is clear that along with temperature rising, the methane emission gradually increasing in time series.

5.3. Discussion and Conclusion

In this chapter, we did a comparison analysis between SCIAMACHY atmospheric concentration data and methane emissions estimated from models. We found a good agreement on seasonal variation and also found some anomalies on SCIAMACHY. The methane has positive growth rate both in model estimation and SCIAMACHY observation. Not only methane emissions (model) but also methane concentration (SCIAMACHY) appeared increasing in growing season and decreasing in early

winter. Mostly the peak values were observed in Jun or July. But for SCIAMACHY, in 2003 and 2009, the peak value observed in September; in 2004, 2006 and 2010 the peak value happened in April. There are some probably reasons could explain it. One is because of temperature. For example, when temperature suddenly dropped down in early winter, the ground surface will freeze quickly and pushed out amount of methane from the soil, so that peak value may appeared in September. In a similar way, when temperature risen early before summer, the amount of methane which accumulated under the ground in previous year will released to the atmosphere along with ground melting, so that the peak value may appeared in April. Another is because of sensor itself, because SCIAMACHY has detector degradation since 2005 and lower tropopause height may cause incorrect observation value. Another is from temperature anomaly,.

From correlation analysis, high Pearson's correlation coefficients appeared between SCIAMACHY and model estimations. Therefore, on the one hand the estimation models made a good simulation of methane emissions; on the other hand, estimation results and SCIAMACHY can check the methane fluctuation each other in permafrost wetland area.

SCIAMACHY atmospheric concentration data is very good and convenient to use. But in high latitude area (> N60), the SCIAMACHY measurement value will smaller than in low latitudes because of low tropopause height. Also, the land-sea distribution, atmospheric circulation and other atmospheric motion will affect on methane concentration. Additionally, the long-lived trace gases concentrations also depend on the topography not only on the strength of emissions. For instance, if the measurement place is located in basin or surrounded by high mountains, the trace gas would be accumulate easily and cause the detection value higher.

Chapter 6

VALIDATION OF METHANE ESTIMATION

6.1. Methane estimation in Lena River Delta

6.1.1 Point scale

According section 4.3.1, the same study point was selected to validate for estimation result. Because of the research at this point located in permafrost wetland area and continuous measurement results had published [20,34].

In this section, the in situ measurement results of 2003 referenced from Wille's [34] report and of 2006 referenced from Sachs' [20] report. For easily understanding, here take same time period of in situ measurement results [20,34] and estimation results to compare, shown in Table 6.1. Based on the assumption in this study, the time period selection neglect minus temperature times and only focus on the days which temperatures are positive. The Equation (4.5) (CH4_ndvi) didn't mention in this comparison, because the satellite data used in Equation has 16 days time resolution, so that cannot represents daily emission condition.

Table 6.1 represents the comparison result of referenced paper and model estimation result. The model in 2012, results of Equation (4.2) and (4.3) are more than 3000 mg/m^2/year, both overestimate the methane emission in the point. Through modify the threshold, in model 2014, Equation (4.4) (CH4_lst) and Equation (4.6) (CH4_Ndl) results more close to in situ measurement results, especially CH4_Ndl. From this comparison we can understand, more parameter consider, more realistic result.

Table 6.1: Comparison of in situ measurement and methane estimation results in 2003 and 2006. The duration in 2003 is 95 days (Jul.20~Oct.22) and in 2006 is 70 days (Jul.9~Sep.16).

		Model (2012)		Model (2014)			CH_4 (*Reference value)
		Eq.(4.2)	Eq.(4.3)	Eq.(4.4)	Eq.(4.5)	Eq.(4.6)	
		CH4_lst	CH4_ndvi	CH4_lst	CH4_ndvi	CH4_ndl	
2003	Emission ($mg/m^2/yr$)	3836.1	3813.6	2043.4	-	1838.6	1737[34]
	Duration(day)	95	95	95	-	95	95
2006	Emission ($mg/m^2/yr$)	3067.3	2886.7	1909.4	-	1681.8	1458[20]
	Duration(day)	70	70	70	-	70	70

*: [34]Christian Wille, etc. 2008, Global Change Biology (2008) 14, 1395–1408;
[20]Torsten Sachs, etc. 2010, Global Change Biology (2010) 16, 3096–3110.

6.1.2 Region scale

Since 1998, the Alfred Wegener Institute (AWI) for Polar and Marine Research in Potsdam in collaboration with the Lena Delta Reserve has operated the Samoylov Station in this region for Arctic system science [40]. Being the largest delta in the Arctic, Lena River Delta (Figure 4.5) is a key region for long-term investigations of the processes of the permafrost formation and decay, transformation and emission of green house gases, thermal and hydrologic studies on the active layer of permafrost in the Siberian Arctic [35]. Hubberten et al. [35] give an overview of the station's facilities and research opportunities. Wagner et al. [41] measured the methane emissiones as well as the fundamental processes of methane production and methane oxidation from the end of May to the beginning of September 1999. Sachs et al. [42] measured methane emissiones on the microsite scale in the Lena River Delta from July to September 2006 by closed chamber measurement.

In this part, we use Schneider et al. [21] results to validate the model estimations. The study area is the Lena Delta, where the same area used in referenced paper. To improve reliability, we extract Lena Delta place from study area and apply CH4_lst, CH4_ndvi and CH4_Ndl three models to estimate methane emissions. Table 6.2 shows the Schneider et al.'s result. In referenced paper shows the mean daily methane emission of the entire Lena Delta was calculated with 10.35 mg CH_4 m^{-2} d^{-1} and mean daily emission is $300.7*10^6$ g d^{-1}.

Table 6.3 shows the model estimations of mean daily emission and emissions on July in last decade (from 2001 to 2010). Compare with referenced results, the modeled mean daily emissions are very close to measurement data, especially from CH4_lst modeling. The CH4_ndvi and CH4_Ndl are underestimated, especially CH4_ndvi, and all mean daily emissiones are overestimated.

Table 6.2: Cited from Schneider et al. paper. The mean daily emission in July is 10.35 mg m^{-2} d^{-1} and mean daily emission is 300.7*10^6 g d^{-1}.

Mean daily methane emission rates for July and annual emission rates for all land cover classes in the Lena Delta

Code	Class	Area	%	Mean daily emission July		Annual emission	
		km²		mg m^{-2} d^{-1}	10^6 g d^{-1}	mg m^{-2} a^{-1}	10^6 g a^{-1}
WT	Wet sedge- and moss-dominated tundra	8277	28.5	16.8	139.1	1452.3	12,020.7
MT	Moist grass- and moss-dominated tundra	2173	7.5	17.2	37.4	1486.9	3231
NV	Non-vegetated areas	1697	5.8	0	0	0	0
MDD	Moist to dry dwarf shrub-dominated tundra	1832	6.3	58.4[a]	107	5048.5	9248.9
DMSD	Dry moss-, sedge- and dwarf shrub-dominated tundra	3519	12.1	0.4[b]	1.4	34.6	121.8
DG	Dry grass-dominated tundra	610	2.1	0.4[b]	0.2	34.6	21.1
DT	Dry tussock tundra	444	1.5	0.4[b]	0.2	34.6	15.4
WB	Water bodies	8894	30.6				
	Rivers and coastal waters	5886	66.2	0[c]	0	0	0
	Lakes (>0.36 ha=4 Landsat-7 pixel)	3008[d]	33.8				
	Thermokarst lakes on 3rd terrace	88.9[d]	3.0	–	–	24,900[e]	2213.6[e]
	All other lakes	2919.1[d]	97.0	3.1[f]	9.0	268	782.3
SW	Shallow water	1590	5.5				
	Vegetated lake margins and shoals	159	10[g]	40.3[h]	6.4	3483.8	553.9
	Sandbanks and shoals in rivers and along the coast	1431	90[g]	0	0	0	0
	Total	29,036	100	10.35[i]	300.7[i]	972.14	28,208.7

[a] Values for class MDD measured in June.
[b] Values adopted from Kutzbach and Kurchatova (2002); measured in the Lena Delta.
[c] According to Semiletov (1999) methane concentrations in the Lena Delta channels and offshore waters were close to his analytical measurement limit (<0.015 µM/l). We therefore set these emissions to zero.
[d] Area of lakes based on Morgenstern (2005).
[e] Value adopted from Walter et al. (2006); measurements cover the whole annual cycle, incl. winter emissions; measured in NE Siberia.
[f] Value adopted from Morrissey and Livingston (1992); measured in Alaskan North Slope region.
[g] Percentage ratio between subclasses is based on visual interpretation of the classification image and the Landsat 7 data.
[h] Values from this study, Wagner et al. (2003), and Spott (2003); all measured in the Lena Delta.
[i] Daily emissions of thermokarst lakes are not included.

Table 6.3: Mean daily emission and emissions from model estimations on July from 2001 to 2010.

	Mean daily emission					
	Emission (mg m^{-2} d^{-1})			Emission (10^6 g d^{-1})		
Year/month	CH4_lst	CH4_ndvi	CH4_Ndl	CH4_lst	CH4_ndvi	CH4_Ndl
2001/7	20.82	32.02	31.34	307.53	262.21	294.44
2002/7	20.73	31.74	31.08	306.18	249.15	291.95
2003/7	20.58	31.79	31.12	303.87	244.50	292.33
2004/7	20.18	30.96	30.41	297.96	199.71	285.67
2005/7	20.53	32.03	31.22	303.20	258.00	293.25
2006/7	20.41	31.82	31.22	301.40	256.78	293.24
2007/7	20.72	32.06	31.43	305.94	262.63	295.27
2008/7	20.67	31.43	30.82	305.23	20 9	289.54
2009/7	19.95	31.46	30.91	294.55	229.45	290.34
2010/7	20.90	32.16	31.64	308.67	273.36	297.24

6.2. Comparison of methane concentration obtained from WDCGG

6.2.1 Introduction

The World Data Centre for Greenhouse Gases (WDCGG) is one of the WDCs under the Global Atmosphere Watch (GAW) programme. GAW focuses on six measurement groups: greenhouse gases, UV radiation, aerosols, ozone, major reactive gases (CO, VOCs, NOy and SO_2), and precipitation chemistry [46]. The purpose of the WDCs is to collect and archive the processed GAW data, and to make them openly available. They also provide support in the quality assurance, and for analysis and explanation of these data for the processes of scientific advances and policy decisions.

The data from WDCGG are organized by NOAA. NOAA supports the sampling and measurements. They archive their data at the WDCGG to make it easy for users to get data from different measurement programs, and those data are also available from their own data server. In very approximate terms, the air sample is representative of large well-mixed volumes of atmosphere (10s to 100s of thousands of square km), has atmospheric concentration unit, ppb. The contributor of the data from WDCGG used in this study is Main Geophysical Observatory (MGO), Russian Federation. For convenience named as “WDCGG data” hereafter.

Among all stations in WDCGG, there are 7 stations available corresponding to the area of interest of this study. Table 6.4 shows the cite essential information of those 7 stations. After checking those points on Google Earth, it was found that points No. 1 to No.3 are in urban areas, not natural wetland; point No.6 is located in bare land; point No.7 is water. Hence, here only two points could be used for comparison. Table 6.5 is the point No.4 and No.5 information with measurement period. This table indicates that the measurement period of No.5 is too short to do long-term analysis.

Table 6.4: Available points information from WDCGG.

No.	Point	Land cover type	Station name	Time interval
1	42.62N 76.98E	Grassland	Issyk-Kul, Kyrgyzstan	Daily/Monthly
2	43.25N 77.87E	Grassland	Plateau Assy, Kazakhstan	Event/Monthly
3	44.45N 75.57E	Grassland	Sary Taukm, Kazakhstan	Event/Monthly
4	69.20N 35.10E	Evergreen Needle forest	Teriberka, Russia	Event/Monthly
5	71.59N 128.92E	Open shrublands	Tiksi, Russia	Event/Monthly
6	44.45N 111.08E	Sparsely vegetated	Ulaan Uul, Mongolia	Event/Monthly
7	43.16N 145.50E	Water	Cape Ochi-ishi, Japan	Daily/Monthly

Table 6.5: Point No.4 and No.5 information from WDCGG.

No.	Point	Land cover type	Covering period	Time interval
4	69.20N 35.10E	Evergreen Needle forest	1999-01 ~ 2013-12	Event/Monthly
5	71.59N 128.92E	Open shrublands	2011-01 ~ 2013-12	Event/Monthly

6.2.2 Data from WDCGG and SCIAMACHY

The data used in this part is from the point Teriberka, Russia (No.4) of WDCGG platform and SCIAMACHY. In convenience to compare, here data are archived monthly basis. The methane is measured by Gas Chromatography (FID) technique.

The SCIAMACHY data is from satellite observation with daily 60km spatial resolution. Data provides the information of methane distribution at lower altitude down to the surface. It is influenced by several elements such as climate (wind, ocean currents and so son), topography (mountain area, plateau, basin and so on) and sensor itself. So that many factors affecting on methane data should be taken into consideration.

The differences between these two measurements are WDCGG can accurate to small region or area, but SCIAMACHY overlay huge area; moreover satellite sensor sometimes cannot detect the earth because of climate reason. Therefore, the difference measurement technique will create difference result at same point and same time.

Figure 6.1 represents the WDCGG and SCIAMACHY curve at Teriberka (ppb). Figure 6.1 (a) shows methane flask at whole covering period (1999 to 2013) of the point No.4 from WDCGG platform. The data appears phenomenal increasing tendency ($R^2 = 0.34848$). Correspondingly, Figure 6.1 (b) overlay the methane curves from WDCGG and SCIAMACHY both. The SCIAMACHY curves also appear increasing trends ($R^2=0.148$) from 2003 to 2010.

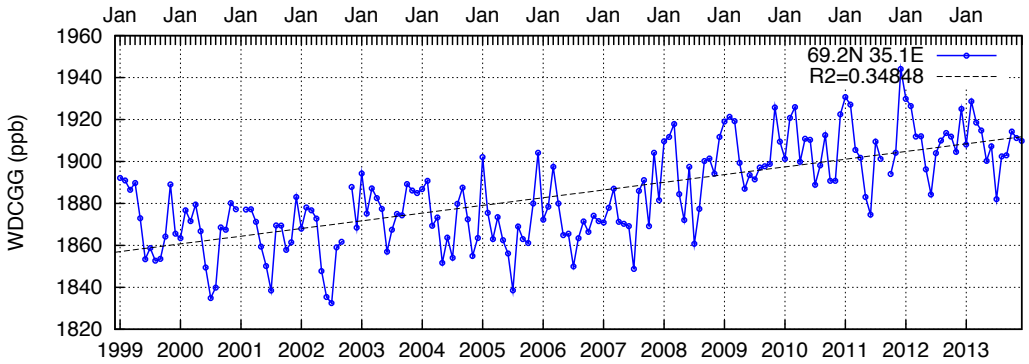

(a)

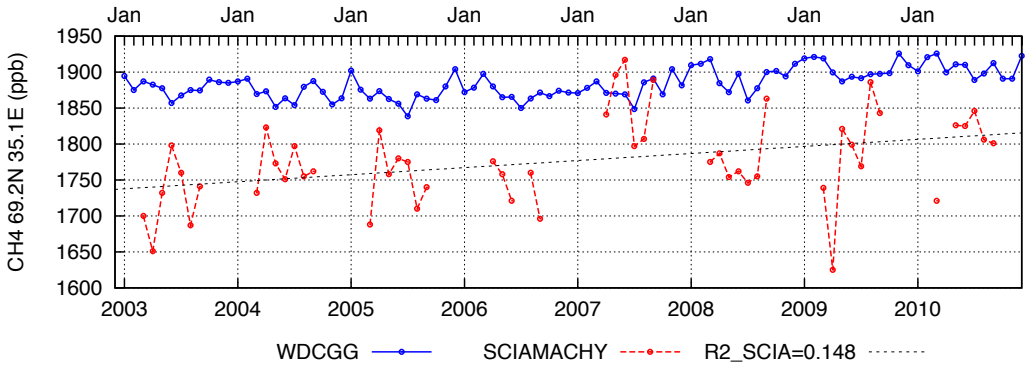

(b)

Figure 6.1: The methane concentration curves at Teriberka from WDCGG and corresponding grid of SCIAMACHY. (a) represents from WDCGG in time series 1999 to 2013. (b) is from WDCGG overlay with SCIAMACHY from 2003 to 2010 because of data shortage.

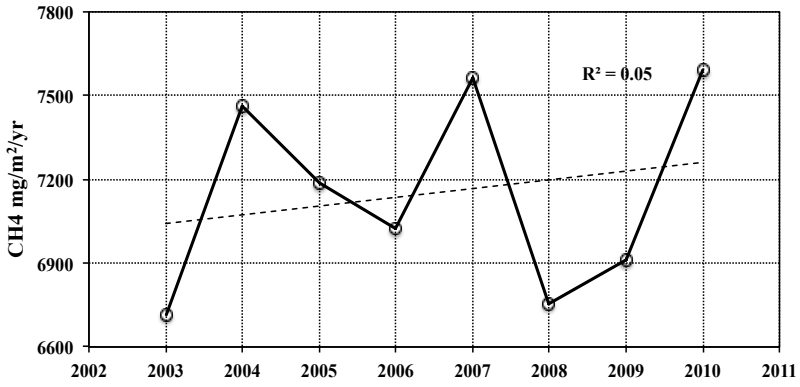

(a)

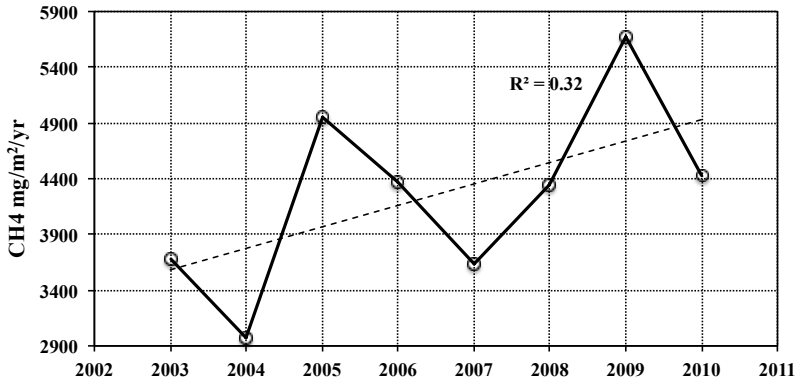

(b)

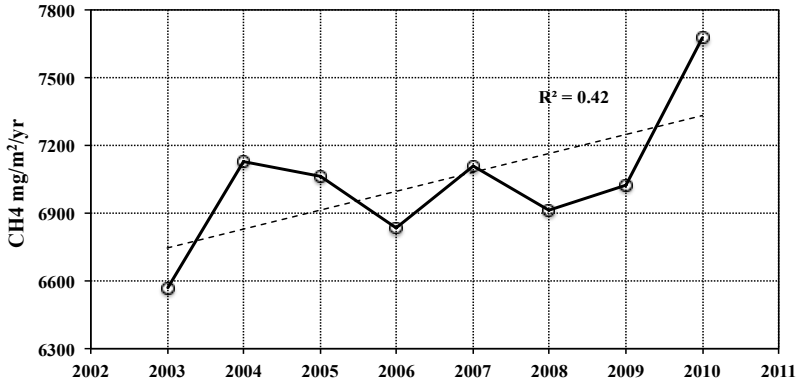

(c)

Figure 6.2: Annual methane emission of modeling estimations from 2003 to 2010. (a), (b) and (c) represent CH4_lst, CH4_ndvi and CH4_Ndl modeling result respectively.

Figure 6.2 represents annual methane emission from modeling estimations. (a), (b) and (c) on behalf of CH4_lst, CH4_ndvi and CH4_Ndl three modeling results separately (mg/m^2/yr). All three curves show increasing tendency same as what was indicated in Figure 6.1.

But in Figure 6.1 (b) appeared a peak value in 2007, which much higher than others. Correspond to this phenomenon, Figure 6.2 (a) and (b) showed increasing methane emission in 2007. Combine with previous section (6.1.2) CH4_ndvi is the worst estimation model in three of them.

6.3. Discussion and Conclusion

In this chapter, we use several kinds of methane measurements to validate the model estimations. Two sections validate the model estimation in two ways. The Lena Delta area estimations focus on the emission amount; and data from WDCGG platform focus on the variation tendency of methane concentration.

The validation results in Lena Delta had a good result both on point and regional scale. The modeling result was very close to the in situ data and the tendency also had an agreement with WDCGG. But the mean daily emission overestimated in regional scale. There are some probable explanations as follows: one is because of the projection distortion of original data from MODIS, area calculation will underestimate; furthermore, wetland land cover map remains uncertainties; third is it is difficult to take all potential impact factors into account for bio-geophysical modeling.

In point scale, Sachs and Wille [20, 34] using eddy covariance method because this technique provides nonintrusive spatially integrated emission data at the landscape scale while chamber measurements makes the soil surface isolated from the

atmosphere [20]. In region scale, Schneider [21] using closed chamber measurement to determine methane emission and quantify the methane emission of the individual land cover classes in object area. Chamber measurement is easy to establish and the result varies by landscape. Therefore, the result of paper more comparable with model estimation.

Atmospheric concentration data cannot directly compare with ground based estimation result. Because identify the source of atmospheric methane is extremely difficult and it related with numerous influence factors. Therefore, even in same measurement point, the difference source and measurement mechanism will lead difference result.

Chapter 7

CONCLUSIONS AND FUTURE WORK

7.1. Conclusions

In this study, no matter point basis or regional scale estimation, the results were good to represents the methane emissions in northern permafrost wetland. Through considered vegetation growing and temperature variations, the improvement models (Equation 4.4, 4.5 and 4.6) became more realistic.

The modeling results had good correlation with SCIAMACHY measurement data, although they were not in the same scale measurement, but show the proximity trends and seasonal changes in time series. In 8-year (2003-2010) methane emission estimation showed, in the course of growing season, the emission concentrate upon June, July and August three months (Figure 4.12). Table 5.2 showed the year growth rate of CH_4 emission, means methane emission has increased in time series. From 2003 to 2012, all three estimations showed positive year growth rate. In this study, onset of methane emission started earlier, offset date delayed and the methane-releasing days were getting longer.

The land surface water coverage also indicated an important role for methane emission response to climate warming. Along with climbing of annual mean temperature, the summer period extended. At the same time the wetland area expanded. Melton et al. [45] report, under higher temperature produce higher methane emission rates; through precipitation changed that changes methane oxidation in the soil and water table position. Wetland methane emissions are also

affected by changes in wetland area that may either increase or decrease locally.

Methane estimations in this study indicate that land surface temperature is one of the most important factor that decide the seasonal fluctuation of methane emission. This phenomenon consensus with many scientific researches. The research done by Hoehler and Alperin in 2014 [43] showed methane production will increase more steeply with temperature than would be captured by climate-change models, and as in Gabriel Yvon-Duroche's in 2014 [44] result showed, the emission of CH_4 and the ratio of CH_4 to CO_2 emissions increase markedly with seasonal increases in temperature. Consequently, the amount of emission and time of releasing are quite depending on temperature. The estimation still under calibration by other referenced publications, these examinations will lead positive effects in near future.

Methane emission is complexly controlled by biological, physical and chemical, factors. Therefore, single-factor environmental relationships are deficient to explain fully the variation in methane emission [18]. Furthermore, the factors must be easily available and workable over a wide area.

The relating factors induce CH_4 emission such as different sources; different soil conditions and water table variations have a lot of uncertainties. These mainly due to the typically large variability of emissions of many CH_4 source categories, leading to large uncertainties of ground based estimates based on activity data and emission factors, or based on biogeochemical models [25]. A major limitation of present satellite observation is the limited number of atmospheric observation sites. Hence, additional a priori information from ground based estimates is usually required in order to overcome the underdetermination of the inverse problem. As a consequence, large uncertainties still exist [23]. The results obtained in this study indicate a potential scientific possible that connection of methane concentration in the atmosphere and land surface. Therefore transport model is an important and

challenging task to solve connection with ground based estimation problem in the future.

7.2. Future work

The study covered a wide range of simulation results and there is high agreement between model results and other field measurements. IPCC 2013 report, climate change by the end of the 21st century will increase wetland CH4 emissions [16]. Therefore climate model for simulate permafrost thawing is quite important.

CH4_Ndl modeling results indicated that more impact factors considered more accuracy results would come. Therefore, collaborate other climate indices like soil moisture, wind speed, atmospheric pressure and so on is the good way to improve estimation model. However, it is difficult to gather every element, which affect methane emission in wetland. In order to let emission and concentration value comparable, the atmospheric transport model should be considered. It is important that doing more investigations and exploring new scientific techniques (instruments) is necessary to remedy those limitations. Furthermore, because of climate warming and methane emission have interactive relationship, so that methane emission reduction method eager to be explored.

REFERENCES

[1] Osterkamp TE. Subsea Permafrost. Chapter in Encyclopedia of Ocean Sciences, SteeleJH, ThorpeSA and TurekianKK, Academic Press: London; 2902–2912, 2001.

[2] Zimov SA, Schuur EA and Chapin FS. Permafrost and the global carbon budget, Science 312, 1612, doi: 10.1126/science.1128908, 2006.

[3] Oechel WC, Hastings SJ, Jenkins M, Riechers G, Grulke NE and Vourlitis GL. Recent change of arctic tundra ecosystems from a net carbon sink to a source, Nature 361: 520-526, 1993.

[4] Vaks A, Gutareva OS, Breitenbach SFM, Avirmed E, Mason AJ, Thomas AL, Osinzev AV, Kononov AM and Henderson GM. Speleothems Reveal 500,000-Year History of Siberian Permafrost, Science 340, 183, doi: 10.1126/science.1228729, 2013.

[5] Sasakawa M, Ito A, Machida T, Tsuda N, Niwa Y, Davydov D, Fofonov A, and Arshinov M. Annual variation of methane emissions from forested bogs in West Siberia (2005–2009): a case of high CH4 and precipitation rate in the summer of 2007, Atmospheric Chemistry and Physics Discussions, 10, 27759–27776; doi:10.5194/acpd-10-27759, 2010.

[6] Denman, KL, G. Brasseur, A. Chidthaisong, P. Ciais, P.M. Cox, R.E. Dickinson, D. Hauglustaine, C. Heinze, E. Holland, D. Jacob, U. Lohmann, S Ramachandran, P.L. da Silva Dias, S.C. Wofsy and X. Zhang. Couplings Between Changes in the Climate System and Biogeochemistry. The Physical Science Basis. Contribution of Working Group I to the Fourth Assessment Report of the Intergovernmental Panel on Climate Change [Solomon, S., D. Qin, M. Manning, Z. Chen, M. Marquis, K.B. Averyt, M.Tignor and H.L. Miller (eds.)]. Cambridge University Press, Cambridge, United Kingdom and New York, NY, USA, 2007.

[7] Anisimov OA. Potential feedback of thawing permafrost to the global climate system through methane emission. Environmental Research Letters, 2-045016 (7pp), 2007.

[8] Christensen TR, Torbjo¨rn Johansson, H. Jonas A kerman, Mastepanov M, Malmer N, Friborg T, Crill P and Bo H. Svensson. Thawing sub-arctic permafrost: Effects on vegetation and methane emissions, Geophysical Research Letters, Vol. 31, L04501, doi:10.1029/2003GL018680, 2004.

[9] Wagner D and Liebner S. Global Warming and Carbon Dynamics in Permafrost Soils: Methane Production and Oxidation, Permafrost soils, Soil biology 16,

doi:10.1007/978-3-540-69371-0, 2009.
[10] Stocker, TF,Qin D, Plattner GK, Tignor M, Allen SK, Boschung J, Nauels A, Xia Y, Bex V and Midgley PM. The Physical Science Basis. Contribution of Working Group I to the Fifth Assessment Report of the Intergovernmental Panel on Climate Change, Cambridge University Press, Cambridge, United Kingdom and New York, NY, USA, 2013.
[11] Vaughan, DG, Comiso JC, Allison I, Carrasco J, Kaser G, Kwok R, Mote P, Murray T, Paul F, Ren J, Rignot E, Solomina O, Steffen K and Zhang T. The Physical Science Basis. Contribution of Working Group I to the Fifth Assessment Report of the Intergovernmental Panel on Climate Change [Stocker, TF, Qin D, Plattner GK, Tignor M, Allen SK, Boschung J, Nauels A, Xia Y, Bex V and Midgley PM]. Cambridge University Press, Cambridge, United Kingdom and New York, NY, USA, 2013.
[12] Kevin S, Lantuit H, Romanovsky V, and Schuur E. Policy implications of warming permafrost, 2012.
[13] Kääb A, Frauenfelder R, and Roer I. On the response of rockglacier creep to surface temperature increase. Global Planetary Change, 56, 172-187, 2007.
[14] Jones BM, Grosse G, Arp CD, Jones MC, Walter Anthony KM, and Romanovsky VE. Modern thermokarst lake dynamics in the continuous permafrost zone, northern Seward Peninsula, Alaska, J. Geophys. Res., 116, G00M03, 2011.
[15] Glaser PH, Chanton JP, Morin P, Rosenberry DO, Siegel DI, Ruud O, Chasar LI, and Reeve AS. Surface deformations as indicators of deep ebullition emissiones in a large northern peatland, Global Biogeochemical Cycles, Vol. 18, GB1003, doi:10.1029/2003GB002069, 2004.
[16] Ciais P, Sabine C, Bala G, Bopp L, Brovkin V, Canadell J, Chhabra A, DeFries R, Galloway J, Heimann M, Jones C, Le Quéré C, Myneni RB, Piao S and Thornton P. Carbon and Other Biogeochemical Cycles. The Physical Science Basis. Contribution of Working Group I to the Fifth Assessment Report of the Intergovernmental Panel on Climate Change [Stocker TF, Qin D, Plattner GK, Tignor M, Allen SK, Boschung J, Nauels A, Xia Y, Bex V and Midgley PM]. Cambridge University Press, Cambridge, United Kingdom and New York, NY, USA, 2013.
[17] Frankenberg C, Meirink JF, van Weele M, Platt U and Wagner T. Assessing Methane Emissions from Global Space-Borne Observations, Science, 308, 1010–1014, 2005.
[18] Nakano T, Kuniyoshi S and Fukuda M. Temporal variation in methane emission from tundra wetlands in a permafrost area, northeastern Siberia, Atmospheric Environment 34-1205-1213, 2000.

[19] Walter KM, Zimov SA, Chanton JP, Verbyla D and Chapin FS. Methane bubbling from Siberian thaw lakes as a positive feedback to climate warming, Nature, Vol 443-7, doi:10.1038, 2006.
[20] Sachs T, Wille C, Boike J, and Kutzbach L. Environmental controls on ecosystem-scale CH4 emission from polygonal tundra in the Lena River Delta, Siberia, Journal Of Geophysical Research, Vol. 113, G00A03, doi:10.1029/2007JG000505, 2008.
[21] Schneider J, Grosse G and Wagner D. Land cover classification of tundra environments in the Arctic Lena Delta based on Landsat 7 ETM+ data and its application for upscaling of methane emissions, Remote Sensing of Environment 113-380–391, 2009.
[22] Gavrilov NM, Makarova MV, Poberovskii AV, and. Timofeyev Yu. M. Comparisons of CH4 ground-based FTIR measurements near Saint Petersburg with GOSAT observations, Atmospheric Measurement Techniques, 7, 1003–1010, doi:10.5194/amt-7-1003, 2014.
[23] Frankenberg C, Meirink JF, Bergamaschi P, Goede APH, Heimann M, Ko¨rner S, Platt U, van Weele M and Wagner T. Satellite chartography of atmospheric methane from SCIAMACHY on board ENVISAT: Analysis of the years 2003 and 2004. JOURNAL OF GEOPHYSICAL RESEARCH, VOL. 111, D07303, doi:10.1029/2005JD006235, 2006.
[24] Frankenberg C, Bergamaschi P, Butz A, Houweling S, Fokke Meirink J, Notholt J, Katinka Petersen A, Schrijver H, Warneke T, and Aben I. Tropical methane emissions: A revised view from SCIAMACHY onboard ENVISAT, Geophysical Research Letters, Vol. 35, L15811, doi:10.1029/2008GL034300, 2008.
[25] Bergamaschi P, Frankenberg C, Fokke Meirink J, Krol M, Gabriella Villani M, Houweling S, Dentener F, Dlugokencky EJ, Miller JB, Gatti LV, Engel A, and Levin I. Inverse modeling of global and regional CH4 emissions using SCIAMACHY satellite retrievals, Journal Of Geophysical Research, Vol. 114, D22301, doi:10.1029/2009JD012287, 2009.
[26] Nakayama T. Estimation of Methane Emission from Natural Wetlands in Siberian Permafrost Area, A doctoral dissertation, Division of Geophysics, Graduate School of Science, Hokkaido University, 1995.
[27] Rast M, Bezy JL and Bruzzi S. The ESA Medium Resolution Imaging Spectrometer MERIS a review of the instrument and its mission, International Journal of Remote Sensing, 20:9, 1681-1702, DOI: 10.1080/014311699212416, 1999.
[28] Bicheron P, Defourny P, Brockmann C, Schouten L, Vancutsem C, Huc M, Bontemps S, Leroy M, Achard F, Herold M, Ranera F and Arino O. Globcover:

Products Description and Validation Report. MEDIAS-France 2008.
[29] Strahler AH, Boschetti L, Foody GM, Friedl MA, Hansen MA, Mayaux P, Morisette JT, Stehman SV and Woodcock CE. Global Land Cover Validation: recommendations for evaluation and accuracy assessment of global land cover maps, Office for Official Publications of the European Communities, Luxembourg, 2006.
[30] Zhuang Q, Melillo JM, Kicklighter DW, Prinn RG, McGuire AD, Steudler PA, Felzer BS, and Hu S. Methane emissiones between terrestrial ecosystems and the atmosphere at northern high latitudes during the past century: A retrospective analysis with a process-based biogeochemistry model, Global Biogeochemical Cycles, Vol. 18, GB3010, doi:10.1029/2004GB002239, 2004.
[31] Christensen TR, Ekberg A, Strom L, Mastepanov M, Panikov N, Oquist M, Svensson Bo H, Nykanen H, Martikainen PJ and Oskarsson H. Factors controlling large scale variations in methane emissions from wetlands, Geophysical Research Letters, Vol. 30, NO. 7, 1414, doi:10.1029/2002GL016848, 2003.
[32] Cao MK, Gregson K and Marshall S. Global methane emission from wetlands and its sensitivity to climate change, Atmospheric Environment Vol. 32, No. 19, pp. 3293—3299, 1998.
[33] Christensen TR, Johansson T, Akerman HJ, Mastepanov M, Malmer N, Friborg T, Crill P and Svensson Bo H. Thawing sub-arctic permafrost: Effects on vegetation and methane emissions, Geophysical Research Letters, Vol. 31, L04501, doi:10.1029/2003GL018680, 2004.
[34] Wille C, Kutzbach L, Sachs T, Wagner D and Pfeiffer EM. Methane emission from Siberian arctic polygonal tundra: eddy covariance measurements and modeling, Global Change Biology 14, 1395–1408, doi: 10.1111/j.1365-2486.2008.01586.x, 2008.
[35] Hubberten HW, Wagner D, Pfeiffer EM, Boike J and Gukov AYu. The Russian-German Research Station Samoylov, Lena Delta -A Key Site for Polar Research in the Siberian Arctic, Polarforschung 73 (2/3), 111 – 116, 2006.
[36] Takeuchi W and Gonzalez L. Blending MODIS and AMSR-E to predict daily land surface water coverage, Proceedings of International Remote Sensing Symposium (ISRS), Busan, South Korea, Oct. 29, 2009.
[37] Iijima Y, Fedorov AN, Park H, Suzuki K, Yabuki H, Maximov TC and Ohata T. Abrupt Increases in Soil Temperatures following Increased Precipitation in a Permafrost Region, Central Lena River Basin, Russia, Permafrost and Periglac. Process. 21: 30–41, DOI: 10.1002/ppp.662, 2010.
[38] Hayashida S, Ono A, Yoshizaki S, Frankenberg C, Takeuchi W and Yan X. Methane concentrations over Monsoon Asia as observed by SCIAMACHY:

Signals of methane emission from rice cultivation, Remote Sensing Environment, 139/246-256, 2013.

[39] Peters W, Jacobson AR, Sweeney C, Andrews AE, Conway TJ, Masarie K, Miller JB, Bruhwiler Lori MP, Petron G, Hirsch AI, Worthy Douglas EJ, van der Werf GR, Randerson JT, Wennberg PO, Krol MC, and Tans PP. An atmospheric perspective on North American carbon dioxide exchange: CarbonTracker, Proceedings of the National Academy of Sciences, U S A, 104, 18925-18930, 2007.

[40] Gukov AYu, Wagner D, Boike J and Hubberten HW. The Russian-German Research Station Samoylov, Lena Delta: A Key site for Long-term Observations of Permafrost Ecosystems in the Siberian Arctic, 2007.

[41] Wagner D, Kobabe S, Pfeiffer EM and Hubberten HW. Microbial Controls on Methane Emissiones from a Polygonal Tundra of the Lena Delta, Siberia, Permafrost Periglac. Process. 14: 173–185, 2003.

[42] Sachs T, Giebels M, Boike J and Kutzbach L. Environmental controls on CH4 emission from polygonal tundra on the microsite scale in the Lena river delta, Siberia, Global Change Biology 16, 3096–3110, doi: 10.1111/j.1365-2486.2010.02232.x, 2010.

[43] Hoehler TM and Alperin MJ. Biogeochemistry: Methane Minimalism, Nature 507, no. 749: 436-437, 2014.

[44] Yvon-Durocher G, Allen AP, Bastviken D, Conrad R, Gudasz C, St-Pierre A, Thanh-Duc N and del Giorgio PA, 2014. Methane emissiones show consistent temperature dependence across microbial to ecosystem scales. NATURE, doi:10.1038/nature13164.

[45] Melton JR, Wania R, Hodson EL, Poulter B, Ringeval B, Spahni R, Bohn T, Avis CA, Beerling DJ, Chen G, Eliseev AV, Denisov SN, Hopcroft PO, Lettenmaier DP, Riley WJ, Singarayer JS, Subin ZM, Tian H, Zurcher S, Brovkin V, van Bodegom PM, Kleinen T, Yu ZC and Kaplan JO. Present state of global wetland extent and wetland methane modelling: conclusions from a model intercomparison project (WETCHIMP), Biogeosciences Discussions 10, 753–788, 2013.

[46] Laurila T, 14th WMO/IAEA Meeting of Experts on Carbon Dioxide, Other Greenhouse Gases and Related Tracers Measurement Techniques. Helsinki, Finland, 10-13 September 2007. (This document (or report) is not an official publication of WMO and has not been subjected to its standard editorial procedures.)

[47] Schrier-Uijl AP, Kroon PS, Hensen A, Leffelaar PA, Berendse F, Veenendaal EM. Comparison of chamber and eddy covariance-based CO2 and CH4 emission estimates in a heterogeneous grass ecosystem on peat, Agricultural and Forest Meteorology 150 825–831, 2010.

[48] GISS Surface Temperature Analysis: 2010 — How Warm Was This Summer? NASA News Release, April, 2013.

[49] Voiland A. How Warm Was Summer 2010? NASA Earth Observatory, 2013-9-30.

[50] Zamolodchikov DG, Karelin DV, Ivaschenko AI, Oechel WC and Hastings SJ. CO2 emission measurements in Russian Far East tundra using eddy covariance and closed chamber techniques, Tellus, 55B, 879-892, 2003.